On The Strategy To Reduce Greenhouse Gas Emissions Of Crew Transfer Vessels;

Towards Zero Emission Crew Transfer Operations

Reinout Sterk
Document No. 2022.038

Delft University of Technology

TU Delft

SIEMENS Gamesa
RENEWABLE ENERGY

On The Strategy To Reduce Greenhouse Gas Emissions Of Crew Transfer Vessels;

Towards Zero Emission Crew Transfer Operations

To obtain the degree of Master of Science
in *Mechanical Engineering* at the
Delft University of Technology

Reinout Sterk

Student number: 4486706

Project duration: Sep. 2021 - Aug., 2022

Supervisors:	Dr.ir. R.A.J. van Ostayen	Delft University of Technology
	Dr.ir. H. Polinder	Delft University of Technology
	Ir. B. van Veldhuizen	Delft University of Technology
	K. Coughlan	Siemens Gamesa
Graduation committee:	Dr.ir. R.A.J. van Ostayen	Delft University of Technology, Chairman
	Dr.ir. H. Polinder	Delft University of Technology
	Dr.ir. S. Nasiri	Delft University of Technology
	Ir. B. van Veldhuizen	Delft University of Technology

TU Delft Delft University of Technology

SIEMENS Gamesa RENEWABLE ENERGY

Cover photo: Wikinger wind farm located offshore Germany in the Baltic Sea
(https://cdn.offshorewind.biz/wp-content/uploads/sites/2/2017/07/2914318/30-wikinger-turbines-in-place.jpg)

Abstract

Due to more stringent greenhouse gas (GHG) emission regulations in the maritime industry, solutions are being sought to decrease the GHG emissions of crew transfer vessels used in offshore wind farms. Multiple alternative fuels and power generating systems can be used to decrease these emissions. In this research, a comparative study is performed on six concept solutions. Four fuel types (hydrogen, HVO, methanol, and renewable energy) and three different power generating system components (proton exchange membrane fuel cells, lithium-ion batteries, and internal combustion engines) are considered. The option of charging a battery-powered ship offshore is also considered. The goal of this research is to identify the most cost-effective system to reduce GHG emissions. The comparison is based on the total cost of ownership, the GHG emissions of fuel production and utilisation, and the GHG emissions of the production of the power generating system. In order to achieve this, the component sizes and lifetimes are calculated based on the constraints of the ship and the operational profile with different transit distances to the wind farm. The lifetime of the fuel cell is based on a cell voltage degradation model developed in this research. A battery electric ship with a methanol genset is found to be the best method with the largest GHG emissions reductions in relation to cost. Without charging offshore for a transit distance up to 18 km, and with offshore charging beyond 18 km. If charging offshore is not considered viable, a combustion engine with hydrogen is the best option for a transit distance of 18 km up to 68 km, and HVO upwards of 68 km.

Table of contents

List of Figures

Acronyms

BoP balance-of-plant. 81
CI compression ignited. 9
CTV crew transfer vessel. 1
DME dimethyl ether. 5
DMFC direct methanol fuel cell. 10
DoD depth of discharge. 12
ECSA electrochemically active surface area. 80
EFC equivalent full cycle. 12
EoL end-of-life. 84
FT diesel Fischer-Tropsch diesel. 7
GDL gas diffusion layer. 79
GHG greenhouse gas. 1
GWP global warming potential. 107
HVO hydrotreated vegetable oil. 8
ICE internal combustion engines. 1
IMO International Maritime Organisation. 1
LCoE levelised cost of energy. 10, 91
LFP lithium iron phosphate. 12
LHV lower heating value. 34
MCFC molten carbonate fuel cell. 10
MEA membrane electrode assembly. 79
MeOH methanol. 6
MGO marine gasoil. 1
NCA nickel cobalt aluminium. 12
NMC nickel manganese cobalt. 12
NO_x nitrogen oxides. 3
OCV open circuit voltage. 83
PEMFC proton exchange membrane fuel cell. 10
PFSA perfluorinated sulfonic acid based ionomer. 80
PM particulate matter. 3
PMSM permanent magnet synchronous machine. 110
RH relative humidity. 85
SCR elective catalytic reduction. 3
SI spark ignited. 9
SO_x sulphur oxides. 3

SoC state of charge. 25
SOFC solid oxide fuel cell. 10
TCO total cost of ownership. 3
TRL technology readiness level. 18
TTW tank to wake. 44, 107
WTT well to tank. 44, 107
WTW well to wake. 44, 107

Symbols

Symbol	Definition	Unit
A	Area	m^2
C_{FC}	Fuel cell cost	€ kW^{-1}
C_B	Battery cost	€ kWh^{-1}
C_{ICE}	ICE cost	€ kW^{-1}
C_{GS}	Genset cost	€ kW^{-1}
C_{SH_2}	Hydrogen storage cost	€ kg^{-1}
C_{EM}	Electric motor and switchboard cost	€ kW^{-1}
C_{Scale}	Propulsion power scaling factor	
C_{SCR}	SCR system cost	€ kW^{-1}
C_{H_2}	Hydrogen price	€ kg^{-1}
C_{rate}	Battery charge/discharge speed	C
D_{SS}	Fuel cell degradation rate	μV h^{-1}
E	Electric energy	kWh
F	Faraday constant	C mol^{-1}
G	Gibbs free energy	J
GED	Gravimetric energy density	kWh kg^{-1}
$\bar{g}$	Gibbs free energy per mol	J mol^{-1}
H	Enthalpy	J
L	Lifetime	h
m	Mass	kg
n_{cell}	Number of battery cells	
n_{cycle}	Number of battery discharge cycles	
n_{days}	Days of operation	
n_1	Number of fuel cell load cycles	
n_2	Number of fuel cell start-stop cycles	
P	Power	kW
$P_{FC_{installed}}$	Installed fuel cell power	kW
P_{min}	Minimum installed power	kW
P_{shaft}	Propulsion power	kW
Q_B	Battery capacity	kWh
q_{cell}	Battery cell capacity	Ah
S	Entropy	J K^{-1}
S_{fuel}	Safety margin fuel capacity	
S_{power}	Safety margin on installed power	
t	Time	s
V	Volume	m^3
V_r	Reversible voltage	V
VED	Volumetric energy density	kWh l^{-1}
$V_{FC_{EoL}}$	Maximum fuel cell voltage loss	V

R	Gas constant	J mol^{-1} k^{-1}
W	Work	J
η	Efficiency	
δV	Cell voltage loss	V
ρ	Density	kg m^{-3}

Acknowledgements

This report has been written to obtain a Master of Science degree in Mechanical Engineering at the Delft University of Technology. I want to acknowledge the people who supported me during this project. First, I want to thank my daily supervisor Berend van Veldhuizen for being a great discussion partner during our meetings and always being available for my questions. Besides, when I was stuck at the project, his expertise and ability to ask good questions helped me find the right direction again.

I want to thank my thesis supervisors Henk Polinder and Ron van Ostayen for their guidance, supervision, and constructive feedback, which helped me to go through the process.

Next, I want to thank Siemens Gamesa Renewable Energy for providing me the great graduation opportunity to work on this exciting and relevant project of decarbonising the fleet. Especially I would like to thank Kenneth Coughlan for his supervision and expertise which helped me to get familiar with the maritime aspect of the offshore wind industry. Also, I want to thank Hugo Cook for his enthusiasm for the project and his expertise in crew transfer vessels.

Also, I want to thank Tom Mehew from Njord Offshore for providing me the practical information needed to execute this project.

Finally, I want to thank my friends and family for their endless support during this project and throughout the rest of my educational journey.

Reinout Sterk
Rotterdam, 30/07/2022

1 Introduction

1-1 Background

To counter global warming, the International Maritime Organisation (IMO) set regulations to lower the shipping industry's emissions, forcing the industry to transition from fossil fuels to cleaner alternatives. According to the initial IMO greenhouse gas (GHG) strategy, the annual GHG emissions from shipping should be decreased by 50% in 2050 compared to 2008 (IMO, 2018). Besides, global efforts are made to replace fossil fuels for electricity production with green alternatives such as solar and wind energy. The government of the Netherlands announced that in 2050 all the electricity used in the Netherlands has to come from renewable sources and foresees a significant role for offshore wind energy, with a target of 21 GW installed in 2030 (Government of the Netherlands, 2020). With this large stake in offshore wind, the use of vessels to install and operate these wind farms will increase. These vessels contribute to a significant part of offshore wind energy's life cycle GHG emissions (Yang et al., 2018).

Traditionally, ships have internal combustion engines (ICE) powered by fossil fuels such as marine gasoil (MGO). Multiple different alternative fuel options are proposed to reduce GHG emissions. Ammonia, bio-diesel, hydrogen, and methanol are often described as promising alternatives (van Biert et al., 2016, McKinlay et al., 2021). Besides, battery technology is an interesting alternative due to its high electrical efficiency. The energy density of these fuels and the storage systems is lower than MGO resulting in less energy on board. More efficient fuel conversion systems such as fuel cells can partially solve this problem. Fuel cells transform chemical energy directly into electrical energy. However, the power density of these systems is also lower than the traditional ICE.

In the offshore wind industry, multiple installation vessels are used: wind turbine installation vessels, cable laying vessels, and jack-ups. During maintenance, a crew transfer vessel (CTV) is used. CTVs are relatively small vessels of 15 to 35m in length that transport the technicians and small cargo between the wind farm and port daily. CTVs can bunker or recharge after each day and are therefore easier to convert to alternative fuel systems than the larger installation vessels. For this reason, CTVs are investigated in this research as a first step into a more sustainable fleet.

1-2 Problem statement and research questions

Multiple alternative fuels and power generating systems exist with many possible combinations. Each combination has its pros and cons in terms of emissions, range, and costs. Previous research is often on large vessels, e.g. cruise ships or ferries (Kim et al., 2020, Inal et al., 2022, Trillos et al., 2021). These ships have completely different operational profiles, length, weight and volume constraints, energy consumption, power characteristics, etc. Therefore, to identify a CTV's future power generating system, knowledge specifically focused on CTVs is needed. Previous studies in alternative power generating systems for CTVs focused on diesel-electric hybrids or hydrogen fuel cell ships (Łebkowski, 2020, X. Wang et al., 2021). However, increasing interest in producing fuels using renewable electricity and captured CO_2 or nitrogen provides new alternatives. To the author's knowledge, no comparative study has been performed which also takes the lifetime of the power generating systems into account. It is known that the lifetime of a fuel cell is highly dependent on how it is used (Ren et al., 2020). As the CTV performs multiple short trips between the turbines each day, there will be a large number of load transients which leads to a shorter lifetime of the fuel cell. Therefore it is essential to investigate the influence of the operational profile on the lifetime of the power generating system. Besides these literature gaps, a secondary problem arises considering the higher costs of these renewable fuels and power generating systems compared to their fossil counterpart. As offshore wind energy is on the boundary of being cost competitive, a large price increase can result in fewer installed wind turbines and thus fewer reductions in GHG emissions. Therefore the cost is an important factor in the economical feasibility of these new systems. In this research, an effort is made to identify the most promising solutions to reduce GHG emissions of CTVs towards zero in the short future, with the following research question:

What is the most economically attractive alternative fuel and power generating system to reduce greenhouse gas emissions of crew transfer vessels used for the operation of offshore wind farms towards zero?

This is divided into the following sub-questions:

- What fuels and power generating systems can be used to reduce GHG emissions towards zero?
- How can the lifetime of the power generating system be taken into account in the evaluation of the different power generating systems?
- What are the GHG emissions associated with the operation of CTVs?
- What are the costs associated with the alternative fuels and power generating systems for a CTV?
- How does the operational profile of the CTV change the choice between the different alternative fuel options?

1-3 Methods

First, multiple concept power generating systems are made out of a selection of fuels and fuel conversion systems. Next, methods to predict the lifetime of these systems are investigated and a fuel cell degradation model is made. Afterwards, the GHG emissions are calculated based on life cycle assessment studies, and the total cost of ownership (TCO) is calculated. To determine the fuel consumption and component sizes of the different system components, the energy and power requirements of the CTV are needed. This will be based on information from sea trials and operational data logs, out of which an operational profile is constructed for multiple transit distances. The cost and GHG emissions will be evaluated for these different transit distances. This will give insights into how the length of the transit will impact the choice between power generating systems.

1-4 Scope

As the lifetime of ships is typically over 20 years, a large fleet of existing ships needs to be converted with these new power generating systems. The possibility of retrofitting an existing ship is investigated in this research. Therefore, vessel design will not be taken into account. However, results from this research will give insights on whether vessels need to be designed differently to fit all the systems on board. The vessel is only considered from a constraints point of view, such as maximum system weight.

The CTV will be used in wind farms. Therefore there will be a focus on fuels that can be produced using wind energy. Besides, only fuels that can drastically reduce GHG emissions towards zero, and that are likely to be available in ports are considered in this research.

Multiple pollutants are emitted during fuel combustion. Under high temperatures, nitrogen oxides (NO_x) are generated by a reaction of atmospheric nitrogen and oxygen. The combustion of fuels containing sulphur will produce sulphur oxides (SO_x) emissions. Additionally, particulate matter (PM) is emitted, originating from the fuel and lubricating oils. State-of-the-art elective catalytic reduction (SCR) systems can reduce NO_x emissions by up to 90% (Baleta et al., 2015). This is sufficient to comply with the most strict IMO tier 3 NO_x regulations of 2 g/kWh. SO_x emissions of alternative fuels are virtually eliminated due to the low sulphur content of most alternative fuels. Therefore, only GHG emissions are evaluated in this work. All concepts will be based to comply with the IMO tier 3 NO_x regulations. Besides the direct emissions from the exhaust, GHG emissions from fuel production and GHG emissions of the power generating system are important to reduce GHG emissions. For example, batteries and fuel cells provide efficient ways to store and produce power. However, the GHG impact during production is higher than ICEs (Simons and Azimov, 2021). Therefore, also the production of the power generating system is taken into account. The recycling of the components after their use-full life is not considered as this is highly dependent on what happens with the components at the end of its lifetime.

The lifetime of the power generating system will be investigated in different depths. The ICE is an established technology, and its durability is proven. The combustion of alternative fuels is however still in development. Thus durability of engines with alternative fuels is not as proven as an ICE with MGO. However, working principles are similar. In this report, it is assumed that the fuel type does not influence durability. The durability of fuel cells has been described as a problem for widespread implementation (van Biert et al., 2016). The durability of fuel cells is highly dependent on how it is operated and hence on the operational profile (Borup et al., 2007). Consequently, a large part of this research will be focused on investigating the degradation mechanisms of fuel cells and mitigation strategies to minimise degradation. Also, a method to estimate the lifetime of the fuel cell will be made. Furthermore, batteries are known to lose capacity over time. Therefore, the capacity fade of the battery is predicted.

The TCO is based on the cost of the power generating system, the cost of the fuel, SCR operational cost, and finally, the cost of the battery charger as a battery charger specifically for the CTV is required due to long charging times. Bunker infrastructure is not included as this is not explicitly needed for the CTV. Maintenance cost is not included as this is hard to correctly predict as little practical knowledge is available about the maintenance of these new systems.

1-5 Document structure & Reading guide

Chapter 1 Introduces the topic of this research, the research questions, the objectives, the methods used in this research, and the scope of work.
Chapter 2 Provides an overview of the alternative fuel options and the power generating systems suitable for CTVs. Besides, Offshore charging is discussed.
Chapter 3 Introduces the concepts that will be investigated further as possible solutions to reduce GHG emissions. Besides, the technology readiness of these concepts is discussed.
Chapter 4 Describes the model and methods used to evaluate the different concepts. Besides, an overview of the made assumptions can be seen.
Chapter 5 Provides the results of the comparison of the different concepts.
Chapter 6 Evaluates the used methods and describes how the results of this work might be influenced by the assumptions made in this thesis. Furthermore, recommendations are made for further research.
Chapter 7 Presents the conclusion and the answers to the research questions are given.

2

Alternative fuels and power generating systems

2-1 Alternative fuels

In this chapter alternative fuels are investigated. The largest part of the emissions from a CTV originates from the combustion of the fuel. In order to reduce these emissions alternative fuels can be used. For fuels that can be produced by multiple methods, the method of using renewable wind energy is used. In this way, the electricity produced by the wind park is also used to produce the fuel needed to operate the wind park.

In the work of Ampah et al. (2021) ammonia, bio-diesel, electricity, LNG, and methanol are described as possible alternative fuels. Xing et al. (2021) also did a review of alternative fuel options and investigated the previously named fuels, in addition LPG and dimethyl ether (DME) are mentioned. In the work of van Biert et al. (2016), LNG, hydrogen, methanol and ammonia are described as possible alternatives to MGO. According to Xing et al (2021) LNG cannot comply with a 50% CO_2 reduction, therefore LNG is not further considered. In the following section, these fuels are discussed further.

2-1-1 Renewable energy

The most direct way of using renewable energy in ships is using it as electricity stored in batteries. Although electricity can technically not be considered a fuel, in this report the use of electricity to propel the CTV is considered an alternative fuel option. Besides the use of renewable energy in batteries, renewable energy can be used to produce hydrogen which will be discussed next.

2-1-2 Hydrogen

Hydrogen (H_2) is an often named alternative fuel option. Hydrogen is at a gaseous state at atmospheric pressure and standard temperature. Hydrogen can be produced in multiple

different ways. Traditionally, hydrogen is produced by natural gas reforming. However, with this process CO_2 is emitted. Therefore, hydrogen is increasingly produced with renewable energy. The production of hydrogen with electricity is done via the electrolysis of water. Hydrogen only consists of two hydrogen atoms; therefore during combustion no carbon is emitted making hydrogen a carbon free fuel during the usage phase. Of all e-fuels hydrogen is the cheapest to produce (TNO, 2022). However, due to the low density of hydrogen, storage is one of the difficulties of hydrogen in ships. Although hydrogen has a very high gravimetric energy density compared to other fuels, the volumetric energy density of hydrogen gas under normal atmospheric pressure is very low. To improve the volumetric energy density of hydrogen it can be compressed to pressures up to 700 Bar or it can be stored as a liquid in special well-insulated tanks at a temperature below -253° C, cryogenic storage. The safety of hydrogen is an often discussed topic. Because the hydrogen molecule is very small and storage is often done at pressures of hundreds of Bars, there is a relatively large risk of leakages. The flammability range of hydrogen is large, between 4% and 74%, increasing the risks of potential leakages (TNO, 2022). With many renewable hydrogen projects launched in recent years, the availability of hydrogen in ports is expected to increase.

2-1-3 Alcohols

In chemistry, an alcohol is an organic material madelarge of at least one hydroxyl group bound to a carbon atom. For alternative fuels, the class of alcohols which includes methanol and ethanol are often described as promising fuels for the marine industry. Because of the possibility of producing methanol from renewable hydrogen, only methanol is considered in this work.

Methanol (MeOH) is a liquid at atmospheric pressure making storage, distribution, and bunkering easier. Methanol can be produced in various ways, from fossil fuels, biomass, and from renewable energy sources in carbon capture and utilisation schemes (Verhelst et al., 2019). The production of methanol using electricity is done via the synthesis of hydrogen and CO_2. Methanol can be a net-zero carbon fuel when CO_2 is captured from, for example, the steel industry. During the operation of a methanol-powered vessel, CO_2 is still emitted. However, the CO_2 emissions during utilisation are compensated by the capture of CO_2 during production. Another benefit of methanol is the SO_x-free combustion, as methanol is a sulphur-free fuel. Methanol has a high autoignition temperature and is therefore more difficult to combust than diesel fuel. In the report of TNO (2020), three possibilities to combust methanol are given: 1) Dual fuel, use a certain amount of diesel to initiate the methanol combustion. 2) Combustion in a spark ignition engine. 3) Use an ignition improver to lower the autoignition temperature such that it can be used in a diesel engine.

2-1-4 Ethers

An ether is an organic compound similar to alcohols. In an alcohol, one of the two hydrogen atoms of water (H_2O) is replaced by an alkyl group: C_nH_{2n+1}. In an ether both hydrogen atoms are replaced by an alkyl group or aryl group. Dimethyl ether (DME) is an ether often described as an interesting option. The chemical formula of DME is CH_3OCH_3. DME can be produced by methanol dehydration in the following reaction:

$$2\,CH_3OH \longrightarrow C_2H_5OH + H_2O \tag{2.1}$$

Alternatively, DME can be produced directly from synthesis gas, a mixture of carbon mono oxide and hydrogen. DME can be stored in liquid form at a pressure of 5 Bar, with a slightly higher energy density than methanol (van Biert et al., 2016). To the author's knowledge there is no large-scale green DME production project running to date. Therefore, the availability of green DME is expected to be low in the coming years. Therefore, DME is not considered further in this work, although it could be an interesting option when production is increased.

2-1-5 Ammonia

Ammonia is a compound of nitrogen and hydrogen with chemical formula NH_3. Storage can be done by compressing it, often to 10 Bar, or stored as a liquid below -33°C. Ammonia has the highest energy density compared to hydrogen, methanol and DME. Similar to methanol, ammonia can be produced by the synthesis of hydrogen. Instead of CO_2, nitrogen (N_2) is used. The nitrogen can be obtained by air separation, in which nitrogen is extracted from the air. The synthesis of hydrogen and nitrogen takes place in a Haber-Bosch reactor with a yield of 70% (Verhelst et al., 2019). A drawback of ammonia is that inhalation of ammonia is toxic. For the shipping industry probably enough safety measures can be taken (Verhelst et al., 2019). One of the largest flaws of ammonia for ICEs are the far from ideal combustion characteristics: small flammability range, high autoignition temperature and low flame temperature (Kobayashi et al., 2019). In Section 2-2, possible power generating systems are described, and no fuel cells are deemed suitable for ammonia onboard of CTVs. Ammonia is not considered in this research because ammonia is not particularly suitable for combustion engines and fuel cells for ammonia are not suitable for CTVs yet.

2-1-6 FT/Bio - Diesel

Diesel can be produced using different feedstocks, traditionally fossil-based, but diesel can also be produced with the Fischer-Tropsch process where hydrogen and carbons are transformed into a mixture of several hydrocarbons, Fischer-Tropsch diesel (FT diesel). Similar to, for example methanol, production can be done with carbon capture and renewable hydrogen, making this a carbon neutral alternative. However, the efficiency of this process is lower compared to methanol production; therefore more hydrogen is consumed during production

(SMART PORT, 2020). This higher hydrogen consumption will increase the emissions and cost. For this reason, FT-diesel is not considered. Bio-diesel is another sustainable form of diesel. Bio-diesel can be produced in several ways. Using biomass, where vegetable oils are hydrogenated to create a fuel similar to diesel with chemical structure C_nH_{2n+2}, hydrotreated vegetable oil (HVO). Different biomass feedstocks can be used. Residual bio-masses, e.g. from used cooking oil or from purpose-grown feedstocks, crops that are specifically farmed for fuel production such as, soybean or rapeseed. A possible feedstock to create HVO is palm oil. However, this is controversial as palm oil is a major driver for deforestation and is coupled with the transformation of carbon-rich peat soils where large amounts of GHG emissions are emitted into the atmosphere and contribute to climate change (WWF, 2022). Therefore palm based HVO is not considered. It could be argued that the use of other purpose-grown crops would also lead to deforestation due to the increase of required agricultural land. Besides, the emissions related to the production of this fuel are still relatively high, this is discussed further in Appendix E. Therefore, only residual feedstocks are considered. The HVO production capacity in Europe was around 3.5 million tonnes in 2021 and could grow to 10 million tonnes in 2030 (SGS Inspire, 2021). Therefore it is expected that there is a sufficient supply for CTVs, but it would not be sufficient for the entire shipping industry.

2-1-7 Sub-conclusion

Ammonia is not considered a viable option due to the poor ignition properties, and DME is excluded due to low expected availability. This leaves hydrogen, HVO, methanol, and renewable electricity as alternative fuel options. The properties used in the coming sections are listed in Table 2-1.

Property	**Unit**	**MGO**	**HVO**	**Hydrogen**	**Methanol**
Density	kg/m^3	855	920	0.090*	791
LHV	MJ/kg	42.8	37.8	120	19.9
Autoignition temperature	°C	210	204	500	464

Table 2-1: Fuel properties at 15 °C. *Density hydrogen at 1 Bar and 0 °C. (EngineeringToolbox, 2022).

2-2 Alternative power generating systems

In this section, possible alternative fuel options and power generating systems are investigated. In the end, a sub-conclusion is drawn about which fuels and systems will be included in the concept solutions.

2-2-1 Internal combustion engine

Instead of changing the power generating system completely in an effort to reduce GHG emissions, the combustion of alternative fuels in a combustion engine is an interesting option due to the limited impact on system design compared to the traditional system. Due to recent developments made by marine engine manufacturers, ICEs running on other fuels such as methanol and hydrogen are expected to be available in the near future (MAN Energy Solutions, 2022). Some offer dual fuel capabilities, making it possible to switch between fuel options, especially useful when the availability of the alternative fuels is not 100%.

Two main types of combustion engines exist, the compression ignited (CI) engine and the spark ignited (SI) engine. CI combustion engines are the marine industry standard due to their high energy efficiency and good durability. Within a CI engine, air is compressed in the cylinders, increasing the temperature to such a high temperature that the injected fuel ignites. For this process, the autoignition temperature, the minimum temperature at which the fuel ignites without a spark or flame being present, is important. From the autoignition temperature in Table 2-1, it can be seen that the autoignition temperature of hydrogen and methanol are considerably higher and are therefore more difficult to combust in a CI engine. Inside a SI engine, the combustion of the air-fuel mixture is initiated by a spark, and this enables fuels to be used with a higher autoignition temperature. Often a distinction is made between ICEs in the marine industry by the RPM of the engine, low, medium and high-speed engines. Low speed, often two-stroke, engines are directly coupled to the propeller. High-speed engines often use a gearbox. For CTVs, high-speed four-stroke engines are used.

Instead of directly connecting the ICE to a gearbox or shaft, it could also be used to generate electricity. In this situation, the ICE is mechanically connected to an electric motor to generate electricity, this combination is called a genset in this report. The produced power can be used by another electric motor connected to the electricity grid via a switchboard and mechanically connected to the driveshaft. An advantage of this topology is that the ICE can operate at its most energy efficient point without having to match the torque and rpm of the driveshaft. Besides, at low power, individual gensets can be switched off to increase efficiency. Also, the generated electrical energy can be stored and utilised later.

NO_x emissions of 3-5 g/kWh were emitted during an emission test on a marine engine with methanol (Dankwa et al., 2021). This is higher than the maximum of 2g/kWh. The NO_x emissions must be reduced to comply with the IMO Tier 3 regulations. For hydrogen combustion even higher NO_x emissions are expected due to the higher combustion temperature.

The most promising way to meet the most strict Tier 3 standards with ICEs is a selective catalytic reduction (SCR) system (Guo et al., 2015). With a reduction up to 90% the most strict targets can be met (Baleta et al., 2015). This process works by injecting urea or ammonia into the engine's exhaust gas. When this mixture is fed through the catalyst converter, the mixture nitrogen oxides are transformed into non-harmful nitrogen (N_2) and water. A schematic of this process can be seen in Figure 2-1.

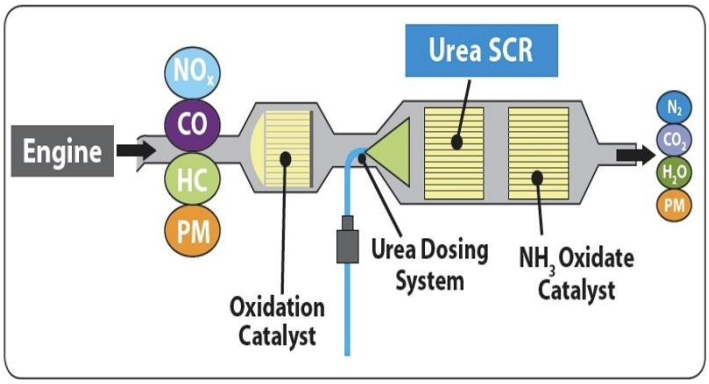

Figure 2-1: Schematic of an SCR system transforming NO_x into N_2 using urea (Moiras et al., 2017).

2-2-2 Fuel cells

Fuel cells are often described as an alternative to ICEs due to their high efficiency and zero local emissions. However, there are also challenges; durability, high cost and limited dynamic performance are often described as drawbacks of fuel cells (van Biert et al., 2016, Larminie and Dicks, 2003). Fuel cells can convert hydrogen, or in some cases, other fuels into usable electric power. There are different types of fuel cells, including solid oxide fuel cell (SOFC), proton exchange membrane fuel cell (PEMFC), direct methanol fuel cell (DMFC), and molten carbonate fuel cell (MCFC). These fuel cells have their own characteristics and differ in terms of efficiency, power density, and fuel options. An overview of different fuel cells and their properties can be found in the work of van Biert et al. (2016). According to Gianni et al. (2021), the power density of SOFC systems is between 8-10 kW/m^3. If one takes the daily fuel consumption of a CTV of around 400 kg of MGO at minimum, this results in roughly 2000 kWh of electrical power at an engine efficiency of 40%. With 10 hours of operation, the minimum fuel cell capacity would be around 200 kW. With a power density of 10 kW/m^3, the resulting system size would be around 20 m^3, excluding battery systems, switchboards, etc. Therefore, SOFCs are not considered further in this research due to the large required volume.

PEMFCs have a much higher power density. A system of 200 kW has a volume of around 2 m^3 (Ballard Power Systems, 2022), a factor ten smaller than the previously described SOFC system. The PEMFC is selected as the fuel cell of choice in this research because of its high power density, high efficiency, and high maturity of technology. When a fuel cell is mentioned is this work, it refers to a PEMFC.

In Appendix B, an in-depth investigation is performed on PEMFCs. The working principles, fuel cell components, fuel cell degradation, and fuel cell degradation modelling are discussed. Besides, a method to calculate the optimal fuel cell size for the lowest levelised cost of energy

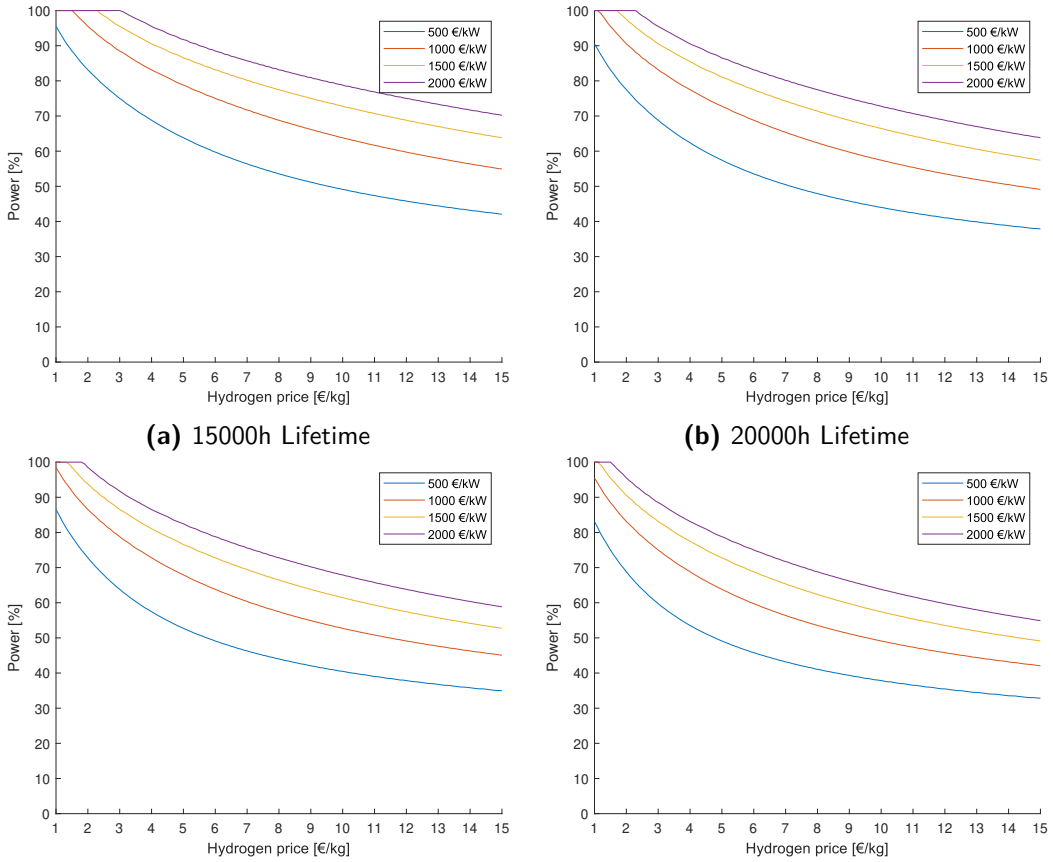

(a) 15000h Lifetime

(b) 20000h Lifetime

(c) 25000h Lifetime

(d) 30000h Lifetime

Figure 2-2: Optimal fuel cell operating power for the lowest LCoE, produced by a fuel cell operating at a constant power, as a function of the hydrogen price for different lifetimes of the fuel cell and different fuel cell prices.

(LCoE) is made. With Equation 2.2 the LCoE of the fuel cell can be calculated. Minimising this equation results in the optimal fuel cell operating power shown in Figure 2-2. Often when a fuel cell system is designed, the smallest fuel cell system is chosen to reduce the CAPEX e.g (TNO, 2019b). However, Figure 2-2 shows that this is not necessarily the best method to have the lowest cost over the entire lifetime. The above optimal fuel cell power is only valid for a fuel cell that is operated at steady-state and when there are no differences in steady-state degradation rates for different power outputs.

$$LCoE = \frac{C_{H_2}}{LHV_{H2} * \eta_{FC}} + \frac{C_{FC}}{L_{FC} * P_{FC}} \tag{2.2}$$

2-2-3 Batteries

Multiple types of batteries exist, including lead-acid, nickel metal hydride, lithium-ion batteries. The energy density of batteries is still far smaller than diesel fuel. Lithium-ion batteries are considered the most suitable battery technology in this study due to their high energy density and long lifetime. Safety is also an important topic with lithium-ion batteries. Lithium-ion batteries can catch fire or even explode. Therefore, safety systems must be included besides the battery cells alone. In the marine industry, the individual cells are often combined into battery packs with the safety system included. These smaller packs can be combined to form a large energy storage system. An example of such a system can be seen in Figure 2-3. Multiple types of lithium-ion batteries exist. Including lithium iron phosphate (LFP) or $LiFePO_4$, nickel cobalt aluminium (NCA), and nickel manganese cobalt (NMC). These different cell chemistries have different properties in terms of energy density, depth of discharge (DoD) and discharge rate. The cycle lifetime is an important parameter for a CTV as they are used intensively. From the above-mentioned cell chemistries, the LFP battery has a considerably higher lifetime (Preger et al., 2020). Besides, the LFP is less sensitive to cycles of 0-100% DoD. In the research of Preger et al. (2020), LFP batteries showed little to no difference in equivalent full cycle (EFC) lifetime between cycles of 40-60% DoD, 20-80% and 0-100%. In the same study, the cycle life of the NMC and NCA battery decreased substantially during complete discharge cycles, up to four times shorter EFC lifetimes. Another advantage of LFP batteries is that LFP batteries are not dependent on the rare earth metals nickel and cobalt. A disadvantage of LFP batteries compared to the other chemistries is the lower energy density. LFP is chosen in this work as the cell chemistry for the batteries of the CTV.

Figure 2-3: Example of a marine battery system (Corvus Energy, 2022).

2-2-4 Sub-conclusion

LFP batteries, PEMFCs, ICEs, and gensets will be included as power generating components within the concept solutions.

2-3 Offshore charging

A possibility to overcome the limited storage capacity of batteries is to charge the batteries in the wind farm when on standby. Multiple companies are working on systems to enable offshore charging of vessels (MEARSK, 2022, Offshore, 2022). These systems, in the form of floating buoys or a connection directly to the turbine, make it possible to connect a ship to the grid of an offshore wind farm. An example charging buoy can be seen in Figure 2-4. In this way, a hybrid or full electric ship can draw power directly from the wind park to charge the batteries. CTVs are on standby for multiple hours each day and could therefore recharge the batteries during the day.

Figure 2-4: Example of an offshore charging buoy for CTVs (Offshore, 2022).

3

Concept generation

In this chapter, concept solutions are made based on the alternative fuels and power generating system options from Chapter 2. Three concepts will be considered. A fuel cell based concept, a concept centred around batteries, and a concept based on ICE using alternative fuels.

3-1 Concept 1 - Fuel cell

The first concept uses hydrogen in combination with a PEMFC. The fuel cell is combined with a large LFP battery pack to account for load changes based on the degradation cost comparison outcome in Appendix B-3, the degradation cost for fuel cell load changes were higher compared to battery load changes. Effectively this is a battery electric CTV with a fuel cell used to extend the range. The concept components are schematically displayed in Figure 2-2. In this schematic, only one of each component is shown for all the concepts, in reality, the concepts consist of two propellers, gearboxes, and motors, each for one side of the CTV. Also, the number of battery stacks and fuel cells is not displayed for simplicity.

3-2 Concept 2 - Battery - Genset

The second concept consists of a large LFP battery pack. The storage capacity can be too little for the entire operating profile, as the battery's energy density is far smaller than diesel fuel. A genset is used to supply additional energy. Besides offshore charging can reduce the required battery capacity. Concept 2 is divided into two concepts: Concept 2A, without the availability of offshore charging and Concept 2B, with the ability to charge at the wind park. However, there is not always a grid connection offshore due to maintenance. The genset can supply the power, when power is unavailable at the wind farm. In this research, we assume a 100% availability in the cost and emissions calculations. However, the space and weight for the genset, and additional fuel are taken into account. Methanol is taken as the fuel for the genset. Hydrogen is not a possibility as the required space to store the hydrogen is not available, the battery pack takes up the space. HVO could also be used. However, this is not done so that a comparison can be made between fuels based on renewable wind energy.

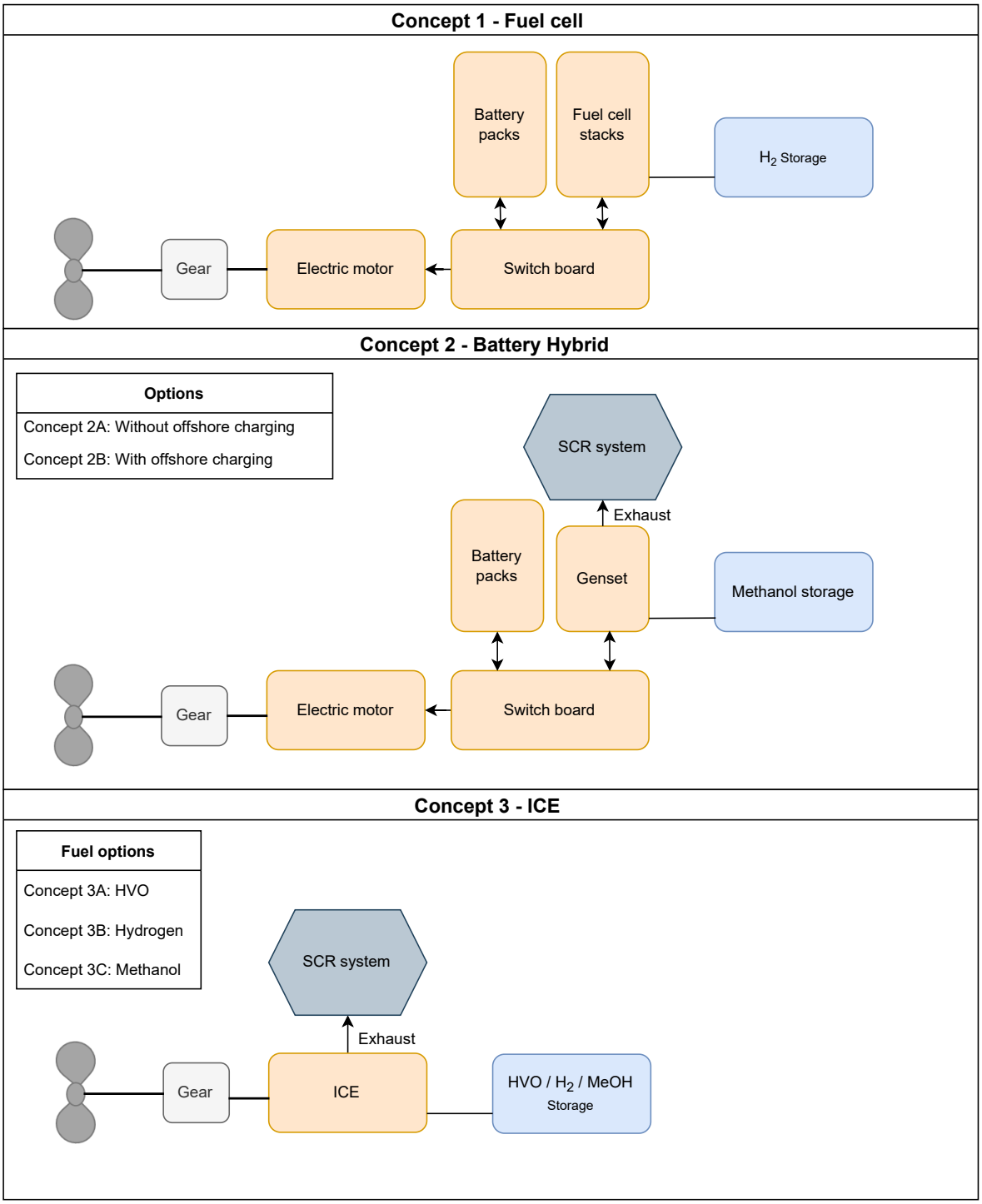

Figure 3-1: Overview of the schematic power generating systems of the different concepts.

3-3 Concept 3 - ICE

The last concept consists of a system similar to the standard system used today. It consists of ICEs with an SCR system to reduce NO_x emissions. For simplification, it is assumed that the engines used for the different fuel types are identical in terms of efficiency, weight, power, and size. Also, no distinction is made between CI and SI engines. The properties of a Volvo Penta D13-800 engine are used for all fuel types (VOLVO PENTA, 2022).

3-4 Fuel storage

For HVO and methanol, no special storage systems are needed as these fuels are in a liquid state at standard temperature and pressure. For hydrogen, the choice between compressed or cryogenic storage is determined by the constraints of the CTV. Compressed hydrogen at 350 Bar is chosen for simplicity if it does not exceed the maximum available space. Otherwise, cryogenic hydrogen is used. Compressed hydrogen has fewer storage difficulties than cryogenic storage such as hydrogen boil-off.

3-5 Charging and bunkering

Bunkering MGO or diesel on a ship is a relatively easy task. However, with hydrogen this becomes more difficult. Also, recharging the battery is a different process. Chargers of several hundreds of kW are required to charge the batteries of the CTV. This would be in the same order of magnitude as the fastest EV chargers currently available. Also, the first electric ships have been demonstrated and are used today. Therefore it is assumed that charging the batteries onshore does not imply insurmountable difficulties. Charging the battery of Concept 2B offshore is however still a new technology. Hydrogen bunkering is more complex than bunkering diesel fuels or other fuels that are liquid under standard pressure and temperature. The way the hydrogen can be bunkered depends on the storage method, either compressed hydrogen or liquid hydrogen must be transferred to the CTV. For compressed hydrogen storage, the hydrogen is transferred using high-pressure hoses. The hydrogen can either be transferred from a high-pressure storage tank onshore, e.g. 500 Bar, and then siphoned to the lower 350 Bar storage without a compressor in between, cascade filling. Or it can be transferred from a lower pressure storage tank with a compressor to the higher 350 Bar storage onboard the CTV. Liquid hydrogen bunkering is done by transferring the hydrogen in a special insulated hose to the storage onboard the CTV.

3-6 Technology readiness level

In this section maturity of technology is investigated. This is done based on the technology readiness level (TRL), a method to assess the maturity level of technology on a scale from 1 to 9, with 9 highest level of maturity. The levels are shown in Figure 3-2. The TRL is estimated for the most important components of the different concepts.

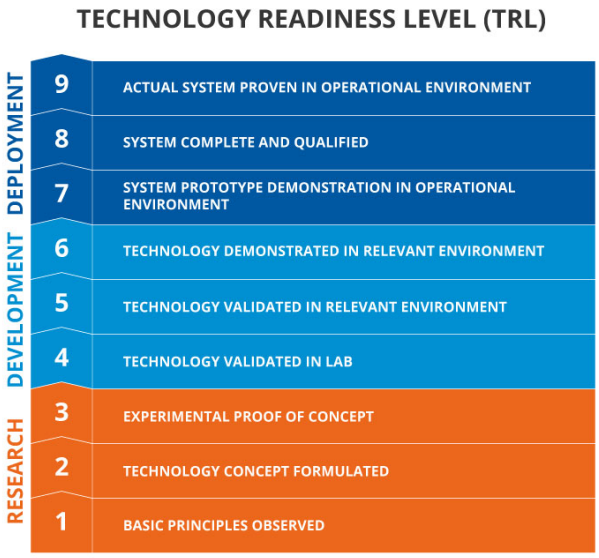

Figure 3-2: Technology Readiness Levels (TWI, 2022).

3-6-1 Power generating system components

Ballard Power Systems recently got the type approval of their marine fuel cell system. A TRL score of 8 is assigned due to few applications. Lithium-ion battery systems have been demonstrated in numerous electric ships worldwide and therefore receive a TRL score of 9. 100% hydrogen combustion engines have been launched (BEHYDRO, 2022). However, no similar engines as the ones used in CTVs are known. Therefore, a score of 6 is assigned. Methanol combustion engines and gensets are used in multiple large ships. To the author's knowledge no projects with a comparable engine to the ones used on CTVs are known, and thus receive a score of 6. HVO engines and SCR systems are widely used and receive a score of 9. Compressed hydrogen storage receives a 9, however cryogenic hydrogen storage onboard ships has not been demonstrated. Cryogenic hydrogen storage is used in other industries and therefore gets a TRL of 6.

3-6-2 Bunker system

Bunkering of HVO, methanol, and charging the batteries onshore receive a TRL score of 9 due to proven systems in operation. Compressed hydrogen bunkering receives a TRL of 8 due to the limited demonstration projects. Bunkering liquid hydrogen facilities have been launched but are not yet demonstrated in the marine industry. However, it is demonstrated in other industries, and therefore receives a TRL of 6. Charging offshore is only shown on prototypes and therefore receives a TRL score of 6 (Offshore, 2022).

3-6-3 Overview

In Table 3-1 the TRL scores of the concept components are given. It can be seen that Concept 3A has the highest TRL as this concept is already in use to date. The TRL of the genset used for Concept 2A and 2B is a limiting factor. This can however be mitigated by replacing methanol as the fuel with HVO. Lastly, the TRL of offshore charging is the lowest overall.

	Concept 1	**Concept 2A**	**Concept 2B**	**Concept 3A**	**Concept 3B**	**Concept 3C**
ICE				9	6	6
Genset		8	8			
Electric motor	9	9	9			
Switchboard	9	9	9			
SCR		9	9	9	9	9
Fuel Cell	8					
Battery	9	9	9			
Storage	9/6*	9	9	9	9/6*	9
Bunkering/charging	8/6*	9	5	9	8/6*	9

Table 3-1: TRL of the components of the different concepts. *for compressed/cryogenic storage.

4

Method

In this chapter, the model elements and the methods used to answer the research questions are described. The structure of this chapter is based on the model structure, this can be seen in Figure 4-1, where the green elements indicate a step of the calculation. All calculations are performed in MATLAB version R2019b. First, the energy and power that are required for the operation of the CTV are determined. Afterwards, the method of how the energy and power demand are divided between the components of the power generating system is described. This energy and power distribution are used in an iterative process to find the component size. Next, the fuel consumption and the lifetime of the components are calculated. Finally, the TCO and GHG emissions are calculated. The following sections elaborate on these steps in more detail.

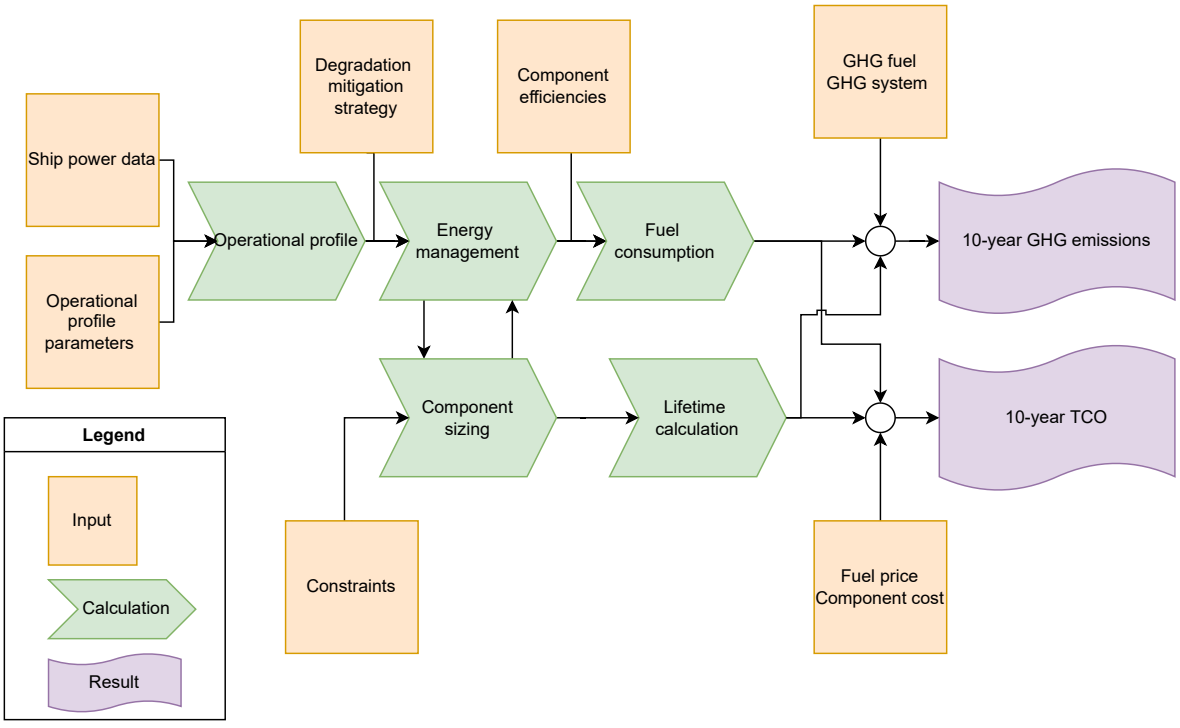

Figure 4-1: Flow chart of the developed model to compare the different concepts.

4-1 Load Profile

In this section, the method of how the power of the CTV is calculated during the day. First, the operational profile of the CTV must be determined. This operational profile contains the information about which task the CTV is performing in chronological order. This profile is then translated into a load profile. The load profile contains the required power over time during the operation of the CTV. To construct the load profile first, an array is constructed which contains the modes of the CTV during the day. The mode is the task the CTV is performing. Five different modes are considered: 1) transit to/from the park, 2) transit in the park, 3) transfer, 4) standby, 5) manoeuvring.

The operational profile is constructed based on a typical day of operation. An estimate is made of what a real operational profile would look like. The operational profile is constructed as follows. First, the CTV transits to the wind farm at the service speed, then, each team is deployed on a specific turbine. Each deployment is modelled as an approach phase where the CTV travels at a slow speed to the turbine, called manoeuvring. When contact is made between the CTV and the turbine, the power is increased to have a firm connection between the CTV and the turbine in order to transfer the technicians. After which, there is a manoeuvring phase again, followed by a lower transit speed in the park. The transit speed in the park is lower to navigate safely between the turbines. As an example, one deployment of technicians will result in the following block, which is placed in the mode array:

$$deploy = [5\ 3\ 5\ 2] \tag{4.1}$$

When all the teams are transferred, the CTV will go on standby, waiting for the next task. When the troubleshoot teams are finished they are collected and transferred to the next turbine, after which the CTV will go on standby again. At the end of the day, all teams are collected, and the CTV transits to port again. With this mode array, the load profile is constructed. When the CTV is in transit the power of the mode is determined by the speed-power characteristics of the CTV. This speed-power relationship is obtained from sea trial data where the engine power output of a CTV is measured for multiple speeds. There were no available measurements of the CTV investigated in this research. Therefore, the available data of a bigger CTV is used and scaled to estimate the power of the CTV used in this research. This scaling is done based on the power at maximum transit speed. It is known that the CTV of this research uses a power of roughly 1100 kW at 22 Kts, the CTV of the original measurements uses 1467 kW. The scaling factor is then calculated using Equation 4.2. The power speed relation is then calculated using Equation 4.3, where the scaling factor at 22 Kts is applied on all transits speeds. The original measurements and the estimated power for the CTV used in this research can be seen in Figure 4-2. In the next chapters and sections, the term P_{shaft} will refer to the required mechanical power from the ICE or electric motor.

$$C_{Scale} = \frac{1100}{1467} \tag{4.2}$$

$$P_{estimate}(v_{transit}) = P_{original}(v_{transit}) * C_{Scale} \tag{4.3}$$

	Assumed value	Unit
Transit speed to/from wind farm	19	kts
Transit speed in wind farm	12	kts
Manouvring speed	4	kts
Average transit distance between turbines	2000	m
Number of daily transfer operations	18	
Average daily standby time	3:30	h
Average transfer duration	6	min
Average manoeuvring duration	3	min
Days of operation per year	330	
Power during transfer / push-on	500	kW
Service teams	3	
Nr. of turbines visited by service teams	1	
Troubleshoot teams	2	
Nr. of turbines visited by troubleshooting teams	3	

Table 4-1: Assumed values for the operational profile.

Based on experience from Siemens Gamesa, it is assumed that 500 kW of propulsion power is used during the transfer operation where the CTV pushes the bow of the CTV against the turbine to provide access for the mechanics to the turbine. The speed and power combined with the power during transfer results in the power corresponding to the modes. From Figure A-1 in Appendix A, it can be seen that up to the year 2024, the furthest wind farm lies 62 km out of coast. This distance does not include the distance to the port. Therefore a distance of 75 km is assumed for the offshore wind farm furthest offshore. Tenders after 2024 will likely be further offshore. In the evaluation of the concepts, the transit distance will vary from 5km up to 100 km. 50 km is taken as the average transit distance of a CTV to the wind farm. This value will be used for analyses which are performed on a specific transit distance.

With the distance and the speed, the duration of each transit is calculated. Besides, for an average crew onboard, it is assumed that there are three teams doing regular maintenance, which visit only one turbine each day, dropped off in the morning and collected at the end of the shift again, and two teams that are doing troubleshoot work, visiting three turbines each day. With the power during the different modes combined with the duration of operation from Table 4-1, the load profile is constructed as an array with a 1s time step, δt. In Figure 4-3 the load profiles with a transit distance of 5 km, 25 km, 50 km, and 75 km can be seen. Generally, service technicians work in shifts of around 12 hours. Therefore, for wind farms further offshore, likely faster vessels will be used, or large vessels that remain offshore for an extended period of time will be used, which are not considered in this research.

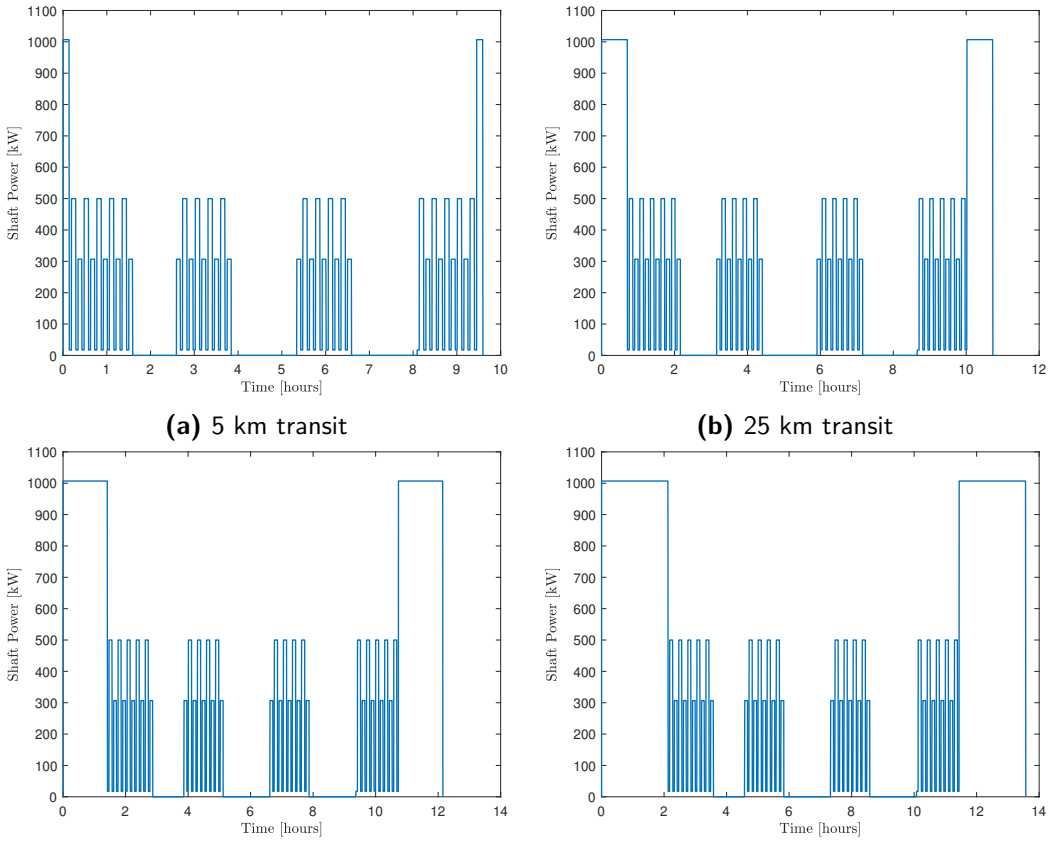

(a) 5 km transit **(b)** 25 km transit

(c) 50 km transit **(d)** 75 km transit

Figure 4-3: Load profiles of the CTV for the different transit distances.

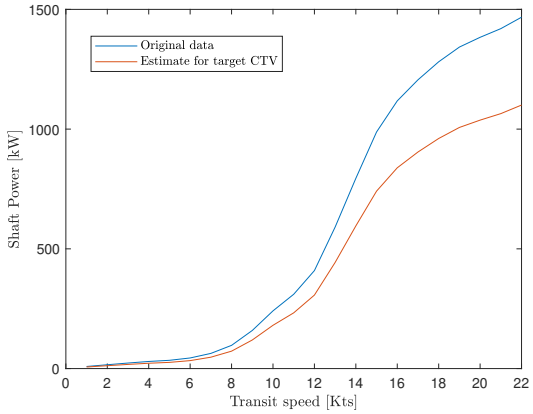

Figure 4-2: Relationship between the shaft power and speed. In blue, the original data from a 26m CTV, and in orange, the estimate used for the 20m CTV of this research.

4-2 Energy management

Multiple energy sources are available on the CTV for some of the concept power generating systems. For example, fuel cell Concept 1 also contains a battery. In this section, the method of how the power demand is divided is described. For Concept 1, 2A, and 2B, the electric power required by the electric motor, P_{emotor}, is calculated using equation 4.4. With P_{shaft} the mechanical propulsion power that is needed to propel the ship at the required speed, this includes all losses in the drivetrain, such as gearbox losses. For Concept 3, the power of the ICE is equal to the shaft power. For each concept, the state of charge (SoC) at the beginning of the day is 95%. This is done to account for capacity loss during the lifetime of the battery. 95% is taken as the average battery capacity between 0% loss and 10% loss. Also, each battery is discharged up to a remaining SoC of 10%. In this way, at the EoL of the battery, the battery can be discharged up to 5% SoC.

$$P_{emotor}(t) = \frac{P_{shaft}(t)}{\eta_{EM}} \tag{4.4}$$

4-2-1 Concept 1 - Fuel cell

Based on the results of Appendix B-3, it is chosen to let the fuel cell operate at steady-state. The battery is used to supply the fluctuating power demand, and the fuel cell delivers the average power. The power from or to the battery is calculated by subtracting the power supplied by the fuel cell from the required power by the electric motor. When little power is required, the fuel cell charges the battery, $P_B(t)<0$, the battery is discharged when $P_B(t)$ is positive. The available power to charge the battery is multiplied by η_B to account for the round trip energy losses from the battery. For simplification, it is assumed that all losses of the battery occur during the charging phase of the battery, in this way the available energy in the battery for propulsion is the same as the SoC of the battery. This results in the equation to calculate the battery power as follows:

$$P_B(t) = \begin{cases} (P_{emotor}(t) - P_{FC}(t)) * \eta_B, & \text{if } P_{emotor}(t) - P_{FC}(t) < 0. \\ P_{emotor} - P_{FC}(t), & \text{otherwise.} \end{cases} \tag{4.5}$$

The SoC is then calculated by subtracting the energy supplied or taken by the battery during the time step from the SoC of the previous time step.

$$SoC_B(t) = SoC_B(t-1) - P_B(t) * \delta t \tag{4.6}$$

Fuel cell power, $P_{FC}(t)$, is calculated differently for two situations. 1) The situation where enough space in the engine room is available for the required battery capacity needed to let the fuel cell operate at a steady low power. In this way the battery accounts for all load changes, both during transit to the park and during the operation in the park. This peaks-shaving results in a smaller fuel cell size, reducing total cost. Besides the efficiency of the fuel

cell is higher at lower power outputs. 2) The situation when there is not enough engine room space available for the required battery capacity. This is the case when the transit distance is large and the battery capacity to supply the energy needed for the long transit exceeds the maximum engine room area constraint. This will be described in the next section in more detail. $P_{FC_{avg}}$ is the fuel cell power for situation 1). For situation 2) the power during transit is $P_{FC_{transit}}$, and $P_{FC_{avg}}$ corresponds to the fuel cell power between transits.

4-2-2 Concept 2 - Battery - Genset

This concept contains two energy sources, the battery and the genset. When the battery capacity, Q_B is insufficient to supply all the required energy during the day, the genset is used to supply the additional energy so that at the end of the day the battery is discharged up to a SoC of 10%. The onshore charger will be used to charge the battery to 95% again.

Concept 2A - Without offshore charging

First, the situation of Concept 2A is considered where the genset is not used. This allows us to calculate the difference between the total consumed energy and the energy that the battery can supply. The power from the battery is calculated as follows.

$$P_B(t) = P_{emotor}(t) \tag{4.7}$$

The SoC of the battery is calculated with Equation 4.6. When not enough energy is available in the battery there will be a negative SoC (which is not possible in reality). The energy that is needed from the genset to reach a minimum SoC of 10% at the end of the day, is calculated as follows.

$$E_{GS} = Q_b * 0.1 - SoC_B(end) \tag{4.8}$$

The power from the genset is calculated by dividing the needed energy by the time the CTV is in operation, not standby, $t_{operational}$.

$$P_{GS} = \frac{E_{GS}}{t_{operational}} \tag{4.9}$$

The battery power is calculated by subtracting the generated power of the genset from the required electrical power P_{emotor}.

$$P_B(t) = P_{emotor}(t) - P_{GS}(t) \tag{4.10}$$

The SoC of the battery is calculated with the new values for $P_{emotor}(t)$ and $P_{GS}(t)$ using Equation 4.6.

Concept 2B - With offshore charging

For Concept 2B, the power from the battery is calculated as follows.

$$P_B(t) = P_{emotor}(t) - P_{GS}(t) - P_{charger}(t) \tag{4.11}$$

$P_{charger}(t)$ is the power of the offshore charger. When the CTV is on standby, $P_{emotor}(t)$=0, and SoC_B is below 95%, the battery will be charged at a C_{Rate} of 0.5, meaning that the battery will be fully charged from 0 to 100% SoC in 2 hours. The total energy charged depends on how long the CTV is on standby. The resulting power is calculated with the battery capacity, Q_B, as follows:

$$P_{charger}(t) = \begin{cases} C_{rate_{OC}} * Q_B, & \text{if } P_{emotor}(t) = 0. \\ 0, & \text{otherwise.} \end{cases} \tag{4.12}$$

The power from the genset, P_{GS}, is calculated by first calculating $SoC_B(t)$ for the situation when the genset is not used, P_{GS}=0, similarly as is done for the genset of Concept 2A. Only now the SoC of the battery at the first time the CTV is on standby is used. The power that is needed from the genset to reach the first time at which the CTV is on standby with a minimum SoC_B of 10% is calculated as follows.

$$P_{GS} = \frac{Q_b * 0.1 - SoC_B(t = first\ standby\ time)}{t_{transit}} \tag{4.13}$$

Where $t_{transit}$ is the transit time to the park. In contradiction to Concept 2A, the genset is only used during the transit as during operation in the park the genset is not required due to the offshore charger. The genset power during the transit back to port is calculated using the same formula only then with the $SoC_B(t)$ at the end of the day.

4-2-3 Concept 3 - ICE

The ICEs are the only source of energy on board the CTV and therefore supply the entire demand. Therefore, no energy management strategy is needed.

4-3 Component sizing

This section explains how the size of the various concept's components is determined. With the dimensional limitations of the ship and safety constraints considered. For all concepts the size of the electric motor or internal combustion, whichever applies for the specific concept, is matched with the originally installed ICE power on the CTV, 2x588kW. How the size of the other components is determined will be discussed in further sub-sections.

4-3-1 Constraints

Besides, a CTV's operational requirements, such as a minimum amount of deck space for cargo, CTVs also have a minimum speed requirement. In an emergency, CTVs are required to reach the technicians within 30 minutes to rescue or help the technicians on a turbine. Therefore, the CTV is required to have a minimum transit speed. The exact minimum depends on the size of the wind park. In this work, the minimum is set on 10 Kts. Often, this is not an important criteria as the cruise speed of a CTV is generally in the range of 15-25 Kts. With the energy management strategy for Concept 1, the battery supplies power during peaks. In an emergency, there must be enough power available to travel at a minimum speed of 10 Kts, even with empty batteries. Therefore there must be a constraint on the minimum fuel cell size so that there is always enough power available during emergencies. From Figure 4-2 it can be seen that the power needed to travel at 10 Kts is around 180 kW. This does not include the losses from the electric motor. Therefore, 200 kW is set as the minimum power P_{min}. For Concept 2, the battery genset CTV the same principle holds. This constraint does not influence the design for all the other concepts, as already enough power is available. Another safety measurement is the minimum needed fuel capacity. A change in weather conditions or additional operations such as rescue operations can result in more fuel consumption. Therefore, a safety margin of 25% extra available fuel on top of the needed fuel for the operational profile is applied. Besides, a safety margin of 10% is taken on the size of the fuel cell and genset to account for changes in the operational profile and sea conditions.

Furthermore, the maximum available volume for fuel storage on the CTV is assumed as 15 m^3. For Concept 2A and 2B this also includes the battery storage. Besides, the maximum available fuel storage space, all the additional power generating system components must fit inside the engine room. Instead of using the power density of different components in kW/m^3, it is chosen to evaluate the required area. Fuel cells and batteries are often built in high racks, where an ICE would not use all the available height. Therefore, required floor space is used. The engine room dimensions are roughly: L: 7m x W: 2.5 x H: 2.5 for both port side and starboard. However, not all the space is available for power generating system components, as also water pumps, electrical equipment, etc is needed. Besides, space between the components must be available to do maintenance. Therefore, the maximum available floor space for power generating systems is assumed to be a conservative 10 m^2. The maximum weight of the power generating system, fuel, and fuel storage is taken as 20 t. For the concepts with hydrogen fuel, compressed hydrogen storage is used if the volume of the hydrogen storage does not exceed the maximum fuel storage volume. Otherwise cryogenic hydrogen storage is used. An overview of all the applied constraints can be seen in Table 4-2.

4-3-2 Component dimensions and weight

Based on manufacturing specification sheets found online, the estimated floor space and weight per indicated unit size for different components can be seen in Table 4-3. For the

Constraint / Variable	Symbol	Value
Minimum installed power	P_{min}	200 kW
Safety margin on fuel capacity	S_{Fuel}	25%
Safety margin power capacity	S_{Power}	10%
Maximum system weight	m_{max}	20 t
Fuel storage volume	$V_{Fuel_{max}}$	15 m^3
Floor space engine room	$A_{Floorspace_{max}}$	10 m^2
Maximum charge/discharge speed battery	$C_{rate_{max}}$	1
Offshore charge speed	$C_{rate_{OC}}$	0.5
Maximum fuel cell voltage loss	$V_{FC_{EoL}}$	10%
Maximum capacity loss battery	$Q_{B_{loss}}$	10%
Volumetric energy density battery	VED_B	0.13 kWh/l
Volumetric energy density compressed hydrogen storage	VED_{CH_2}	0.5 kWh/l
Volumetric energy density cryogenic hydrogen storage	VED_{LH_2}	1.2 kWh/l
Gravimetric energy density compressed hydrogen storage	GED_{CH_2}	2.3 kWh/kg
Gravimetric energy density cryogenic hydrogen storage	GED_{LH_2}	2.5 kWh/kg

Table 4-2: Variables and constraints used in this work.

floor space of the genset the floor space of the combustion engine and the electric motor are added. All electrical equipment needed such as circuit breakers and converters are included within the switchboard dimension. The total floor space and weight is linearly scaled to the component size e.g. the floor space of a fuel cell of 250 kW would be: 1.25*0.9m^2.

Part	Unit size	Floorspace	Weight	Source
Fuel cell	200 kW	0.9 m^2	900 kg	(Ballard Power Systems, 2022)
Battery	77 kWh	0.35 m^2	440 kg	(Corvus Energy, 2022)
ICE	588 kW	2 m^2	1500 kg	(VOLVO PENTA, 2022)
Electric motor	588 kW	0.5 m^2	230 kg	(Nordelof et al., 2019)
Genset	588 kW	2.5 m^2	1730 kg	ICE + Electric motor
SCR system	PU	1 m^2	500 kg	(YANMAR, 2020) ,estimate
Switchboard	PU	2 m^2	1000 kg	estimate

Table 4-3: Required floor space and weight of power generating system components

4-3-3 Concept 1 - Fuel cell

The installed fuel cell and battery size are based on the engine room space constraint, maximum C_{Rate}, and minimum and maximum SoC. As described earlier in the energy management section of Concept 1, the battery size is increased until the maximum area of the engine room

is exceeded. The way this is modelled can be seen in Figure 4-4. First, initial values for Q_B and $P_{FC_{avg}}$ are taken. Then the battery size is increased until values for Q_B and $P_{FC_{avg}}$ are found which comply with the conditions of the maximum Crate and with a maximum SoC of 95%. This is done by letting the value of $P_{FC_{avg}}$ converge to a value for which the minimum SoC is 10%. If the maximum SoC is larger than 95% the battery is too small and the process is started again with a larger battery capacity. When this first loop does not result in a value for Q_B and $P_{FC_{avg}}$ that comply with the constraints, the initial values for the battery are initiated again, and a similar process is started. Only this time, there is not a fixed fuel cell power during the entire operating profile but a fuel cell power during transit, $P_{FC_{transit}}$, and the fuel cell power between transits, $P_{FC_{avg}}$. For each iteration of $P_{FC_{avg}}$ the transit power is determined. Again, this is iterated until the constraints are met. The installed fuel cell capacity is calculated as follows.

$$P_{FC_{installed}} = max(P_{FC_{transit}} * (1 + S_{Power}), (P_{FC_{avg}} * (1 + S_{Power}), P_{min}) \tag{4.14}$$

The results of Appendix B-5 show that running the fuel cell at a 100% power output is not the most cost-effective method. Therefore, an investigation is performed on the safety factor S_{Power}, to see if a larger installed capacity than the minimum required fuel cell size results in lower cost.

4-3-4 Concept 2 - Battery - Genset

The battery size is based on the available space in both the fuel storage space and the engine room. The volume of the required methanol must be known to calculate the available space for the battery. The volume of methanol is based on the safety factor, S_{Fuel}. Scaling the battery with 25% to meet the requirement of 25% extra energy for safety is impossible due to the constraints on volume and weight. Therefore, the additional fuel is methanol. For Concept 2A the needed methanol is based on 25% of the energy used by the electric motor in kWh, E_{emotor}, and calculated with Equation 4.15.

$$V_{MeOH_{2A}} = \frac{S_{Fuel} * E_{emotor}}{\eta_{GS} * LHV_{MeOH} * \rho_{MeOH}} \tag{4.15}$$

For Concept 2B the methanol storage requirement also includes the needed methanol when offshore charging would not be available, the needed energy from the genset for this situation is calculated based on the electricity supplied by the electric motor with the fuel safety factor included minus the battery capacity. The subtraction of the battery capacity from the energy of the electric motor gives the energy that the offshore charger would normally supply, hence the different calculation method as for concept 2A. The storage volume of methanol for Concept 2B is calculated as in Equation 4.16.

$$V_{MeOH_{2B}} = \frac{((1 + S_{Fuel}) * E_{emotor} - \frac{Q_B}{(1+S_{Fuel})})}{\eta_{GS} * LHV_{MeOH} * \rho_{MeOH}} \tag{4.16}$$

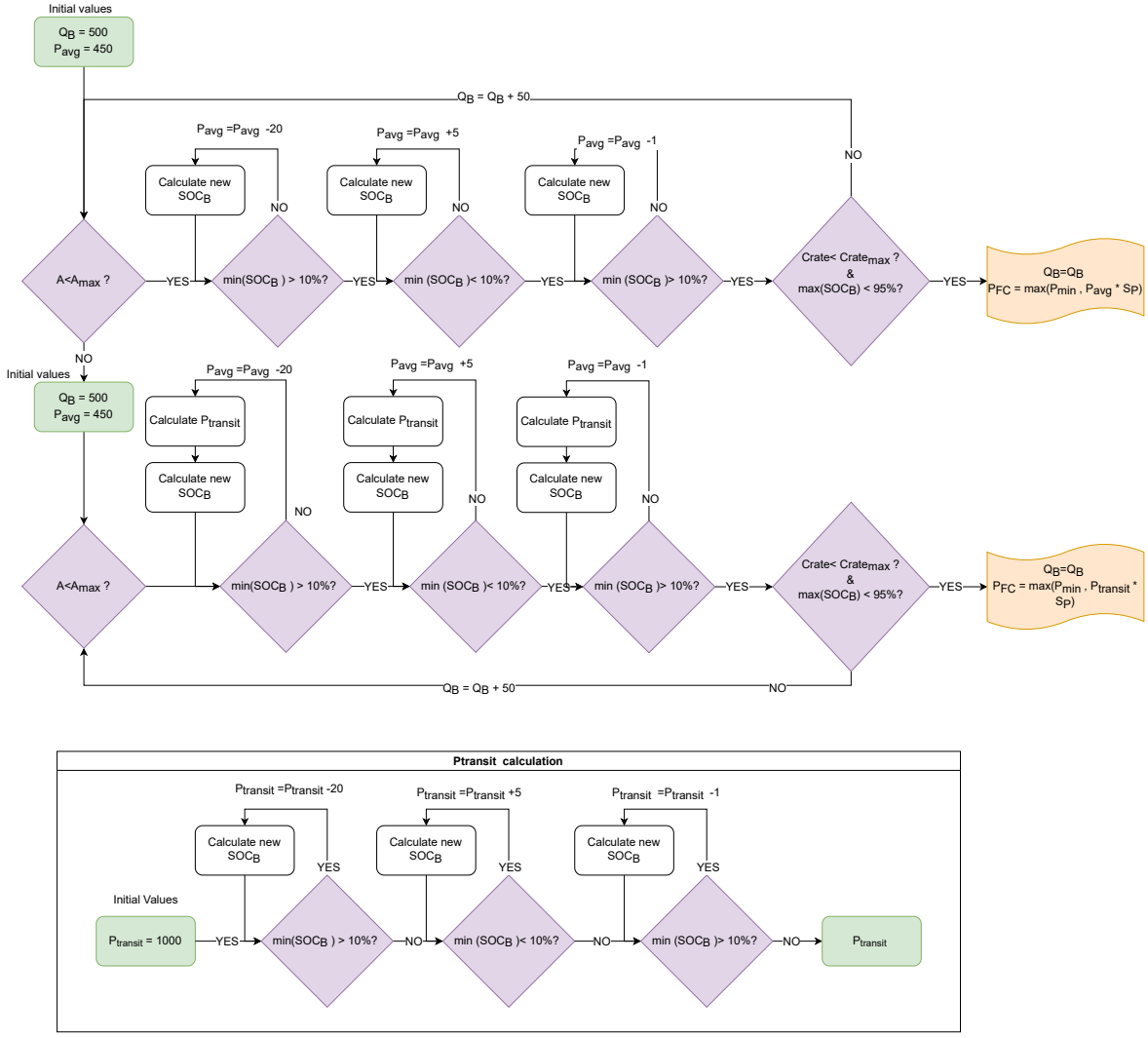

Figure 4-4: Graphical representation of battery and fuel cell size calculation of Concept 1.

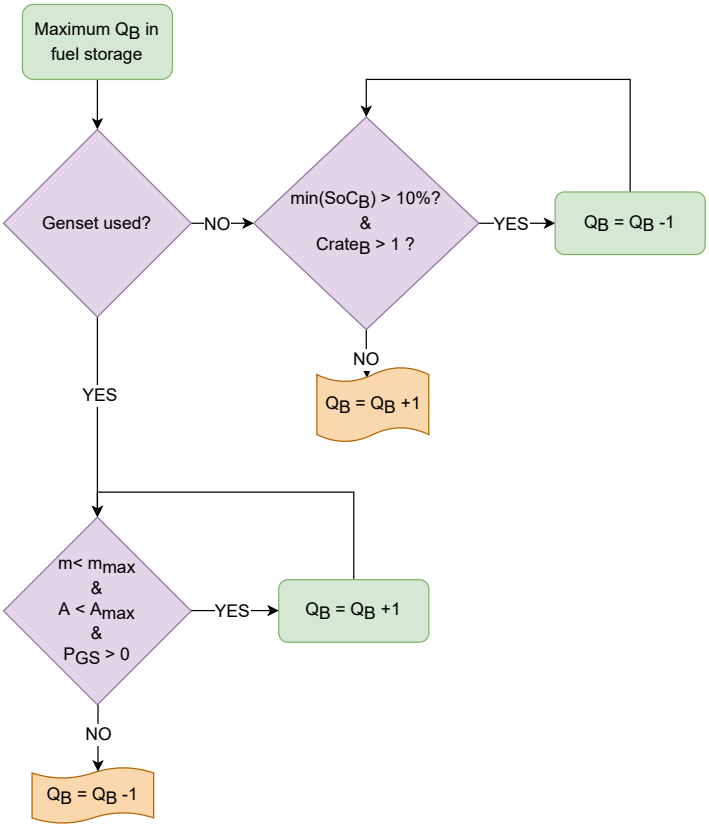

Figure 4-5: Graphical representation of battery size calculation of Concept 2.

The battery capacity of Concept 2A and 2B is calculated differently for two situations. The first situation, when the genset is not used, the battery capacity is sufficient to operate on battery power only. The second, when the battery power is not sufficient to operate on battery power alone and the genset is used. At the start of the calculation, the battery capacity is based on the maximum possible battery capacity that fits in the fuel storage space using Equation 4.17. For the first situation, the battery size is decreased until either the discharge speed constraint, $C_{rate_{max}}$ is met or until the minimum SoC is below 10%. For the second situation, the battery capacity is increased by adding batteries in the engine room until either the weight constraint m_{max}, the engine room area constraint $A_{Floorspace_{max}}$, or until the genset is not used anymore (and thus the battery capacity is sufficient). A graphical representation of both situations can be seen in Figure 4-5.

$$Q_{B_{C2}} = (V_{Fuel_{max}} - V_{MeOH}) * VED_B \tag{4.17}$$

	Symbol	Assumed value
Electric motor efficiency	η_{EM}	92%
Converter efficiency	η_C	98%
Battery efficiency	η_B	90%
ICE efficiency	η_{ICE}	37%
Genset efficiency	η_{GS}	35%

Table 4-4: Assumed efficiencies for different system components

4-3-5 Concept 3 - ICE

The size of the ICEs is based on the originally installed power, two 588 kW ICEs.

4-4 Fuel consumption

In this section, the method of how the fuel consumption is calculated is described for each concept. In general, the efficiencies used for the calculations can be seen in Table 4-4.

The required electrical energy to charge the battery of Concept 1, Concept 2A, and Concept 2B in port is calculated as follows.

$$E_{shore} = \frac{0.95 * Q_B - SoC_B(end\,of\,day)}{\eta_B} \tag{4.18}$$

The charging losses of the charger itself are not taken into account. In the following subsection, the fuel consumption calculations of each concepts are given.

4-4-1 Concept 1 - Fuel cell

The fuel cell efficiency used to calculate the hydrogen consumption can be seen in Figure 4-6, this is the efficiency at beginning of life. At the EoL, the cell voltage will be 10% lower due to degradation. Therefore, the fuel consumption is calculated with an average efficiency over the lifetime, 95% of the original efficiency. Besides, the fuel consumption is multiplied by the converter efficiency, η_C account for losses due to the DC converter losses between the fuel cell and the switchboard. The fuel consumed is calculated with the following function.

$$m_{H_2} = \int \frac{P_{FC}(t)}{0.95 * \eta_C * \eta_{FC}(P_{FC}) * LHV_{H_2}}\, dt \tag{4.19}$$

With m_{H_2} the amount of hydrogen consumed in kg. The fuel cell efficiency $\eta_{FC}(P_{FC})$ as function of the fuel cell power $P_{FC}(t)$ and finally the LHV of hydrogen.

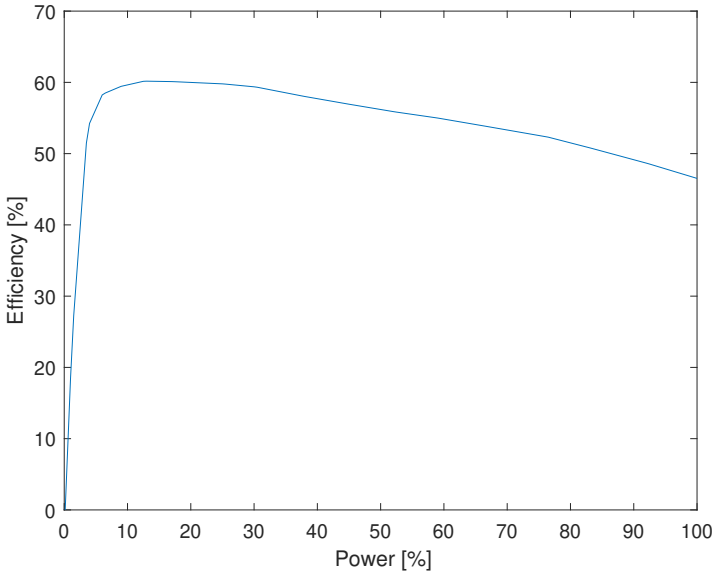

Figure 4-6: Estimated fuel cell system efficiency at beginning of life.

4-4-2 Concept 2 - Battery- Genset

The mass of methanol, MeOH, consumed is calculated using Equation 4.20. With η_{GS}, the thermal efficiency of the genset based on the lower heating value (LHV).

$$m_{MeOH} = \int \frac{P_{GS}(t)}{\eta_{GS} * LHV_{MeOH}} dt \tag{4.20}$$

4-4-3 Concept 3 - ICE

The amount of fuel used is calculated based on the supplied power of the ICE, P_{shaft}, a fixed efficiency, η_{ICE}, and calculated using Equation 4.21, with m_{fuel} and LHV_{fuel} corresponding to either HVO, hydrogen or methanol.

$$m_{fuel} = \int \frac{P_{shaft}(t)}{\eta_{ICE} * LHV_{fuel}} dt \tag{4.21}$$

4-5 Fuel cell lifetime

In this section, the method of how the fuel cell lifetime is calculated is described.

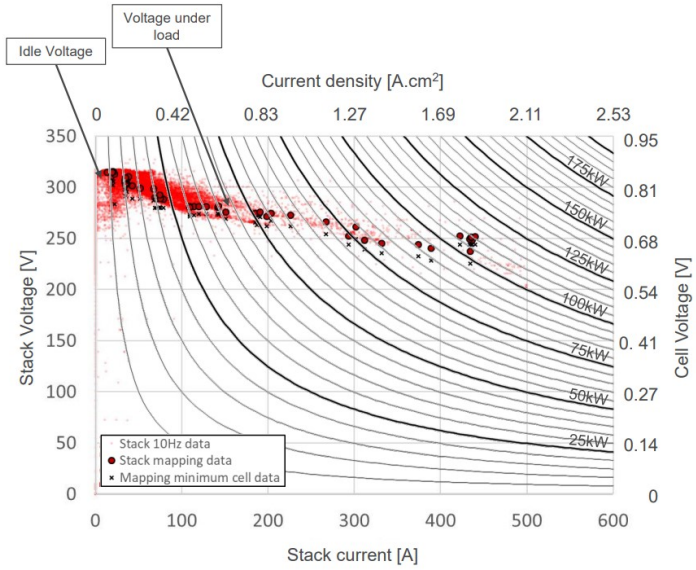

Figure 4-7: Toyota Mirai fuel cell stack voltage measurements (Argon national labratory, 2018).

4-5-1 Fuel Cell Polarisation curve

The polarisation curve is needed to calculate the degradation as a function of the cell voltage. Fuel cells can differ a lot in for example, cell voltage, cell area, and maximum current density. Therefore, it is important to obtain the polarisation curve of a similar fuel cell. The polarisation curve is obtained from a Toyota Mirai fuel cell, a 114kw stack consisting of 370 cells with an area of 237 cm^2. The original measurements can be seen in Figure 4-7. The measurements of Figure 4-7 are approximated to the relationship that can be seen in Figure 4-8, which is used to calculate the voltage dependent degradation.

If one uses the number of cells and the cell area of respectively 370 and 238 cm^2 the voltage over the power output can be calculated. In Figure 4-9 the voltage over the power output can be seen with a power of 100% corresponding to a current density of 2.1 A/cm^2. This voltage-power dependency will later be used to determine the voltage-dependent steady state degradation rate.

4-5-2 Model description

The lifetime of the fuel cell will be calculated based on the potential loss of a single cell. The operational conditions of the CTV will be evaluated based on three different potential losses based on the described degradation mechanisms in Appendix B-2. 1) Potential loss due to steady state operation, $\delta V_{Steady-State}$. 2) Potential loss due to load cycles, $\delta V_{LoadCycle_{day}}$ 3) The potential loss due to start-stop cycles $\delta V_{Start-Stop}$. The ambient conditions are not

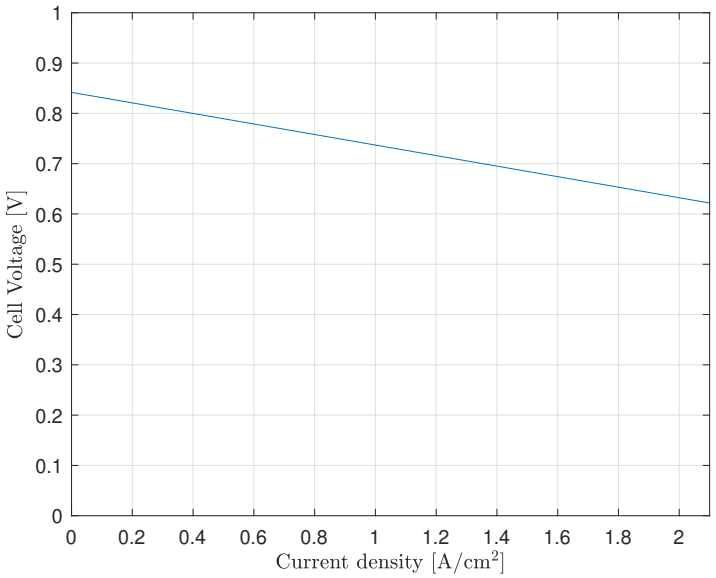

Figure 4-8: Fuel cell Polarisation curve approximation.

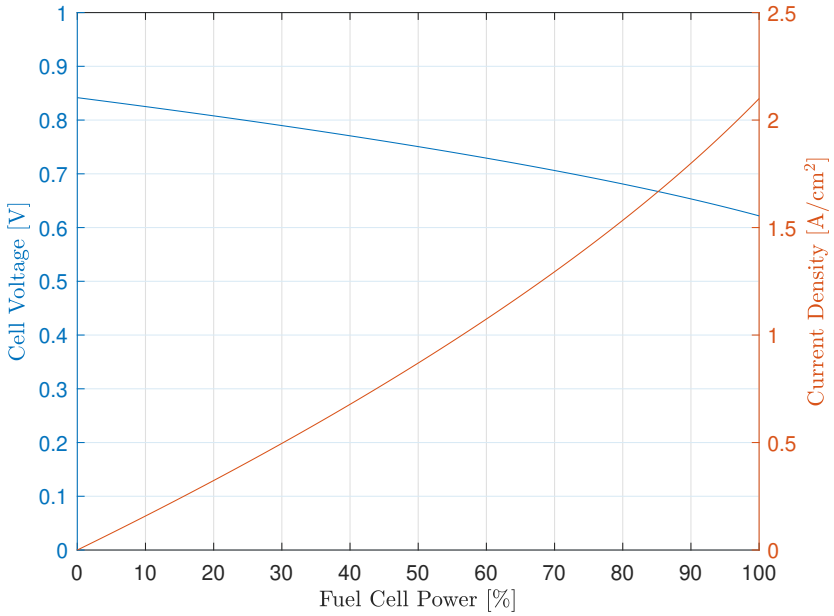

Figure 4-9: Toyota Mirai cell voltage and current density approximation.

taken into account. It is assumed that the impurities in the air and fuel are filtered out or not present and thus does not lead to extra degradation. Second, freezing of the fuel cell is also not taken into consideration. The total degradation is then calculated by adding the individual contributors from one day of operation of the CTV as follows.

$$V_{loss_{day}} = \delta V_{SteadyState_{day}} + \delta V_{LoadCycle_{day}} + \delta V_{Start-Stop_{day}} \tag{4.22}$$

The lifetime of the fuel cell can then be calculated from the maximum potential loss from the EoL condition. A 10% performance loss is used as the EoL condition, at a potential of 0.7 V this corresponds to a maximum potential loss of 0.07V, this is taken as the value for δV_{EoL}. The fuel cell lifetime in days, L_{FC}, is then calculated as follows:

$$L_{FC} = \frac{\delta V_{EoL}}{V_{loss_{day}}} \tag{4.23}$$

In the next sub-sections, the method of how the individual contributors are calculated is described. In Appendix C an in-depth investigation is performed on fuel cell degradation rates, the resulting values are used in the next subsections.

Steady-State

As described in Appendix B-2, degradation from the idling, the ECSA loss and the membrane degradation are likely voltage-dependent. This can also be seen by the loss of ECSA due to different potential holds in Figure C-1. The degradation due to the flooding of the fuel cell at high power is not considered. Because in Figure 4-7 there are no additional concentration losses at high power (linear voltage decline versus output power), thus it can be assumed that flooding does not occur as there would be a large decline in voltage due to the limited oxygen supply. This leaves the ECSA loss and chemical membrane degradation as the main influencing factors, which are mostly voltage dependent. Therefore, the degradation due to steady-state operation is calculated as a function of the power output of the fuel cell. The degradation rates of the first three experiments of Table C-1 are used as the degradation rate as a function of the fuel cell voltage. The three experiments are performed on the same heavy-duty fuel cell by the same researchers. The degradation as a function of the cell potential can be seen in Figure 4-10, where the degradation rate is linearly interpolated/extrapolated between/outside the experimental data points.

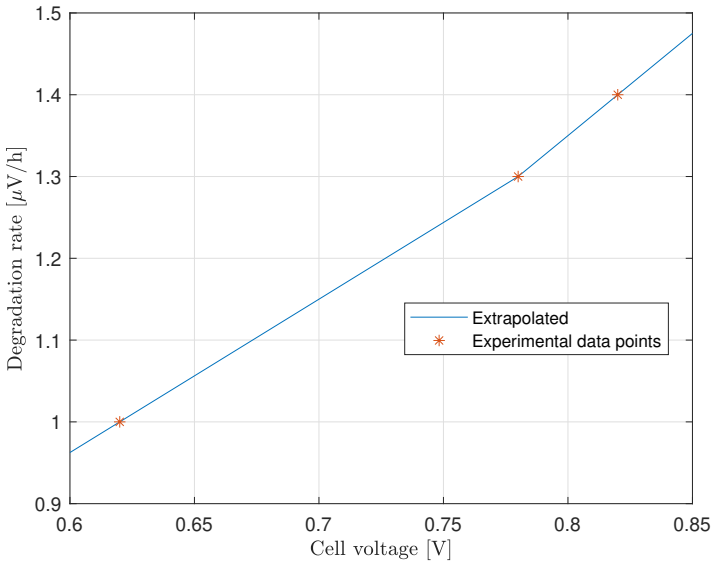

Figure 4-10: Extrapolated degradation rate as function of cell voltage based on the degradation rates found in the work of de Bruijn et al. (2008).

With the polarisation curve from Figure 4-8, the degradation rate as a function of the fuel cell power can be calculated. This can be seen in Figure 4-11.

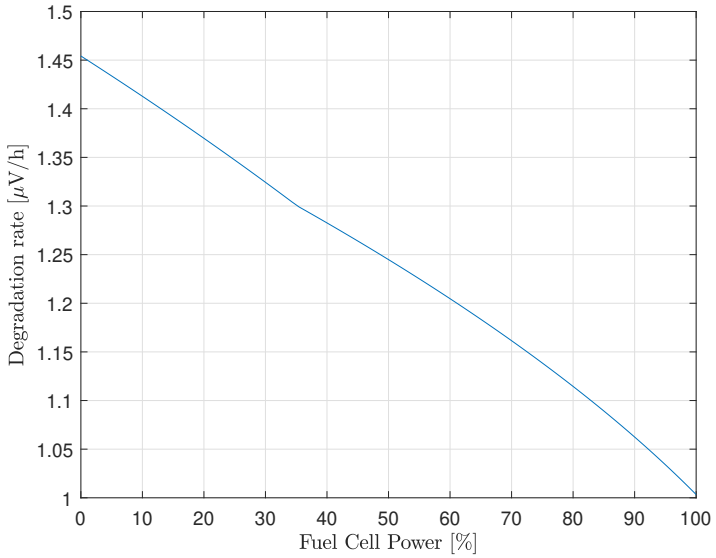

Figure 4-11: Estimated fuel cell degradation rate as function of the fuel cell power.

The steady-state fuel cell degradation is then calculated by using Equation 4.24. With D_{SS}

the degradation rate as a function of the output power of the fuel cell.

$$\delta V_{SteadyState_{day}} = \int D_{SS}(\frac{P_{FC}(t)}{P_{FC_{installed}}})\,dt \tag{4.24}$$

Load cycle

The degradation due to load changes is mostly mitigated due to the combination of fuel cells and batteries. The batteries allow the fuel cell to deliver a steady power demand. Therefore, the fuel cell is not required to perform fast transients as the changes in power demand are powered by the battery. Therefore, little additional ECSA loss due to load changes is expected, as ECSA loss due to load cycles comes mostly from fast transients of the fuel cell (Ren et al., 2020). Therefore, it is assumed that most of the degradation due to the load cycles that are still present originates from membrane degradation. Within membrane degradation, the chemical degradation of the membrane is already accounted for in the steady state degradation rate. The mechanical stresses due to the swelling of the membrane due to the change of humidity in the fuel cell is however not accounted for in the steady state degradation rate. The mechanical stress due to the expansion and contraction cycles can be seen as fatigue stress. For fatigue loading, small individual stress cycles are equal to the combined large stress cycle with the combined amplitude of the smaller stress cycles. This principle will be applied to the membrane degradation due to mechanical stress. The daily degradation is then calculated as the degradation due to one complete load cycle, $\delta V_{LoadCycle}$ multiplied by the equivalent number of full load cycles. With $\delta V_{LoadCycle}$ taken as 1 μV. The number of full load cycles n_1 is calculated with the rainflow counting algorithm of Matlab R2019b. The algorithm is applied on the fuel cell power $P_{FC}(t)$ divided by $P_{FC_{installed}}$. The algorithm outputs a matrix with the corresponding amplitudes of the cycles and a corresponding value of either 0.5 for half cycles and 1 for complete cycles (up and down). Multiplying the amplitude of the cycle with 1 for complete cycles and the half cycles with 0.5 gives the total fluctuation of power in equivalent full load cycles of the fuel cell. Finally, the number of start-stop cycles is subtracted because the load fluctuation during the start-up and shutdown phase is already accounted for in the start-stop degradation. The degradation due to start-stop cycling is calculated with n_2 taken as 1, as there is only one start-stop cycle each day, as follows.

$$\delta V_{LoadCycle_{day}} = \delta V_{LoadCycle} * n_1 \tag{4.25}$$

Start-stop

The degradation due to start-stop cycles is calculated by Equation 4.26, with n_2 the number of daily start-stop cycles. $V_{LoadCycle}$ is taken as 14 μV from the work of Pei et al. (2008).

$$\delta V_{start-stop_{day}} = \delta V_{start-stop} * n_2 \tag{4.26}$$

4-6 Battery lifetime

The capacity fade of the battery due to charging and discharging is described in this section. The charge/discharge profile of the battery differs from a normal charge-discharge profile. For example, the battery of an EV discharges during the drive and is charged again after the drive. However, the battery from, for example, Concept 1 has many small charge and discharge cycles. Therefore, a degradation model based on complete cycles is not suitable. The model used in this research is a model based on the Ampere-hour throughput. In this way, the battery degradation is not dependent on the DoD. This makes it possible to apply the model to the SoC profile of the battery of this research. The battery degradation is simulated based on a capacity fade model from J. Wang et al. (2011). In this model, the capacity fade of the LFP battery is described as a function of current throughput based on experimental results from different ageing experiments. Results showed little dependence of lifetime on DoD for low C-rates, which is in line with the experimental results of Preger et al. (2020). The general lifetime equation for the battery capacity loss Q_{loss}, in percentage, is as follows.

$$Q_{loss} = B * exp(\frac{-31.700 + 370.3 * C_{Rate}}{RT})(Ah)^{0.55} \tag{4.27}$$

With dimensionless variable B, T; the temperature in Kelvin, R; the gas constant, Ah; the current throughput of a single cell. As the discharge speed or C_{Rate} of the different concepts is below 1 C, with a mean below 0.5 C the capacity fade model for a C_{Rate} of 0,5 C is used, as there was no experimental data available for a lower C_{Rate}. The capacity loss model at 0.5 C is then given as follows.

$$Q_{loss} = 30330 * exp(\frac{-31.500}{RT})(Ah)^{0.552} \tag{4.28}$$

For cycles with a distinctive charge and discharge cycle, the current throughput, Ah, can be calculated using Equation 4.29.

$$Ah = n_{cycle} * DoD * q_{cell} \tag{4.29}$$

To calculate the current throughput from the SoC profile of the battery from this research the SoC profile of the entire battery that is expressed in kWh must be converted to Ah throughput of a single cell. The number of cells in the battery back must be calculated. This is done via Equation 4.31. With Q_B the rated battery capacity in kWh, V_{nom} the nominal cell voltage of a single battery cell, and q_{cell} the capacity of a single cell in Ah.

$$n_{cell} = \frac{Q_B[kWh]}{q_{cell} * V_{nom}} \tag{4.30}$$

To determine the current throughput for a single cell for one day of operation, all the individual charge/discharge cycles during a day of operation must be added. This is done with a rain flow counting algorithm of Matlab R2019b. The rainflow counting algorithm is used to calculate the amplitude of every small charge and discharge cycle and all the individual cycles can be

added which results in the total energy throughput, $E_{battery}$ in kWh. This energy throughput is then converted to the current throughput of a single battery cell in Ah, this is done using equation 4.31.

$$Ah_{cycle} = \frac{E_{battery}}{n_{cell} * V_{nom}} \tag{4.31}$$

The total current throughput is then calculated using the following equation:

$$Ah = Ah_{cycle} * n_{cycle} \tag{4.32}$$

The lifetime of the battery system is then calculated with the number of cycles, n_{days}, it takes to reach the EoL criteria, a residual capacity of 90% of the original battery capacity.

4-7 ICE /Genset lifetime

The lifetime of the ICE is taken as 9000h based on operational experience from Siemens Gamesa. The same lifetime is considered for the genset. The lifetime of the ICE and genset, L_{ICE} and L_{GS}, is days, is calculated by dividing the lifetime in hours by the total time the ICE or genset is turned on.

4-8 Cost Calculation

This section describes how the costs are calculated for each concept. The costs are based on 10 years of operation with 330 days of operation each year. The costs that are included are fuel cost, cost of the power generating system, hydrogen storage, and cost of the charger.

4-8-1 CAPEX

Component	Symbol	Value	Unit	Source
Lithium-ion Battery	C_B	500	€/kWh	(TNO, 2019b)
PEM Fuel cell	C_{FC}	1500	€/kW	estimate
ICE (MGO,HVO)	$C_{ICE_{HVO/MGO}}$	120	€/kW	Siemens Gamesa
ICE (H_2, Methanol)	$C_{ICE_{H_2/MeOH}}$	180	€/kW	estimate
Genset	C_{GS}	240	€/kW	estimate
Hydrogen storage	C_{SH_2}	1000	€/kg	(TNO, 2019b)
Electric motor and switchboard	C_{EM}	580	€/kW	(TNO, 2019a)
SCR system	C_{SCR}	50	€/kW	(IACCSEA, 2013)

Table 4-5: CAPEX of different power generating system components

The CAPEX is based on the major system parts and replacements during 10 years. No replacements are assumed for the components other than the ICE, genset, battery or fuel cell. The values of Table 4-5 are used in the next sections. The cost of an ICE running on hydrogen or methanol is expected to be higher compared to the ICE made for diesel due to immature technology, costs are assumed to be 50% higher. The genset is also expected to be more expensive due to the additional electric machine and electronics, the cost is estimated to be twice as high as an ICE. The cost of the fuel cell, battery, ICE, and genset is calculated based on the lifetime of the component. The total cost due to replacements is calculated by dividing the days of operation by the component's lifetime multiplied by component cost with a minimum of one, as seen in Equation 4.33. The actual costs due to replacements will be higher during the 10-year period as the cost is calculated based on a fraction rather than multiplying the number of replacements by the cost. However, this would not result in a fair comparison, there could be a large part of residual lifetime available when a replacement would be required near the end of the 10 year period. The storage cost is only included for hydrogen as the expected cost for storage of the other fuels is expected to be negligible. The storage cost are based on compressed hydrogen storage, although the cost is lower for cryogenic hydrogen storage (cryoworld, 2021), it is expected that this advantage is reduced due to the required additional equipment, such as a vaporiser to bring the liquid hydrogen into the gaseous state again. The CAPEX of a specific concept is then calculated by adding the CAPEX contributions of all the components of the concept.

$$CAPEX_{FC} = P_{FC_{installed}} * C_{FC} * max(1, \frac{n_{days}}{L_{FC}}) \tag{4.33a}$$

$$CAPEX_{B} = Q_{B} * C_{B} * max(1, \frac{n_{days}}{L_{B}}) \tag{4.33b}$$

$$CAPEX_{ICE} = 2 * 588 * C_{ICE} * max(1, \frac{n_{days}}{L_{ICE}}) \tag{4.33c}$$

$$CAPEX_{GS} = C_{GS} * P_{GS_{installed}} * max(1, \frac{n_{days}}{L_{GS}}) + C_{SCR} * P_{GS_{installed}} \tag{4.33d}$$

$$CAPEX_{EM} = 2 * 588 * C_{EM} \tag{4.33e}$$

$$CAPEX_{Storage} = m_{H_2} * (1 + S_{Fuel}) * C_{SH_2} \tag{4.33f}$$

4-8-2 Charger

The cost of the bunkering installation is not considered as these costs are included in the fuel price. The cost of the charger is included as this is not part of the electricity price, and charging times are long, therefore a charger specifically for the CTV is required. The cost of the charger needed to charge the battery electric vessel onshore is obtained from an EV supercharger cost evaluation. Nicholas (2019) reports a cost of roughly €190k for equipment and installation of a 350kW charger in California. However, marine equipment is generally more expensive. In the TCO a total cost of €200k is assumed for Concept 2 and €100k

is assumed for the charger of Concept 1 as the battery of Concept 1 is smaller compared to the battery of Concept 2 and therefore needs less charging power. Charging the batteries offshore comes with a lot more challenges; a buoy with all the electrical equipment needs to be installed offshore, the power must be drawn from the high voltage grid and a connection from the CTV to the buoy must be made, etc. Therefore the cost of the charging infrastructure is expected to be much higher compared to the onshore counterpart. It is difficult to get a correct estimate of the cost, a cost of 1 million euros is assumed during the 10-year time span.

4-8-3 OPEX

Fuel	Price	Unit	Source
Electricity	0.1	€/kWh	(StatLine, 2022)
Hydrogen	6	€/kg	(SMART PORT, 2020)*
HVO	2.1	€/kg	(FullTank, 2022)
Methanol	1.45	€/kg	(SMART PORT, 2020)*
MGO	1.1	€/kg	(BICX, 2022)
OPEX SCR	3	€/MWh	(IACCSEA, 2013)

Table 4-6: Fuel prices used for cost calculations. *With adjusted electricity price to 0.1€/kWh

In Table 4-6 the used fuel prices are displayed. Hydrogen and methanol prices are based on the cost reported in the SMART Port report (2020). The price used for electricity in the report is 50€/MWh, whereas the electricity cost in this research is taken as 100€/MWh. According to the authors, electricity is the main share of the hydrogen production costs, therefore the cost of hydrogen is doubled to account for the higher electricity price. This results in approximately €5/kg for hydrogen and €1.45/kg for methanol. No transportation costs are assumed as the hydrogen production facilities will likely be around ports. For hydrogen, €1/kg is added for fuel station cost and the cost of compression or liquefaction. For the other fuels, the cost of the fuel station is neglected due to the low cost: €4/t for methanol and €7/t for diesel (SMART PORT, 2020). The operating cost of the SCR consists of catalyst replacements and urea costs. Based on the cost analysis of the IACCSEA a value of 3€/MWh produced by the ICE is used (IACCSEA, 2013).

$$OPEX_{Fuel} = m_{fuel} * n_{days} * C_{fuel} \tag{4.34a}$$

$$OPEX_{SCR} = E_{ICE} * 0.003 \tag{4.34b}$$

4-8-4 TCO

The TCO of each concept is then simply calculated using Equation 4.35.

$$TCO = CAPEX + OPEX + C_{Charger} \tag{4.35}$$

4-9 GHG emissions

The GHG emissions of the concepts are based on GHG emissions from the fuel and GHG emissions of the production of the power generating system components. For the fuel emissions, two phases are considered. First, the well to tank (WTT) emissions are the GHGs emitted during fuel production. This typically includes the extraction of raw materials, fuel production, fuel compression for storage, and fuel transport. However, it is a challenge to obtain the correct values for the emissions during the transportation phase as life-cycle assessment studies from literature investigate different locations. Therefore transportation emissions are not included. Next are the tank to wake (TTW) emissions, the emissions from fuel combustion. The combined WTT and TTW emissions are the well to wake (WTW) emissions. Both WTT and TTW in CO_2 equivalent are based on a kWh of fuel. The reported values found online and in articles are often described in different units, e.g. in g CO_2-eq/kg fuel, to transfer this to g CO_2-eq/kWh of fuel, the fuel properties of Table 2-1 are used. For the TTW emissions of fuels which capture and utilise CO_2 during the production phase of the fuel, the CO_2 emissions are not included as due to the capture of CO_2 during production the CO_2 emissions are net-zero. The emissions originating from the fuel can be seen in Table 4-7. The GHG emissions from the component production are based on the values from Table 4-8. Appendix E shows how these values are obtained. The total GHG emissions of a particular system is calculated with Equation 4.37, with the minimum GHG emission of one system if the lifetime is longer than 10 years. Equation 4.36 is used to calculate the fuel GHG emissions.

	WTT	**TTW**	**WTW**
MGO	51	270	321
HVO	39	4.5	43.5
Wind energy	12	0	12
Hydrogen	32	0	32
Methanol	49	3.9	52.9

Table 4-7: Overview of WTT, TTW, and WTW of different fuels in g Co2-eq per kWh of fuel.

$$GHG_{Fuel} = m_{Fuel} * n_{days} * WTW_{Fuel} \tag{4.36}$$

$$GHG_{system} = Size_{component} * GHG_{Component} * max(1, \frac{n_{days}}{L_{component}}) \tag{4.37}$$

Component	Unit	GHG	Source
ICE	kW	42	(Simons and Azimov, 2021)
Fuel cell	kW	45	(Simons and Azimov, 2021)
Lithium-ion battery	kWh	114	(Simons and Azimov, 2021)
PMSM	kW	5	(Nordelof et al., 2019)
Genset	kW	47	(Simons and Azimov, 2021, Nordelof et al., 2019)
Compressed hydrogen	kg	368	(Elgowainy et al., 2012)
Cryogenic hydrogen	kg	200*	(Elgowainy et al., 2012)

Table 4-8: GHG emissions of different power generating system components in kg CO_2-eq per indicated unit. *Estimated based on the values for cryogenic compressed hydrogen storage

4-10 Parameter investigation

A parameter investigation is performed to see the influence of several assumed parameters. For the analysed parameter, a range of values will be taken in order to see how a deviation from the original value will change the outcome of the comparison. A study will be performed on the prices of hydrogen, HVO, MGO, methanol, and electricity. Besides, the fuel cell and battery prices and lifetimes are varied. The results will be shown in the results section.

4-11 Overview and assumptions

Table 4-9 shows an overview of what is included and what is not included in this study.

	Weight	Lifetime	GHG	TCO
ICE	✓	✓	✓	✓
Fuel cell	✓	✓	✓	✓
Lithium-ion battery	✓	✓	✓	✓
Genset	✓	✓	✓	✓
SCR system	✓	✗	✗	✓
Electric motor	✓	✗	✓	✓
Electronics	✓	✗	✗	✓
Hydrogen storage	✓	✗	✓	✓
MGO/HVO/MeOH storage	✗	✗	✗	✗
Charger	N/A	✗	✗	✓
Maintenance	N/A	N/A	✗	✗
Installation	N/A	N/A	N/A	✗

Table 4-9: Overview of what is included in this study

The most critical assumptions made in this work are:

- The power speed relationship of a 26m CTV is scaled to the CTV of this work.
- Approximated load profile.
- Fuel cell degradation rates originate from multiple studies.
- No fuel cell degradation from impurities, ambient conditions, and vessel motions.
- Battery capacity fade at fixed C_{rate} of 0.5C.
- No efficiency or size distinction is made between ICEs for different fuels.
- Efficiencies of the components are based on the assumed values of Table 4-4.
- All electric storage losses of the battery are taking place during charging.
- Minimum continuous speed requirement for safety: 10 Kts.
- 10-year lifetime is assumed for components besides ICE, genset, battery, and fuel cells.
- 100% availability of power from the offshore charger.
- Cost of the offshore charger of €1 million.
- No transportation costs of fuels.
- Price cryogenic hydrogen storage based on compressed hydrogen storage.
- ICE and genset prices for different fuels estimated based on regular diesel ICE.

4-12 Verification and validation

In this section, the methods used to verify and validate the results of this work are described.

4-12-1 Verification

Multiple checks are performed to verify the calculations performed by the model. First, an energy balance check is performed, meaning that the total consumed energy is compared to the total supplied energy. For Concept 1, Concept 2A and 2B this is done using Equation 4.39. With $E_{B_{loss}}$ the energy loss of the battery during operation. $E_{charger}$, the energy from the charger, which is also multiplied by the battery efficiency, to calculate the part of the energy that can be used. This check cannot and do not need to be performed for Concept 3A, 3B, and 3C, as only an ICE is present and the used fuel is directly calculated from the power.

$$E_{error} = sum(P_{emotor}(t)) + E_{B_{loss}} - sum(P_B(t)) - sum(P_{FC}(t)) - sum(P_{GS}(t)) - E_{charger} * \eta_B \tag{4.38}$$

Furthermore, a power check is performed, meaning that the power supplied at each time step of the calculation is the same as the used power.

$$P_{error} = P_{emotor}(t) - P_B(t) - P_{FC}(t) - P_{GS}(t)) - P_{charger} * \eta_B \tag{4.39}$$

The maximum allowable error was set on 1 kWh for E_{error} and 0.1 kW for P_{error}, which were not exceeded during the calculations.

Next, the model's outcome with a simplified load profile is compared with manual calculations. This profile consists of two one-hour-transits at 1000 kW separated by one-hour standby. If possible, the energy and component sizes are calculated manually beforehand and compared to the outcome of the model. If it is impossible to easily calculate the component size by hand beforehand, the results of the model are checked afterwards. In Appendix D, the calculations can be seen. From these calculations, it can be concluded that the outcome of the model is in line with the manual calculations for this profile, Indicating that the model correctly calculates the component sizes and fuel consumption for the given profile.

4-12-2 Validation

The fuel consumption of a day of operation is compared to a mimicked operational profile, to validate if the load profile approximates real-life operation. The example day had an average transit duration of 11 min, average transfer of 5 min, and 12 transfers. A total of 386 kg of HVO was consumed. The model of this research predicts a fuel consumption of 397 kg HVO. Which is similar, although there is a large chance that this is luck, as a lot of additional variables influence the model. The chance that the model can predict a day of operation with the same accuracy as obtained in this example is small. However, it indicates that the results of the model are in the same ballpark.

5

Results

In this chapter, the results of the comparison of the concepts will be given and discussed, divided into five sections. First, a section about the constraints, as some concepts exceed the available space on the CTV. Afterwards, a section about the TCO of the different concepts for multiple transit distances. Next, GHG emissions of the different concepts will be discussed. Afterwards, a section of the results of the fuel cell and battery lifetime calculations. Finally, the results of the parameter investigation. As a reminder, an overview of the concepts is given in Table 5-1.

		Fuel	System parts	Specialty
Concept 1		Hydrogen & electricity	Fuel cell & battery	
Concept 2	A	Electricity & methanol	Battery & genset	
	B	Electricity & methanol	Battery & genset	Offshore charging
Concept 3	A	HVO	ICE	
	B	Hydrogen	ICE	
	C	Methanol	ICE	

Table 5-1: Overview of the evaluated concepts.

5-1 Fuel Volume, Area, Weight

In Table 5-2 an overview of the used area by the power generating systems in the engine room is given, the total weight of the fuel and power generating system, and the occupied volume by the fuel and or battery system. It can be seen that for a transit distance of 75 km, the required volume for the hydrogen storage of Concept 3B exceeds the maximum volume, $V_{Fuel_{max}}$, of 15 m^2. **The hydrogen storage exceeds the available storage space upwards a transit distance of 68 km for concept 3A and upwards a distance of 92 km for fuel cell Concept 1**,this can be seen in Table F-1 in Appendix F. Besides, in this table the hydrogen storage method, compressed or cryogenic, can be seen for all transit distances. Furthermore, Table 5-2 shows that for Concept 1 the engine room space is a restricting constraint. For

Concept 2A and 2B, the weight of the battery system limits the maximum battery capacity. The weight of 19994 kg is not equal to the m_{max} of 20000 kg due to the size of the increments in the battery sizing method.

	5 km			**25 km**			**50 km**			**75 km**		
	Area [m^2]	Weight [kg]	Fuel vol. [m^3]	Area [m^2]	Weight [kg]	Fuel vol. [m^3]	Area [m^2]	Weight [kg]	Fuel vol. [m^3]	Area [m^2]	Weight [kg]	Fuel vol. [m^3]
Concept 1	8.3	10147	5.6	8.1	11574	14.0	10.0	14559	8.6	10.0	16249	12.7
Concept 2A	6.4	17046	15.0	8.4	19994	15.0	9.0	19994	15.0	9.5	19994	15.0
Concept 2B	4.9	10542	8.5	4.9	12447	11.3	7.1	17699	14.9	8.9	19973	14.8
Concept 3A	6.0	7645	0.6	6.0	8344	1.0	6.0	9219	1.5	6.0	10093	2.0
Concept 3B	6.0	9111	11.8	6.0	10481	8.1	6.0	12414	12.2	6.0	14348	16.2
Concept 3C	6.0	7645	1.4	6.0	8344	2.2	6.0	9219	3.3	6.0	10093	4.4

Table 5-2: Overview of the occupied, area in the engine room, weight, and fuel volume of the different concepts.

5-2 TCO

In Figure 5-1, the TCO for the different concepts can be seen for transit distances between 5 km and 100 km. First, there are substantial differences in cost between the various concepts. For a transit distance of 60 km, the TCO of Concept 3C is 86% higher than the TCO of Concept 2B. Besides, all concepts are not yet cost-competitive compared to the benchmark CTV running on MGO, with a difference of at least €1.1 million between the concepts and the benchmark.

Fuel cell Concept 1 is only cost-competitive at a transit distance of 5 km compared to the other concepts, excluding concept 2A. The biggest difference in TCO between concept 1 and concept 3B is about €1 million. This indicates that hydrogen fuel cell technology is still more expensive compared to hydrogen combustion engines.

Concept 2A, the battery-powered CTV without offshore charging, has the lowest TCO up to a transit distance of 18 km. The all-electric range of Concept 2A lies at a transit distance of 12 km to the wind farm. Afterwards, methanol is used to extend the range, increasing the TCO substantially. If the option of offshore charging is unavailable, Concept 2A has the lowest TCO up to 27 km. After 27 km the hydrogen combustion Concept 3C has the lowest TCO.

For almost the entire transit distance range, from 18 km up to 93 km, Concept 2B has the lowest TCO. However, as the fuel volume of concept 3B exceeds the available storage space for this transit distance, this is not a possible solution. Therefore Concept 2B has the lowest TCO up to 97 km afterwards, Concept 3A has the lowest TCO. The all-electric range of Concept 2A is up to a transit distance of 61 km. Afterwards, methanol is used. At the distance of 61 km the largest cost advantage compared to the other concepts can be achieved.

Concept 3A and 3B are similar in cost with a slight increasing advantage for Concept 3B with increasing transit distance. If offshore charging is not an option, these concepts provide the lowest TCO for a transit distance from 28 km onwards. Finally, Concept 3C has the highest cost for almost the entire range.

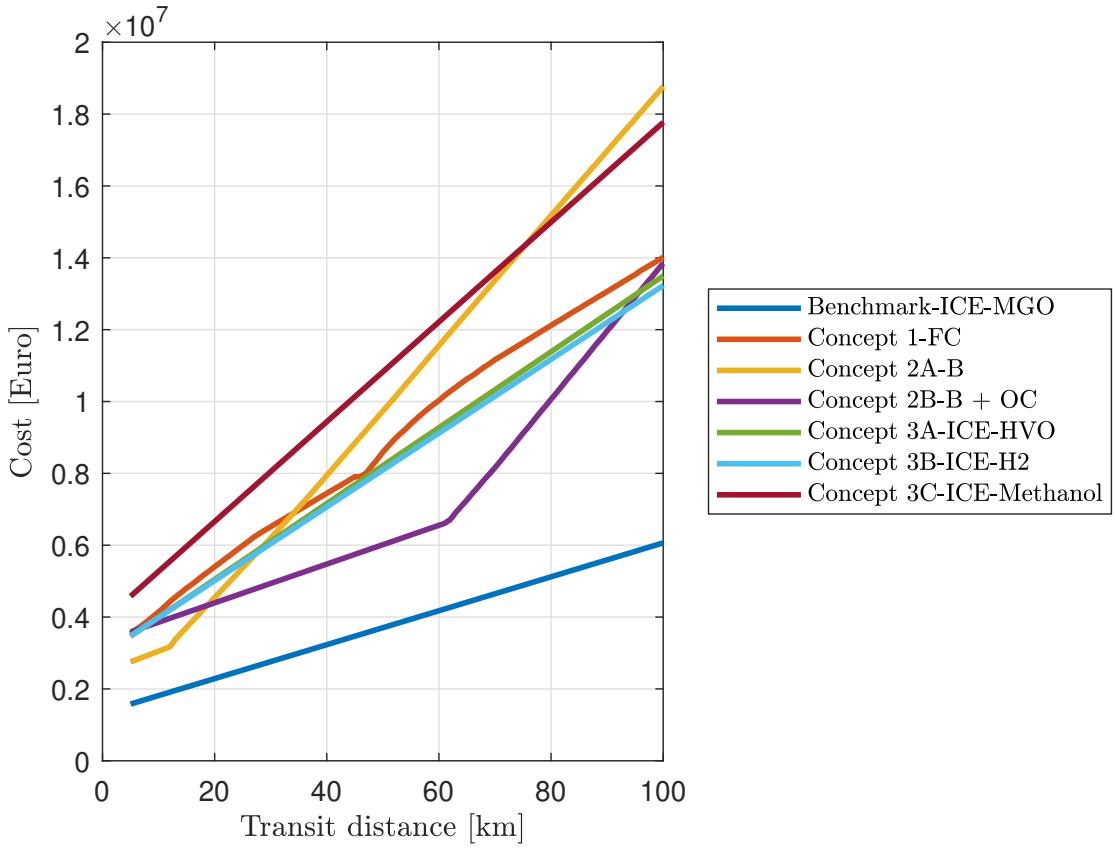

Figure 5-1: 10-year TCO as function of the transit distance to the wind farm.

In Figure 5-2 the TCO elements for each concept are displayed for the transit distances of 5, 25, 50 and 75 km. The cost of the power generating system, the CAPEX, for Concept 1, Concept 2A, and Concept 2B contributes to a significant part of the total cost. For a transit distance of 5 km, the CAPEX contributes to more than half of the total cost in these concepts. As expected, the share of the CAPEX on the TCO reduces with increasing transit distances due to the increasing OPEX, indicating that a component price reduction of fuel cells and batteries will have the largest percentage-wise impact on short transit distances. Also, Offshore charging is only a good investment for longer transit distances. Furthermore, for all the ICE concepts, the CAPEX contributes to only a small part of the total cost.

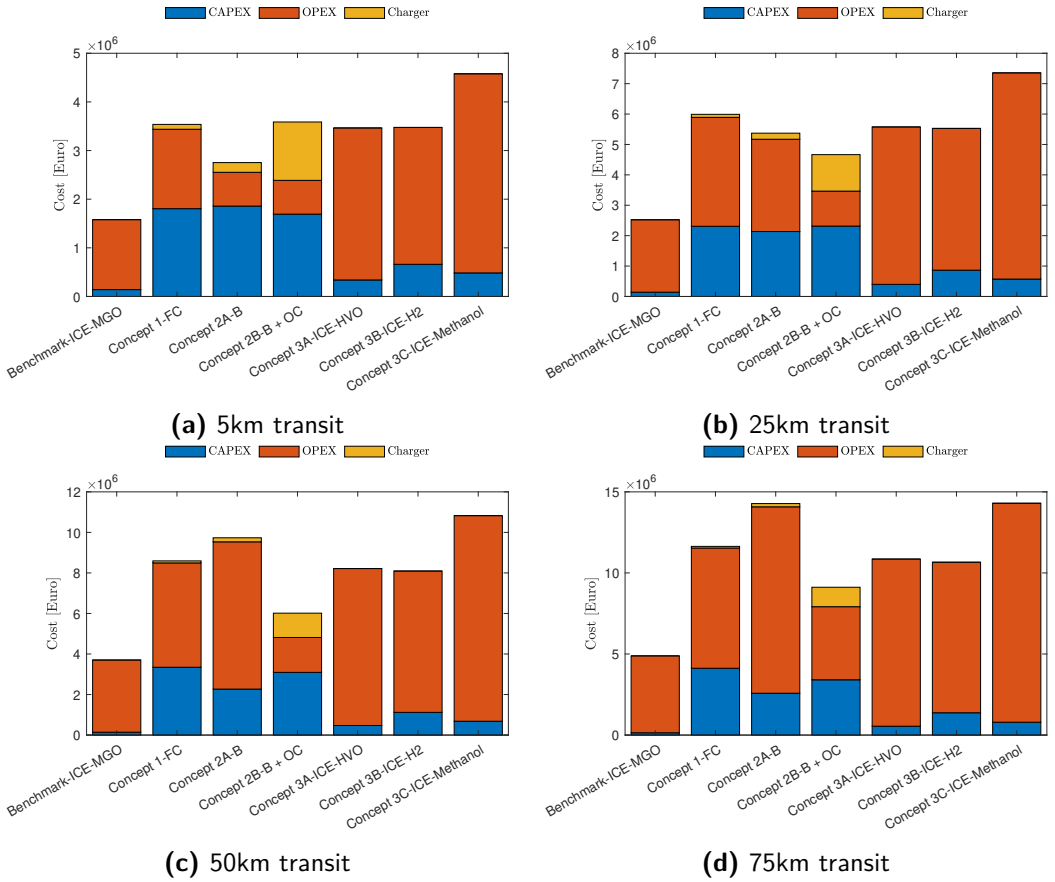

(a) 5km transit **(b)** 25km transit

(c) 50km transit **(d)** 75km transit

Figure 5-2: 10-year TCO for 5 km, 25 km, 50 km, and 75 km transit distances consisting of CAPEX, OPEX, and charger cost.

5-3 GHG emissions

The total GHG emissions of the different concepts are shown next to the benchmark in Figure 5-3. It shows that all considered concepts reduce the emissions by at least 80% compared to the MGO benchmark. The highest reduction is 94% for concept 2B up to transit distances of 62 km.

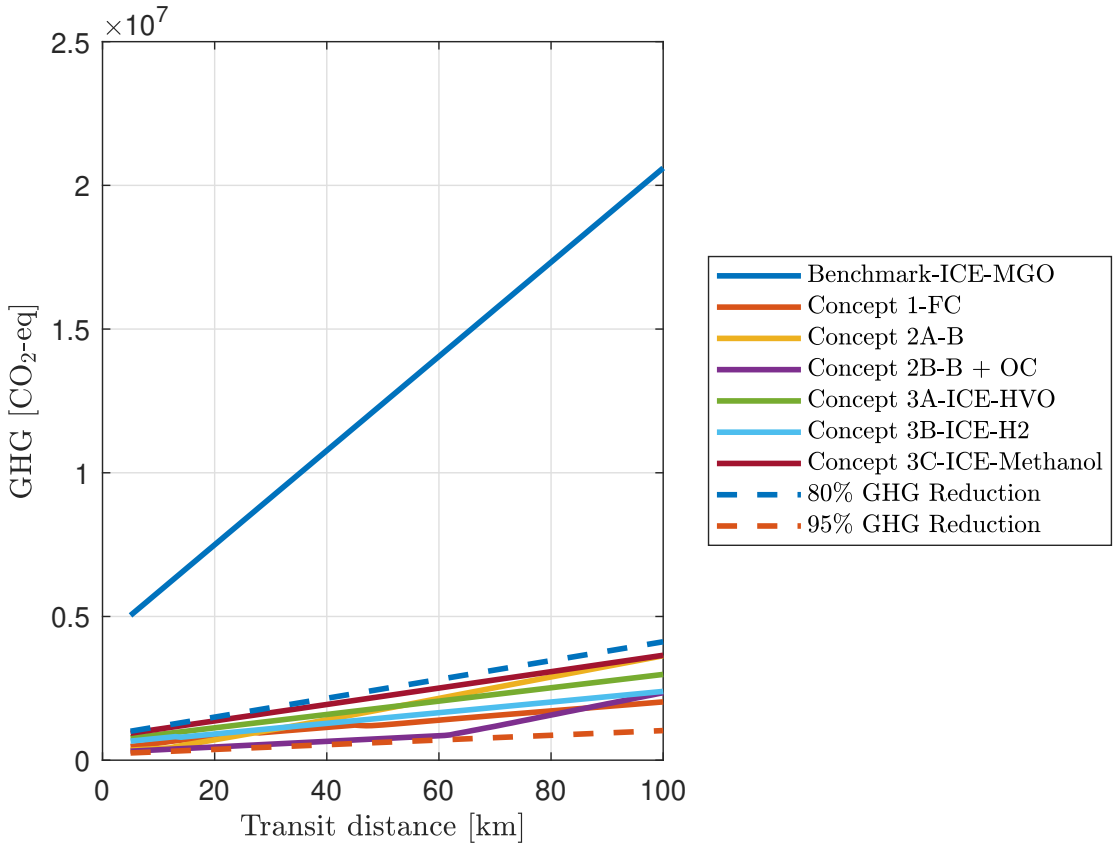

Figure 5-3: Total GHG emissions over a 10-year operating period for transit distances of 5 km up to 100 km.

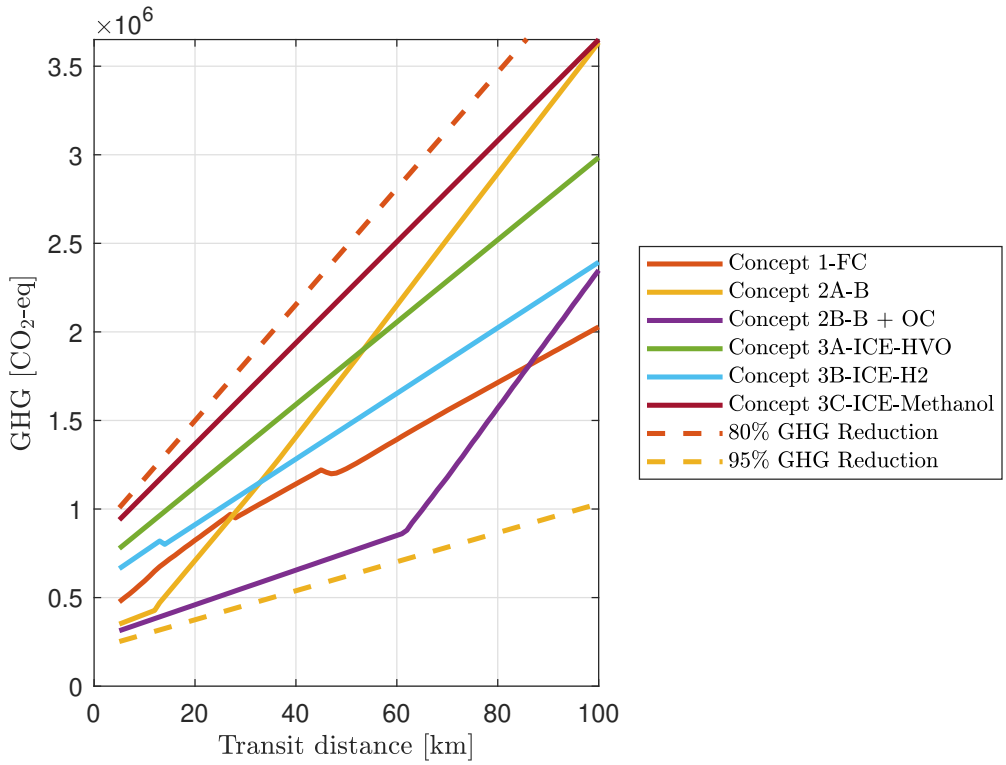

Figure 5-4: 10-year GHG emissions for transit distances of 5 km up to 100 km.

The total GHG emissions of the concepts are displayed in Figure 5-4 without the MGO benchmark for a better overview. Concept 1 has the lowest GHG emissions for a transit distance of 84 km upwards if offshore charging would not be an option. Concept 1 has the lowest GHG emissions from 28 km upwards. The production GHG of cryogenic hydrogen storage is lower than compressed hydrogen, this explains the slight reduction at 27 km, due to the transition of the hydrogen storage method. The irregularity at 45 km is due to the transition from a situation where the battery is used to account for the increased power during transit, to the situation where fuel cell power is increased during transit. Keeping the fuel cell power at a low average power results in a smaller required fuel cell capacity. However, it increases the emissions due to the electric storage losses and more battery replacements. Furthermore, it can be seen that Concept 2B has the lowest emissions for transit distances of 5 km upwards to 86 km. The GHG emission of the battery is calculated by the days of operation in 10 years divided by the lifetime of the battery, with a minimum of one system if the lifetime is longer than 10 years. This explains the slight advantage at low transit distances of Concept 2B compared to 2A, as there is still a residual lifetime of the battery of 2A after the 10-year scope.

At transit distances up to 12 km Concept 2A has low emissions, which rise quickly with

increasing transit distance due to the used methanol. From the fuel options of Concept 3, hydrogen has the lowest GHG emissions followed by HVO. Methanol has the highest emissions.

Finally, the contributions of the GHG emissions from fuel production, fuel consumption, and power generating system production are considered. In Figure 5-5 the GHGs of four transit distances are displayed. For Concept 1, the power generating system contributes to a relatively large part of the total emissions at 5 km transit. This contribution decreases with larger transit distances. For a transit distance of 5 km, the GHG emissions originate largely from of the production emissions of the power generating system. For the ICE concepts, the power generating system only contributes to a small part of the total GHG emissions.

Besides, if one would not consider the power generating system in the total GHG emissions, the comparison of the concepts remains the same relatively. The order of lowest to highest GHG emissions would still be the same. This indicates that in future work this calculation is less important if similar power generating systems and operational profiles are considered.

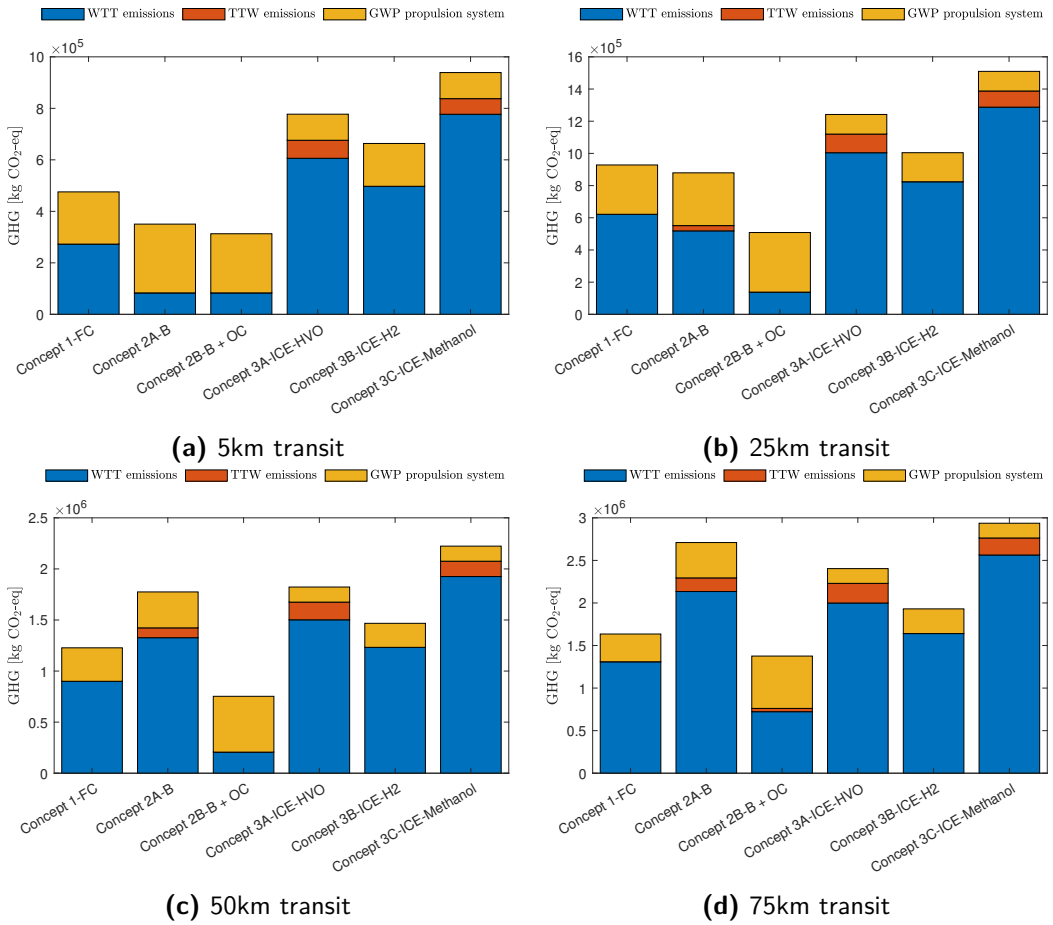

(a) 5km transit **(b)** 25km transit

(c) 50km transit **(d)** 75km transit

Figure 5-5: 10-year WTT, TTW, and power generating system GHG emissions of the concepts.

5-4 Reduction of GHG compared to increased cost

The reductions of GHG emissions in relation to the added costs are compared in this section. This will provide the answer to the research question. In Figure 5-6 the reduction of GHG relative to the increased cost can be seen. The GHG reduction is calculated by subtracting the GHG of a concept from the MGO benchmark. For the cost increase, the MGO benchmark costs are subtracted from the TCO of a concept. It can be seen that both Concept 2A and 2B result in the best ratio of reduced GHG emissions for each extra euro spend. With 2A up to transits of 18 km and Concept 2B from 18 km up to 100 km. Besides, the figure shows two peaks for Concept 2A and 2B, this is the limit of the all-electric range. After the peak, the methanol genset is used which reduces the ratio of emissions savings to cost.

When offshore charging would not be available, the hydrogen combustion concept has the best ratio between GHG reduction and added cost from 28 km upwards. Finally, it can be seen that Concept 3C has the lowest relative reduction of GHG compared to costs. Concept 3B performs slightly better than Concept 3A and Concept 1.

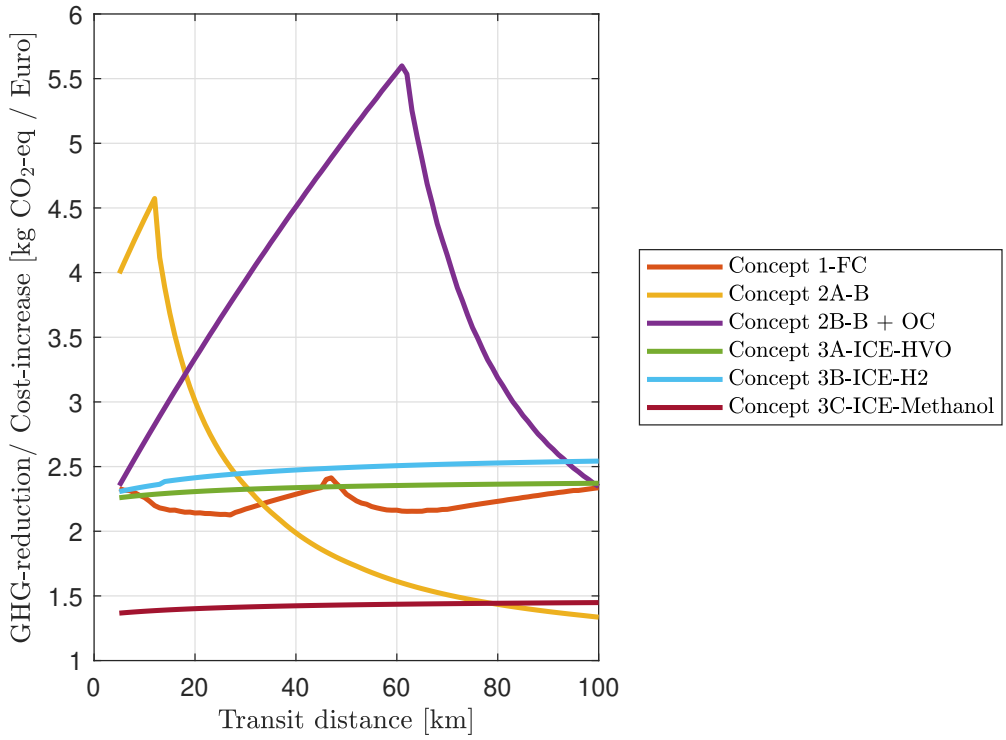

Figure 5-6: Total GHG emissions reduction as a function of cost as function of the transit distance.

5-5 Lifetime battery and fuel cell

The lifetime of the fuel cell and battery are given in Table 5-3. The lifetime of the fuel cell without battery, is the lifetime calculated for a situation where a fuel cell with the size of the original ICE power, of 2x 588kW, would supply the power of the electric motor. It can be seen that the lifetime of the fuel cell of Concept 1 is, as expected, much longer compared to a fuel cell without a battery. Up to a 60% longer lifetime. Besides this lifetime advantage, the cost of the fuel cell is largely reduced by the decreased fuel cell capacity. In Table 5-4 the fuel cell sizes can be seen. It shows that especially for shorter transit distances the fuel cell is substantially smaller. The shorter lifetime of the fuel cell at a transit distance of 5 km in Table 5-3, can be explained by more start-stop cycles compared to the operating hours. As the degradation due to start stop-cycling has a relatively large contribution to the overall degradation, operating profiles with longer transits will have more operating hours per start-stop cycle and thus a longer fuel cell lifetime. The slight decrease in lifetime at the transit distance of 25 km compared to 50 km can be explained by the increased fuel cell size. In that situation, the fuel cell will run at a lower cell potential and thus the steady-state degradation losses are higher.

	5 km	**25 km**	**50 km**	**75 km**
Lifetime fuel cell Concept 1 [hours]	25263	28436	27995	29068
Lifetime fuel cell without battery [hours]	15668	17653	18559	19862
Battery Concept 1 [days]	1432	1249	1249	1248
Battery Concept 2A [days]	3572	3055	2661	2309
Battery Concept 2B [days]	1997	1366	1368	1374

Table 5-3: Lifetime of the fuel cell and the batteries of the different concepts and a fuel cell lifetime for a hypothetical situation where no battery is used and the fuel cell follows the load profiles power demand.

	5km				**25km**				**50 km**				**75 km**			
	Battery [kWh]	Fuel cell [kW]	ICE [kW]	GEN [kW]	Battery [kWh]	Fuel cell [kW]	ICE [kW]	GEN [kW]	Battery [kWh]	Fuel cell [kW]	ICE [kW]	GEN [kW]	Battery [kWh]	Fuel cell [kW]	ICE [kW]	GEN [kW]
Concept 1	970	200	0	0	840	282	0	0	850	687	0	0	520	1038	0	0
Concept 2A	2228	0	0	200	2644	0	0	200	2438	0	0	354	2233	0	0	500
Concept 2B	1091	0	0	200	1424	0	0	200	2338	0	0	200	2618	0	0	278
Concept 3A	0	0	1176	0	0	0	1176	0	0	0	1176	0	0	0	1176	0
Concept 3B	0	0	1176	0	0	0	1176	0	0	0	1176	0	0	0	1176	0
Concept 3C	0	0	1176	0	0	0	1176	0	0	0	1176	0	0	0	1176	0

Table 5-4: Size of components of different concepts

5-6 Influence of operational profile

In this section, the results of different operational profiles are considered. Changes are made in transit distance, power during transfer, and number of transfer operations. The used variables of the different operational profiles can be found in Appendix F. In Figure 5-7 the original and three other load profiles can be seen with the corresponding TCO. Although the absolute value of the TCOs for each concept differs for each profile, the relative order from lowest to highest TCO does not change. Indicating that other parameters besides the transit distance have a limited effect on the cost-wise performance of a specific concept. In Table 5-5 the component sizes are displayed for each profile. It can be seen that the installed fuel cell capacity of Concept 1 for the three different profiles are in the range of the installed fuel cell capacity with the original profile. Indicting that the power generating system of the original profile is able to supply the energy demand for the other three profiles.

	Original profile				**Second profile**				**Third profile**				**Fourth profile**			
	Battery [kWh]	Fuel cell [kW]	ICE [kW]	GEN [kW]	Battery [kWh]	Fuel cell [kW]	ICE [kW]	GEN [kW]	Battery [kWh]	Fuel cell [kW]	ICE [kW]	GEN [kW]	Battery [kWh]	Fuel cell [kW]	ICE [kW]	GEN [kW]
Concept 1	850	687	0	0	960	580	0	0	850	690	0	0	890	652	0	0
Concept 2A	2438	0	0	354	2498	0	0	346	2445	0	0	320	2534	0	0	369
Concept 2B	2338	0	0	200	2152	0	0	200	2189	0	0	200	2061	0	0	200
Concept 3A	0	0	1176	0	0	0	1176	0	0	0	1176	0	0	0	1176	0
Concept 3B	0	0	1176	0	0	0	1176	0	0	0	1176	0	0	0	1176	0
Concept 3C	0	0	1176	0	0	0	1176	0	0	0	1176	0	0	0	1176	0

Table 5-5: System sizes for different operating profiles for a transit distance of 50 km.

	Original profile				**Second profile**				**Third profile**				**Fourth profile**			
	Elect. [kWh]	HVO [kg]	H2 [kg]	MeOH [kg]	Elect. [kWh]	HVO [kg]	H2 [kg]	MeOH [kg]	Elect. [kWh]	HVO [kg]	H2 [kg]	MeOH [kg]	Elect. [kWh]	HVO [kg]	H2 [kg]	MeOH [kg]
Concept 1	806	0	247	0	909	0	217	0	721	0	242	0	841	0	200	0
Concept 2A	2303	0	0	1354	2359	0	0	1083	2309	0	0	1335	2393	0	0	911
Concept 2B	5215	0	0	0	4688	0	0	0	5179	0	0	0	4353	0	0	0
Concept 3A	0	1111	0	0	0	999	0	0	0	1104	0	0	0	928	0	0
Concept 3B	0	0	350	0	0	0	315	0	0	0	348	0	0	0	292	0
Concept 3C	0	0	0	2111	0	0	0	1898	0	0	0	2096	0	0	0	1762

Table 5-6: Fuel consumption for the original 50 km transit profile and the three extra profiles.

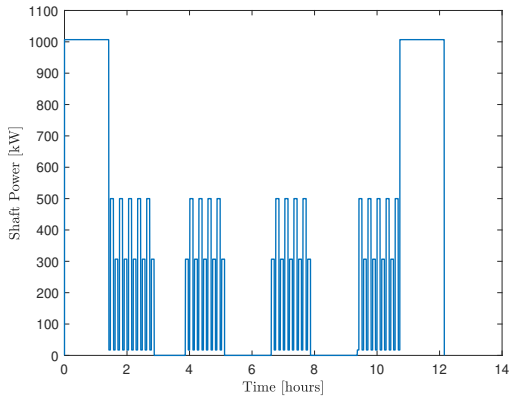

(a) Original profile 50 km transit

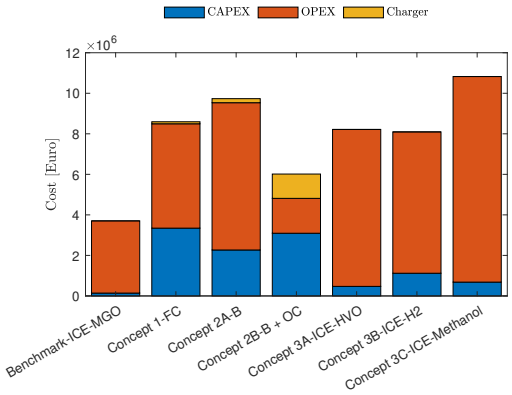

(b) Original profile 50 km transit

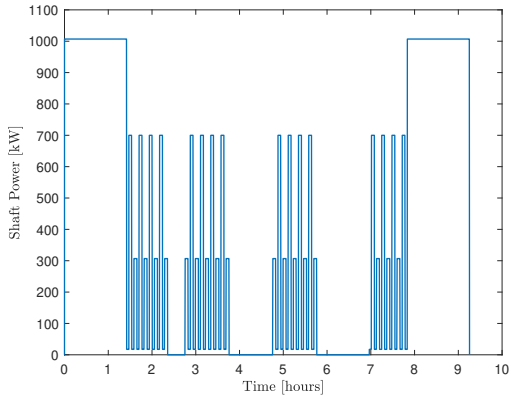

(c) Second profile 50 km transit

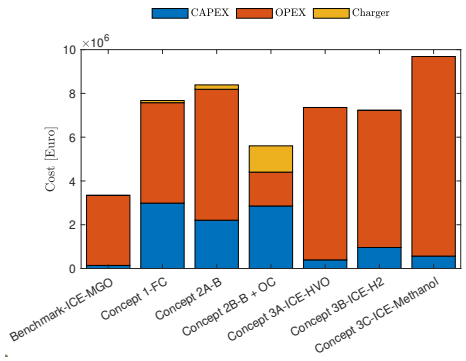

(d) Second profile 50 km transit

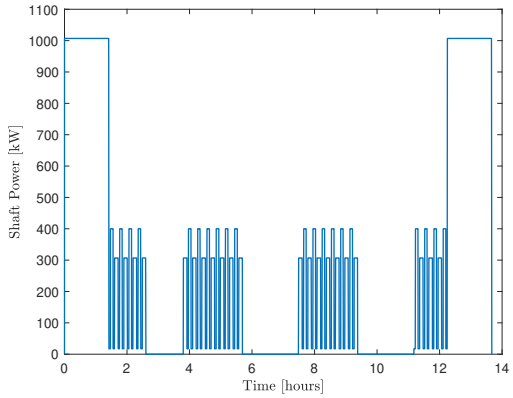

(e) Third profile 50 km transit

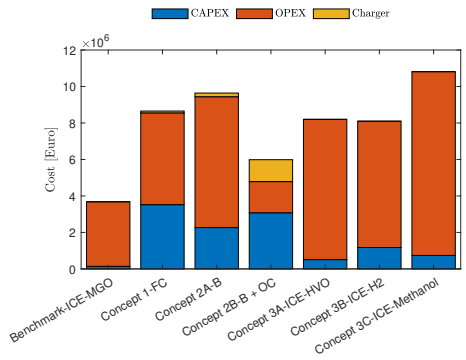

(f) Third profile 50 km transit

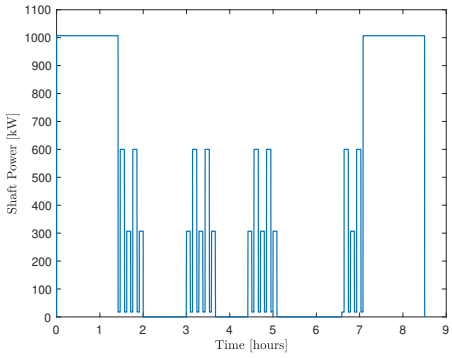

(g) Fourth profile 50 km transit

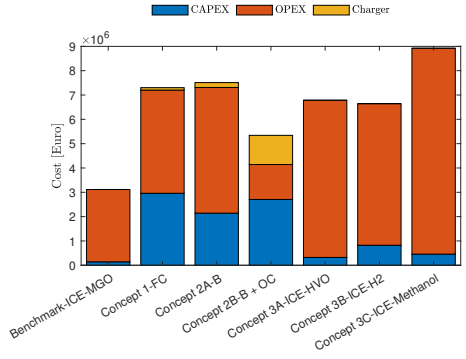

(h) Fourth profile 50 km transit

Figure 5-7: Original 50 km load profile and three adapted load profiles with the corresponding TCO

5-7 Fuel cell Size

The results of varying the power safety factor, S_{power}, of Concept 1 are discussed in this section. This is done to see if the minimum fuel cell size also results in the lowest cost. In Figure 5-8 the TCO of Concept 1 is displayed at each transit distance for multiple values of S_{power}. At low transit distances, the value of S_{power} does not influence the total cost. This can be explained by the constraint P_{min}, which determines the installed fuel cell capacity in this case, and not the maximum power output of the fuel cell. At transit distances up to around 40 km, higher values of S_{power} reduces the total cost slightly. This is in line with what is expected from the results of Appendix B-5. However, the impact of the different values of S_{power} on the cost is limited compared to the original value of 1.1. A sudden rise in cost for higher values of S_{power} can be seen around a transit distance of 40km. At this point, the constraint of $A_{Floorspace_{max}}$ is limiting, meaning that the battery capacity is smaller for a larger installed fuel cell capacity. Due to this, the battery capacity is too small to supply the increased power demand during transit and will therefore result in a higher fuel cell power during transit. The fuel cell size is then determined by the fuel cell power during transit, $P_{FC_{transit}}$. This indicates that installing a larger fuel cell is only beneficial when the battery can still be sufficiently large for peak shaving during the transits. When the fuel cell size is determined by the power peaks of the transit it is no longer beneficial to increase the installed fuel cell capacity.

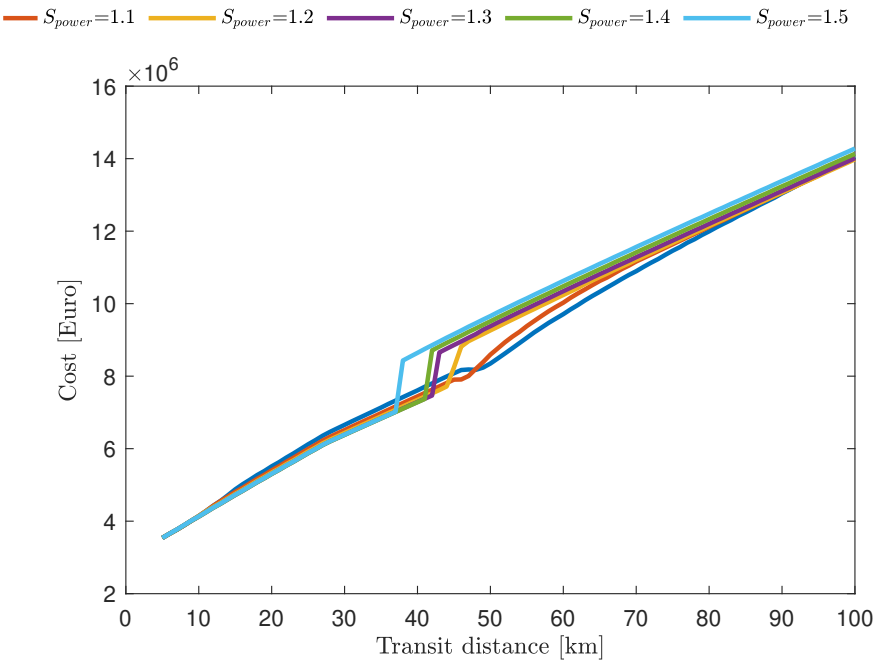

Figure 5-8: TCO of fuel cell Concept 1 with different fuel cell safety factors S_{power}.

5-8 Parameter investigation

In the previous sections the results of the comparisons of the different concepts are based on fixed values for certain parameters. In this section, the influence of the value of some of these parameters is investigated. In this way, one can see how a change in value results in a different outcome of the comparison. Besides, multiple lifetimes of the fuel cell and battery are investigated to see what the influence is on the comparison between concepts. All calculations are performed with a transit distance of 50 km. 50 km is chosen as this is roughly the average transit distance of a CTV in the Netherlands as can be seen in Appendix A-1.

5-8-1 Fuel price

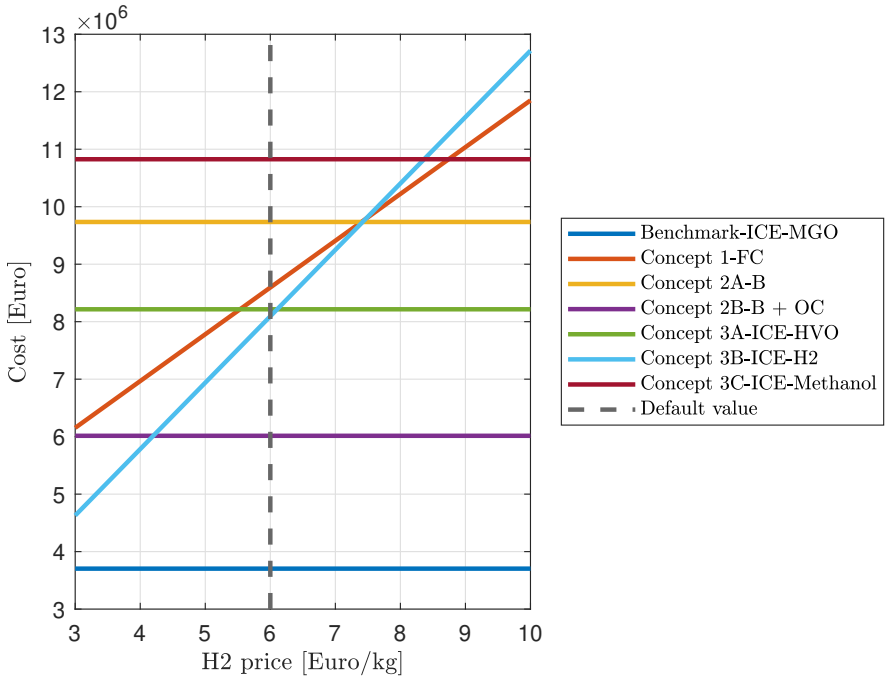

Figure 5-9: TCO for a range hydrogen prices with a 50 km transit.

In Figure 5-9, the TCO as function of the hydrogen price can be seen. For a hydrogen price above 7.4 €/kg the TCO of Concept 1 is lower compared to Concept 3A.

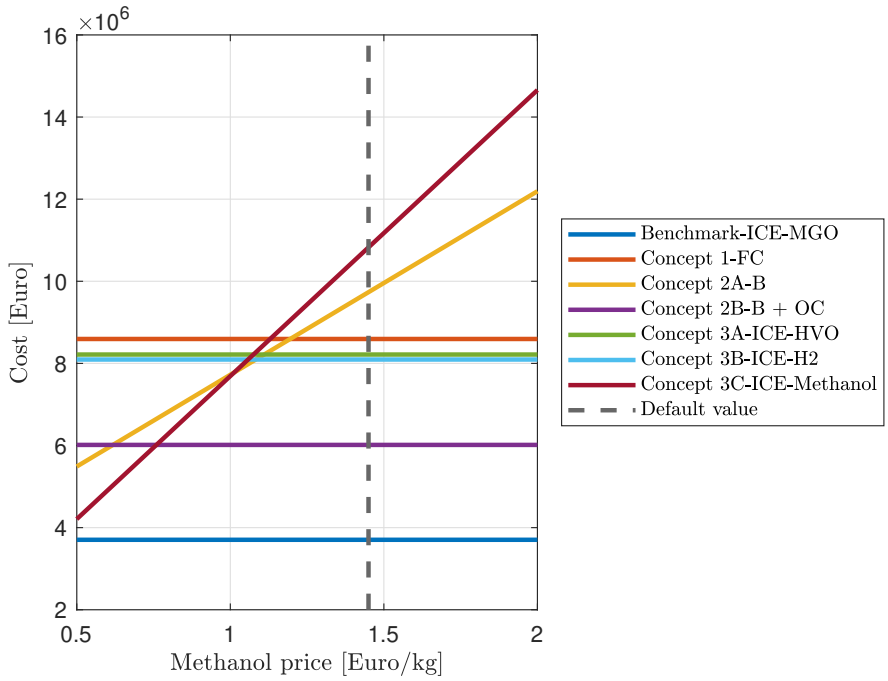

Figure 5-10: TCO for a range methanol prices with a 50 km transit.

In Figure 5-10, the TCO as function of the methanol price can be seen. For a methanol price just above 1 €/kg Concept 2A is more attractive than Concept 3C.

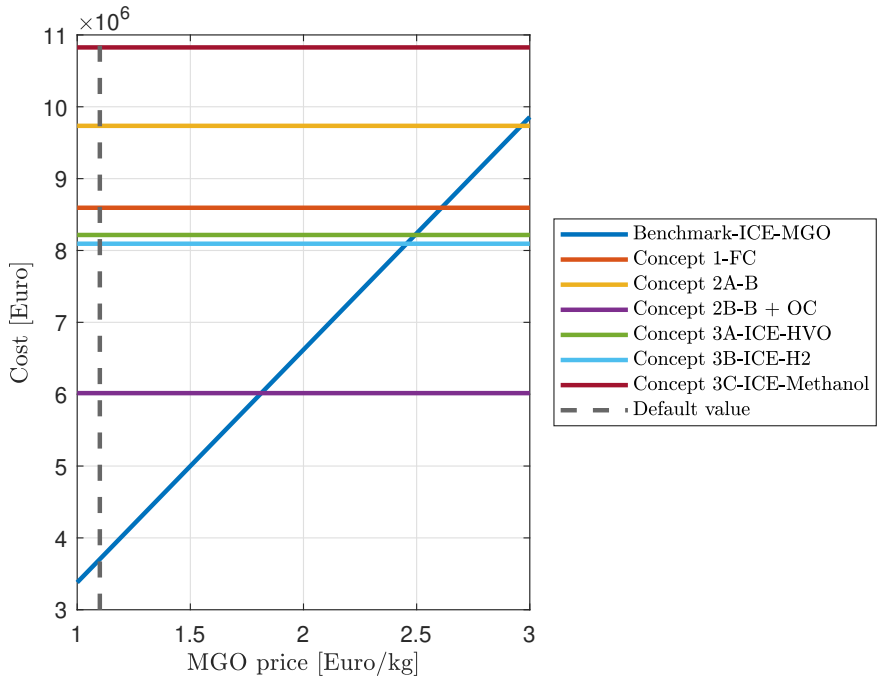

Figure 5-11: TCO for a range MGO prices with a 50 km transit.

In Figure 5-11, the TCO as a function of the MGO price can be seen. For an MGO price of 1.8 €/kg Concept 2B becomes cost competitive. Only at very high prices around 2.5 €/kg the other concepts become cost competitive.

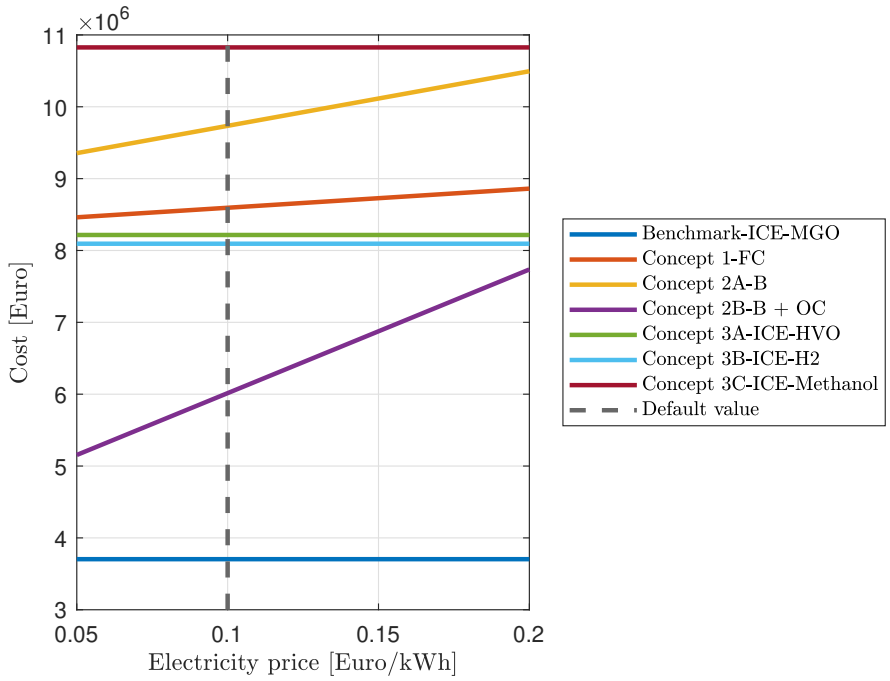

Figure 5-12: TCO for a range electricity prices with a 50 km transit.

In Figure 5-12, the TCO as a function of the electricity price is displayed. For all considered electricity prices Concept 2B has the lowest TCO. Besides, the electricity price does not influence the order of lowest to highest TCO for the considered prices.

5-8-2 Component lifetime

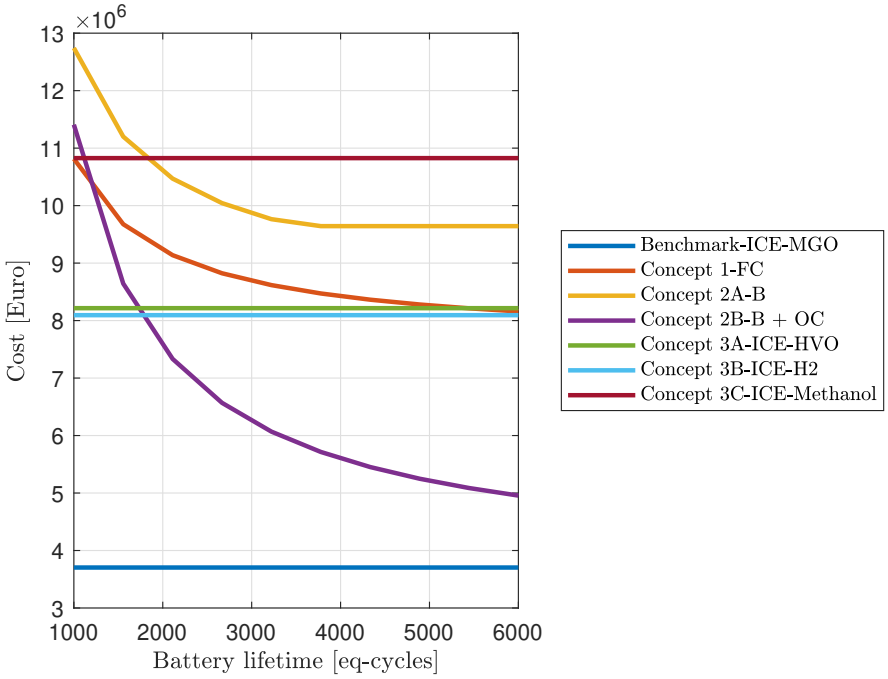

Figure 5-13: TCO for a 50 km transit as a function of the battery lifetime.

The battery's lifetime in equivalent full cycles (EFC) is evaluated to investigate the influence of the battery life on the TCO. It can be seen that for battery lifetimes below 1800 EFC, Concept 2 is not an interesting solution anymore. This indicates that cycle life is indeed an important parameter for selecting the battery type. The cycle life of NMC and NCA batteries are below 1000 EFC for 100% DoD cycles (Preger et al., 2020), therefore these chemistries are less favourable and would result in very high costs.

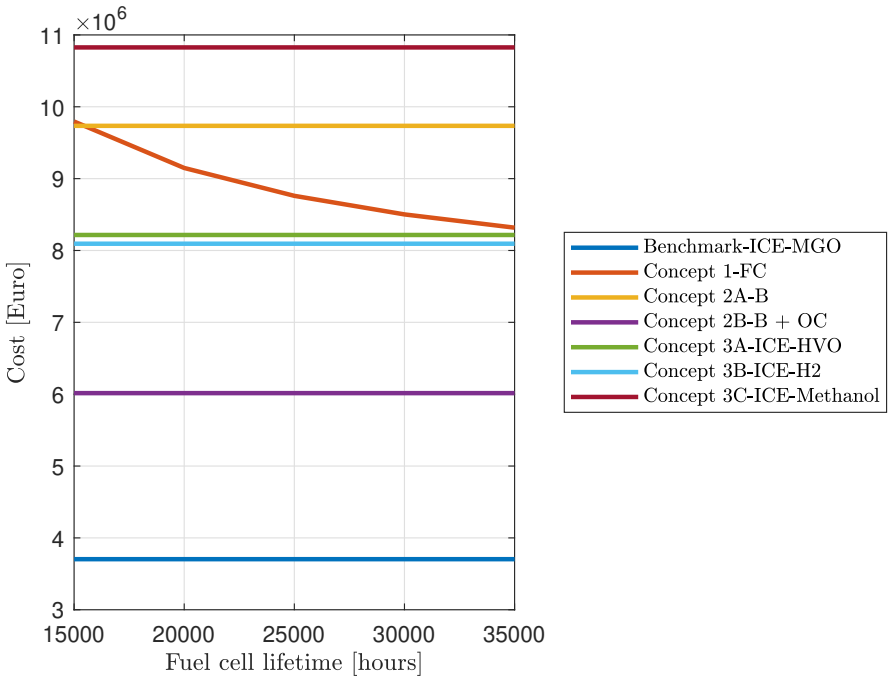

Figure 5-14: TCO for a 50 km transit as a function of the fuel cell lifetime.

In Figure 5-14 the TCO as a function of the fuel cell lifetime can be seen. Only for a lifetime over 35k hours, fuel cell Concept 1 approaches the cost of battery Concept 2B. These lifetimes are not yet reached by marine fuel cells to date.

5-8-3 Component price

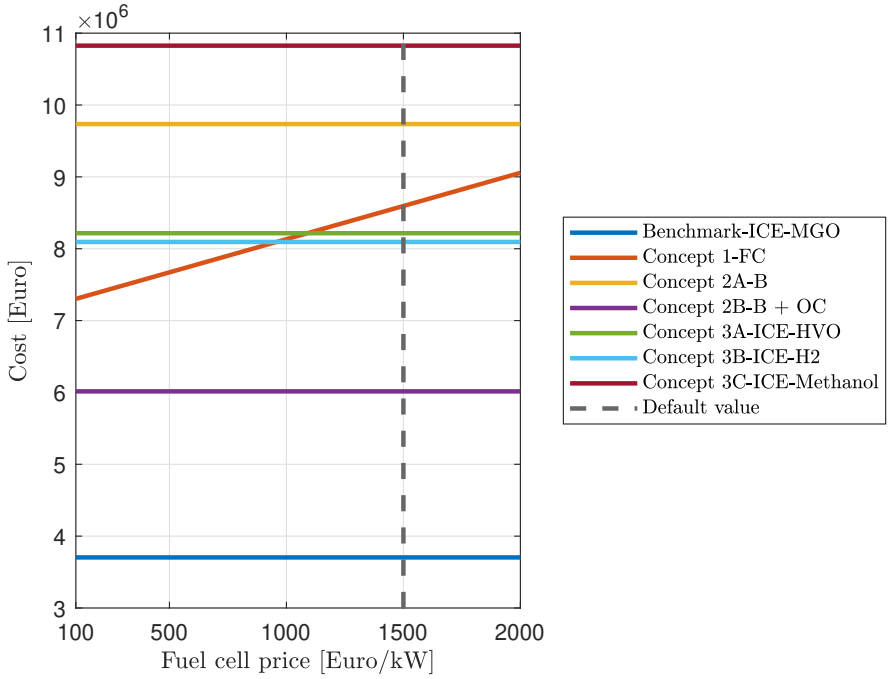

Figure 5-15: TCO Fuel cell price sensitivity for a 50 km transit.

In Figure 5-15 the TCO as a function of the fuel cell price is displayed. For a fuel cell price of €1000/kW fuel cell Concept 1 has the same costs as Concept 3C. This indicates that a reduction of one-third of the price used in this research of €1500/kg is needed to be cost-competitive with the ICE technology. The U.S. Department of Energy (2020) has set a 2030 price target of $80/kW for fuel cell systems of heavy-duty trucks. Besides the U.S. Department of Energy indicates that for 2019 the estimated heavy-duty vehicle fuel cell is estimated to cost $190/kW, this would result in a substantially lower TCO compared to the ICE concepts, including hydrogen combustion.

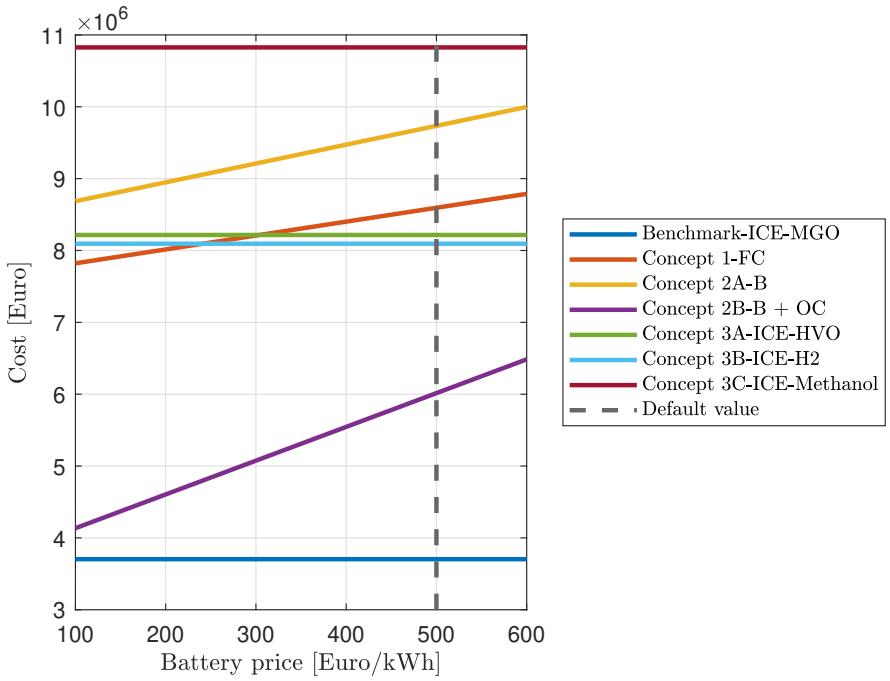

Figure 5-16: TCO Battery price sensitivity for a 50 km transit.

In Figure 5-16 the TCO as a function of the battery price is displayed. For a battery price of 100 €/kWh Concept 2B approaches the total cost of the MGO benchmark. This price of 100 €/KWh is not far away from the cost of an EV battery pack today. BloombergNEF (2021) reports an average EV battery pack price of $132/kWh in 2021 and that this is likely $100/kWh by 2024. When production volumes of marine battery systems scale, the price should come closer to the cost of EV battery systems. Besides, also for Concept 1, a battery price of 240 €/kWh results in equal cost compared to Concept 3B.

6

Discussion

From the previous results, it can be seen that there are substantial differences between the compared concepts. Both the GHG emissions and costs deviate strongly between concepts. In this research, a concept is considered best performing if the ratio of reduced GHG emissions divided by extra cost is the highest. Figure 5-6 shows that for concept 2B, up to 3.8 times as much GHG emissions can be saved compared to methanol concept 3C. An interesting finding as in the shipping industry in general, methanol is often considered a promising solution. This indicates that there is no one-of-a-kind solution for the entire industry, as vessels are substantially different from each other. Besides, in Figure 5-6 it can be seen that ICE concepts with hydrogen and HVO and the fuel cell with hydrogen have comparable GHG reductions compared to increased cost. However, there are some limitations of this work, these will be discussed in the next sections.

Comparison criteria

This research focused on fuels which are produced using wind energy. More methods to produce for example, green hydrogen and green methanol, exist. This might change the outcome of this study as the prices and the emissions can change relative to each other. In the scope of this research, the concepts are compared on cost and GHG emissions. However, there are more important factors that influence the decision-making process. For example, the use of (scarce) materials, safety, and the remaining NO_x emissions of some concepts. Also, the energy footprint of alternative fuels is an important factor that should be taken into account. Not enough renewable energy is available to supply the entire energy demand at this moment. Using more renewable electricity for ships can therefore increase fossil-based electricity elsewhere. The energy consumption of the fuels is indirectly taken into account in this research. With each conversion from electricity to hydrogen and hydrogen to methanol, the efficiency losses result in a higher fuel price and more electricity used. This is also in line with the results of this work. The direct use of electricity results in the lowest GHG emissions followed by hydrogen, and the use of methanol results in the highest GHG emissions. Besides, including the power generating system produciton GHG emissions did not change the outcome of the comparison between the concepts. Indicating that the power generating system production emissions seem to be less relevant to include in future research.

Load profile

The load profile of the CTV used in this research is a strong simplification of reality. Constant powers are assumed, while in real-life operation fluctuations are expected as a result of waves, wind, and actions of the captain. These changes in conditions are not taken into account and might, for example, result in shorter battery life. Also, the load profile is based on the power-speed characteristics of a different CTV and is scaled to the size of the CTV considered in this research as actual data was not available. This is a simplification of reality and is likely not completely accurate. For a better result, the actual power-speed characteristics must be determined. If possible, it would be beneficial to obtain actual power measurements of multiple days of operation. In this way, different weather conditions can be compared, and system designs can be made that suit all the operational profiles instead of a system sizing performed on one particular profile.

Another important simplification that has been made is that the weight of the power generating system does not influence the ship's fuel consumption. As can be seen in Table 5-2, the combined weight of the fuel and power generating system differs between the concepts. In the model of this research, added resistance due to the added weight is not taken into account. The battery CTV was found to be the best economically attractive method. However, this is also the heaviest power generating system. For a transit distance of 50 km, this results in a system of 17.7 t where the total weight of the power generating system of a CTV running on HVO would only weigh 9.2 t. Therefore, the difference between these two concepts will be smaller in reality. However, the difference in TCO and GHG emissions between the battery-powered concepts and the other concepts are large. Therefore, the outcome is expected to be the same when the added resistance is taken into account.

In this research, auxiliary power consumption is not considered. The auxiliary is expected to be little compared to the energy used for propulsion. For the concepts containing a battery for energy storage, powering the auxiliary load is expected to have a small influence on the system design. However, for Concept 3, there would need to be an additional genset, as is done today on CTVs, adding cost and weight.

Lifetime

Fuel cell

The lifetime of the fuel cell in this research is based on experimental data found in literature from multiple studies. The fuel cells used in these studies are not the same as fuel cells used in the marine industry in terms of power output, number of cells, cell area, materials, etc. Therefore, actual degradation rates could differ from the values used in this research. Besides, the voltage losses of the operational conditions of start-stop cycling, load cycling, and steady-

state operation are added, assuming that the individual contributors do not impact each other. However, it is likely that these factors will influence each other as ageing mechanisms can be similar. The measurements used for the steady-state degradation, obtained from the work of de Bruijn et al. (2008), have lower current densities at a given cell voltage compared to the Toyota Mirai polarisation curve used in this research. To the author's knowledge, the current density alone does not influence the ageing mechanisms. However, the degradation rates are likely different in reality as the conditions in the cell change with a change in current density. For example, a different relative humidity, which is known to affect degradation Borup et al. (2007). Besides, the degradation rate for only three cell potentials was known, and linearly extrapolated for other cell potentials. More data points are required to see if this linear dependency is correct. Next, degradation due to load cycling is simplified. Load cycling degradation is calculated by the equivalent number of full load cycles. However, a lot of factors influence the degradation due to load cycling, such as the rate at which the load increases and the cycle's amplitude. In this research, a battery accounts for almost all changes in the power demand. The impact of simplifying the load cycle degradation is therefore limited as almost no load changes happen for the fuel cell. However, this makes the method of degradation calculation less suitable for other applications with more fluctuations in the output power of the fuel cell. The experimental data used in this research could be outdated as recent fuel cell developments might have improved durability. In conclusion, the fuel cell lifetimes obtained (25263 hours - 29068 hours) in this research are in the range of what can be expected from the lifetime of 24k-30k hours indicated by marine fuel cell suppliers (Ballard Power Systems, 2022, Nedstack, 2022). Therefore, for the cost and GHG calculations of this research, this method is deemed sufficient. However, if one is interested in the exact contributions of different ageing mechanisms, the method of this research is less suitable. To obtain more insights into the contributions of different mechanisms, more research is necessary on the degradation rates of large heavy-duty fuel cells. This will provide accurate degradation rates that apply to fuel cells in the marine industry. Besides, future research could develop a method to relate single cell lifetime to full-scale fuel cell lifetime. In this way, single-cell experiments can be used for full-scale fuel cells in real-life operations. This would increase the usefulness of research on single-cells tremendously. Also, if the degradation behaviour for transient powers of these fuel cells is understood better, energy management strategies can be developed that can reduce the total cost of operation. In this research, the energy management strategy of the fuel cell was based on the cost of degradation due to a load cycle compared to battery degradation cost. No difference was made between small and large cycles, as there is, to the author's knowledge, no representative data available. When degradation rates are known for different ramp rates in kW/s, energy management strategies can be developed that optimise battery degradation versus fuel cell degradation. It is a challenge to obtain such data as both the hydrogen needed and the fuel cell itself are costly. As there are more and more hydrogen ships in operation, it might be a good method to obtain the data of these ships with different operating profiles and compare it to accelerated lifetime experiments. The accelerated lifetime test will give insights into how the degradation rates of the different operational conditions compare to each other, and the operational data will provide the absolute values of the degradation rates.

Battery

The method to calculate the lifetime of the battery is based on an ampere-hour throughput capacity fade model. A fixed C_{rate} of 0.5 was taken as the discharge rate to calculate the lifetime. Different fluctuating rates are present in reality. Besides, the lifetime calculation method used in this research depends on the temperature and is taken as a constant of 20 °C. This can differ in reality. Also, for Concept 2A and Concept 2B gensets are used, which can increase the temperature of the engine room. The lifetime of the battery is expected to be lower at higher temperatures. This could be overcome by making engine room compartments or by better ventilation. At the used temperature of 20 °C the used battery capacity model predicts a lifetime of 3295 equivalent full cycles, similar to the lifetimes from the work of Preger et al. (2020) for a capacity fade of 10%. In future work, the EoL criteria of the battery can be investigated to see how the total GHG emissions and cost change with a varying battery EoL condition. Replacing the battery sooner will, for example, result in less methanol used by the genset to extend the range due to the higher remaining capacity. In that case, there will be more battery production emissions.

ICE/genset

The lifetime of the ICE and genset is taken as 9000 operating hours. Which might be different in reality. The cost of the ICE and genset is only a small part of the total cost. Therefore, the influence of this assumption is expected to be small.

TCO

The TCO is based on a scope of 10 years of operation, because this is often the length of a service contract of a CTV. Possible price changes during this period might change the outcome of this research. The cost of replacing, for example, the fuel cell and battery are likely lower due to price improvements. The results of the parameter investigation will provide a method to compare the concepts for adjusted prices. Besides, maintenance cost is not included as little information is known due to limited application. If one compares the maintenance cost of a diesel truck and hydrogen fuel cell truck, respectively \$0.17/mile and \$0.17/mile. This is only a small part of the total cost of \$2/mile (U.S Department of Energy, 2020). Low maintenance costs are expected for the battery concepts, which are already high performing in terms of TCO. Therefore, not including maintenance is expected not to have a large influence. Also, the cost of the offshore charger, which is taken as €1 million, is uncertain. This is hard to predict as it is not a commercial product yet.

Efficiency ICE and genset

For the thermal efficiency of the ICE and genset a fixed value was used for all power outputs. The efficiency is dependent on a lot of factors: torque, RPM, power output, etc. The torque and RPM of the ICE could not be calculated, as there was no information available about the propeller demand curves of the different gear settings of the CTV. Getting the correct efficiency for each power output is therefore difficult. An assumed average was used in this research. This is an important simplification for the comparison between the fuel cell and hydrogen ICE. This might change the comparison between these concepts when for example, the efficiency of the ICE in real-life conditions is lower.

Other ship types

Technicians on a CTV often work in shifts of up to 12 hours. At transit distances above 50 km the duration of the operational profile in this research exceeds 12 hours. There are multiple solutions for this, a large service operating vessel which stays offshore for multiple days to weeks can be used, or a faster CTV can be used. For example, a 26 m CTV with a service speed of 25 Kts, has a total 2060 kW of installed engine power. 75% more than the CTV used in this research. With a maximum weight of 30 t, 50% more as the CTV in this work (Njord OFFSHORE, 2022). Assuming that the installed ICE capacity is a good indicator of the energy consumption, it is likely that concept 2B would perform less for this faster ship type. Another option is a service effect CTV, having a service speed of 27 kts, with 1324 kW installed power (Cwind, 2022). Likely, this ship would have a lower maximum weight compared to a normal 26 m CTV due to the fans that have to lift the CTV out of the water. For concept 2B it is expected that a smaller battery can be installed for this CTV type. However, less energy is used. It would be interesting to investigate the comparison of these CTV types for far offshore use in future work. In Appendix G, the use of a gripper system to reduce the power during transfer is investigated. A potential GHG emissions saving of 1.9 million kg CO_2-eq during 10 years was found. For future research, it would be interesting to include such systems. The outcome of this research has shown that weight is an important limitation for battery-powered CTVs. Indicating that for new-build vessels, hull types with a high weight capacity are more suitable for battery-powered concepts. Besides, it was shown that more fuel storage volume is required for a hydrogen CTV at large transit distances.

The CTV's operational profile is unique compared to other vessels. Therefore, the outcome of this research is not directly applicable to other vessels. Besides, CTVs used in offshore wind have a unique situation where the working area is a large energy source, enabling the offshore charging option. This is often not the case for other ships outside the wind energy industry. To the author's knowledge, the ship types with the most similar profile, profiles with high peak loads and large intermittent standby times, would be small ferries and work ships used around ports. The method of this research could be applied to these ship types.

Practical aspects

The outcome of the comparison of the concepts has given insights into how multiple concepts would perform relative to each other. In practice, the outcome might be different due to practical limitations. For example, in the sizing of the components, the exact component size is likely not commercially available. Besides, the maximum fuel storage volume does not take form factors into account. As an example, the hydrogen storage energy density is calculated based on the volume of the smallest square that could surround the cylinder and the hydrogen content in that cylinder. Because the available storage dimensions were unknown, the maximum hydrogen storage is calculated with the energy density and the maximum volume. Not with the actual number of cylinders that fit in this space. Similarly, this is also done with the maximum battery capacity. A better approach for this would be to take the dimensions of the available spaces and then determine the actual number of components that fit in this space. Another practical limitation is that the weight distribution is not considered. As an example, the changed weight distribution compared to the state-of-the-art CTV can change the dynamic motion of the ship. Besides the technical difficulties, seasickness of the technicians after the transit is a large problem. Therefore, it is beneficial to make actual vessel designs for the different concepts, which enable the investigation of the vessel motions in future research.

7

Conclusion

This research aimed to identify the most economically attractive power generating system for a CTV to reduce GHG emissions. Multiple fuels and power generating systems have been investigated. Methanol, hydrogen, and electricity, all based on wind energy, and besides HVO, were selected as possible fuels. PEM fuel cells, LFP batteries, and ICEs were selected for these fuels to form multiple concepts. The GHG emissions of these fuels and power generating systems have been identified. The study into the degradation of fuel cells identified the main degradation mechanisms and resulted in a method to calculate the expected lifetime based on a cell voltage loss model. Besides, a model to calculate the cost, GHG emissions, and the component sizes of the concepts was developed. The model finds the previous values for the operational profile for different transit distances to the wind farm considering the constraints of the ship.

All considered concepts can reduce GHG emissions by more than 80%, meeting the IMO GHG target for 2050. However, there are substantial differences in cost. The battery genset concept (2A) is the most cost-effective method to reduce GHG emissions for a transit distance of up to 18 km. Beyond 18 km up to 100 km, the same power generating system, with the ability to charge the CTV offshore (2B), is the most cost-effective method to reduce GHG emissions. This distance includes all wind farms in operation in the Netherlands to date. This concept requires a battery life above 1800 EFC for a transit distance of 50 km to maintain the cost advantage over other concepts.

If offshore charging is unavailable, the hydrogen combustion concept (3B) is the best method to reduce the GHG emissions in relation to cost up to 68 km transit, and HVO combustion (3A) upwards of 68 km. Major cost improvements are possible for the fuel cell concept, as the CAPEX accounts for up to 50% of the TCO. With the fuel cell and battery price of vehicles today, the TCO of the fuel cell concept is already significantly lower than the TCO of ICE concepts. Besides, the fuel cell concept has a longer range than the ICE concept. Together, this makes fuel cell technology the most interesting technology for future applications if offshore charging would not be available.

All in all, this thesis provides new insides on the comparison between different alternative fuels and power generating systems for the CTV of this study. The potential of charging the CTV offshore is proven as a promising solution towards zero emissions. Besides, it is shown where

the biggest reductions in GHG emissions can be made for each euro, providing information for decision-makers on where the greatest GHG reductions can be achieved in relation to cost. Next, it has been shown that batteries can mitigate the degradation issues related to fuel cells in a CTV with a transient load profile. The battery can extend the fuel cell lifetime by up to 60% for the considered profiles. Also, it has been shown that the smallest possible fuel cell does not necessarily result in the lowest TCO. Future work could select promising concepts and focus on combining actual operational data and fewer detailed concept solutions.

A

Wind farm sites of the Netherlands

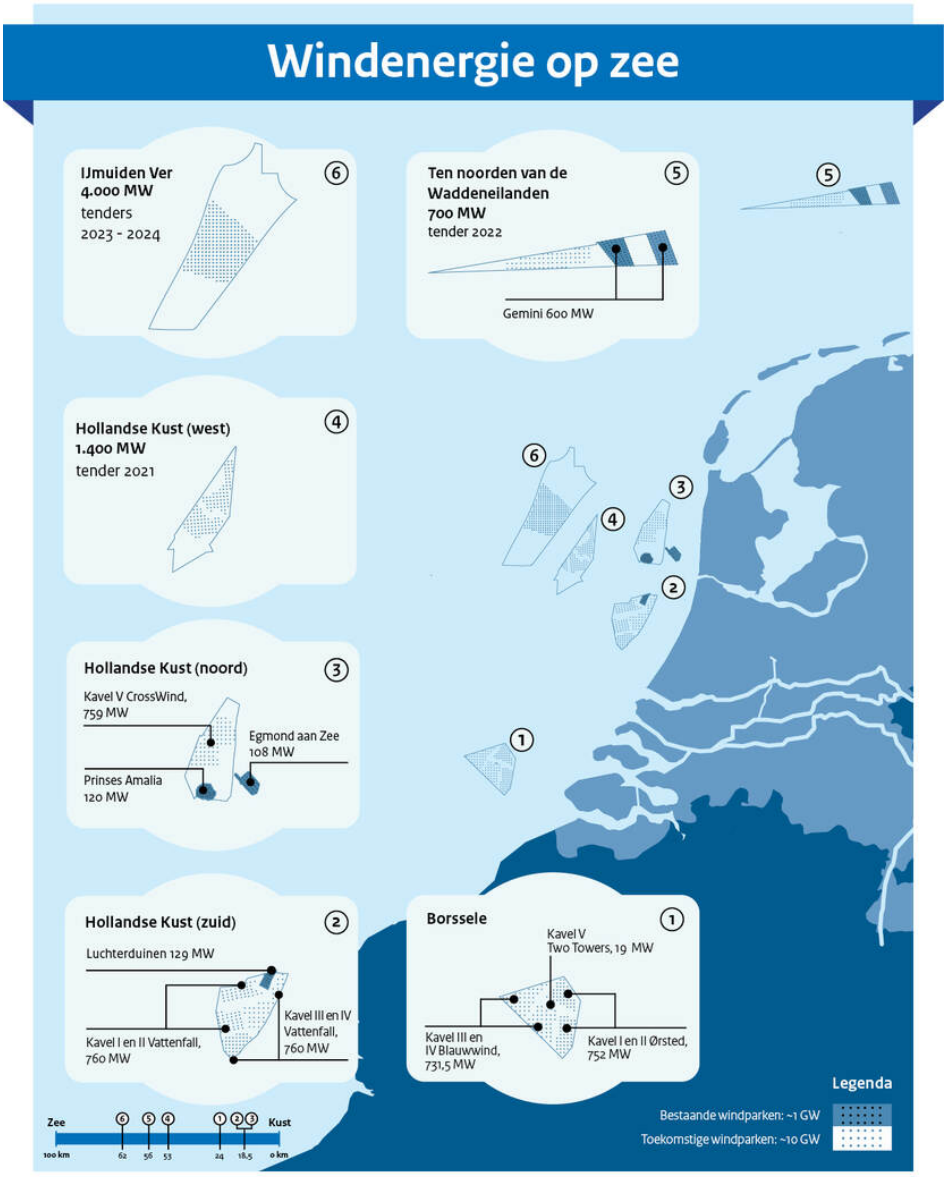

Figure A-1: North Sea Wind farm sites of the Netherlands until 2024 (Government of the Netherlands, 2020).

B

Proton Exchange Membrane Fuel Cell

To determine how a PEMFC would perform on board a CTV, it is valuable to explain how a PEMFC works. Therefore, this chapter describes the components of the PEMFC, how PEMFCs work, and the performance decay of the fuel cell decays over its lifetime. With this understanding of the degradation mechanisms of PEMFC, mitigation strategies are investigated to find methods to extend the lifetime of the fuel cell. The information on how the fuel cell ages can then be used to estimate the lifetime of a fuel cell on board of a CTV.

B-1 System components and working principle of PEMFC

In this section, the basic cell components and the system components of the PEMFC are listed, fuel cell efficiency is discussed, and the working principles are described.

B-1-1 Cell components

An individual cell consists of two electrodes, the anode and cathode, separated by an electrolyte membrane which are displayed in Figure B-1. Each electrode has a gas diffusion layer (GDL) and an electrocatalyst layer. The GDL distributes the reactant gasses and collects the current generated by the cell. The GDL typically consists of two layers, a macroporous layer and a microporous layer. Because of the low voltage of an individual cell, multiple cells are placed on top of each other forming a stack, as can be seen in Figure B-2. The individual cells are electrically connected in series to increase the potential. Bipolar plates are placed between the individual cells. The bipolar plates have multiple functions, electrically connect the individual cells, distribute the reactant gasses across the active membrane electrode assembly (MEA), remove heat through the cooling channels and provide structural integrity. The individual cells are compressed together with end plates on either side of the stack to provide a leak-free assembly. Directly adjacent to the bipolar plates are the GDLs to distribute the gasses to the catalyst layer, conduct electrical current, and transport the liquid water from the MEA to the flow channel. In the centre three layers, the MEA, the electrochemical process that drives the fuel cell reaction occurs. The MEA consists of the two composite electrocatalyst and a polymeric layer in between. The electrocatalyst layers

are commonly made of nanoparticles of platinum deposited on a high-surface-area carbon support. The amount of platinum catalyst surface area which drives the reaction is expressed as the electrochemically active surface area (ECSA). Nafion, a perfluorinated sulfonic acid based ionomer (PFSA), is often used as membrane material for PEMFCs (Borup et al., 2007).

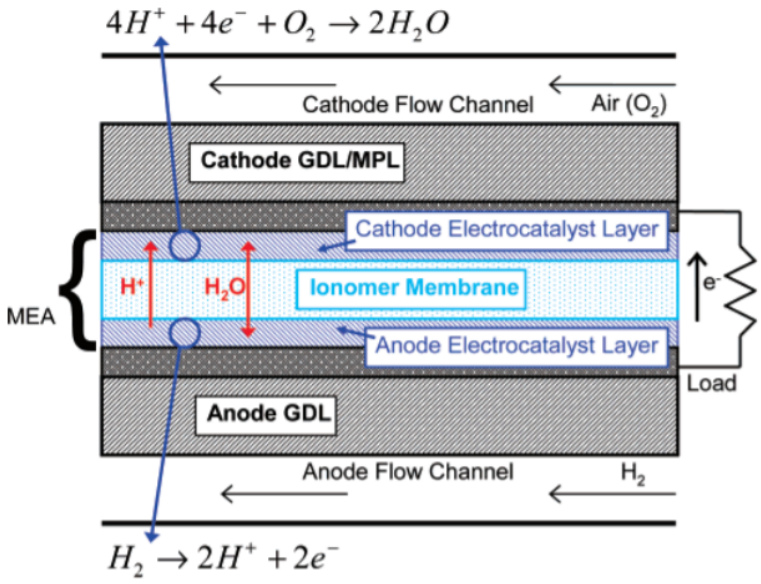

Figure B-1: Schematic cross-section of a typical single cell of a PEMFC (Borup et al., 2007).

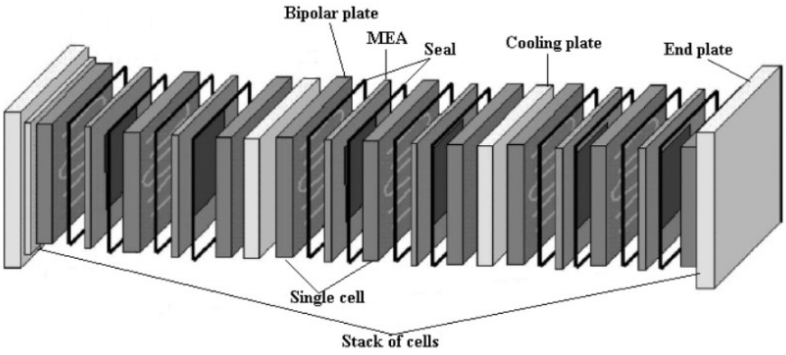

Figure B-2: Schematic cross-section of a typical PEMFC stack (J. Zhang, 2008).

B-1-2 Balance of plant

The previously described cells that together form a fuel cell stack are only a part of the complete fuel cell system. In order to let the fuel cell system work properly, additional

components are needed. These components are called the balance-of-plant (BoP). The extra components fulfil multiple roles such as cooling the stack, controlling the stack's power output, compressing and humidifying the inlet air and much more. A systematic overview of some of the basic components can be seen in Figure B-3.

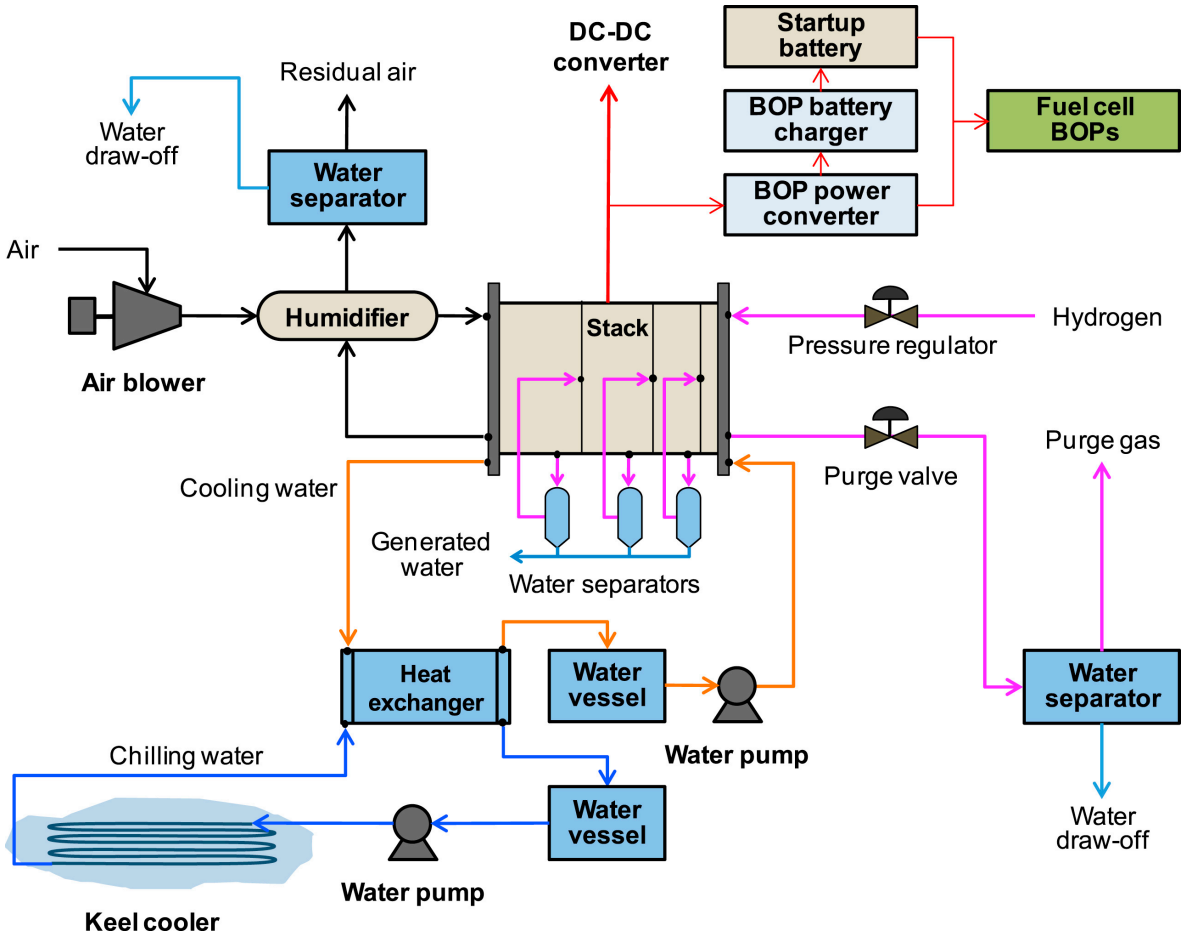

Figure B-3: Schematic overview of the components of a PEM fuel cell system (Choi et al., 2016).

B-1-3 Marine systems

Marine fuel cell systems often come in modules in the range of 100-200 kW. These modules contain the fuel cell stack and the BoP. The modules can be coupled when higher power is required. Due to the intensive use of fuel cells in the maritime industry, a long lifetime is required. According to Nedstack, their marine fuel cell would require a replacement after 24k- 30k running hours (Nedstack, 2022). Ballard reports a similar lifetime of the stack of over 30k running hours (Ballard Power Systems, 2022). According to de Bruijn et al. (2008)

the cost of the fuel cell is directly related to the lifetime of the fuel cell, a reduction in cost can be achieved with less or less expensive materials; less platinum or thinner membranes. Therefore, marine fuel cells are expected to be more expensive than fuel cells for cars. The indicated lifetime by the manufacturers could however be different as the lifetime of the fuel cell is strongly dependent on how it is operated. This will be discussed further in Section B-2.

B-1-4 Working principle

A PEMFC converts the hydrogen electrochemically using two half-reactions. At the anode side, hydrogen is oxidized, electrons are released and H^+ ions are formed following Equation B.1a. At the cathode side, the oxygen reacts with the H^+ ions and electrons from the anode, forming water as in Equation B.1b. The combined reaction on the anode and cathode side will result in the total reaction of Equation B.1c.

$$2H_2 \rightarrow 4H^+ + 4e^- \tag{B.1a}$$

$$O_2 + 4H^+ + 4e^- \rightarrow 2H_2O \tag{B.1b}$$

$$2H_2 + O_2 \rightarrow 2H_2O \tag{B.1c}$$

On the anode, H^+ ions and electrons are released, at the cathode, H^+ ions and electrons are consumed to form H_2O. The transportation of the H^+ ions or protons happens through the electrolyte. This electrolyte is a polymer membrane with mobile H^+ ions, therefore the H^+ ions can travel through the membrane. The electrons will travel from the anode through an electrical circuit to the cathode, creating a usable current (Larminie and Dicks, 2003).

B-1-5 Gibbs free energy

The Gibbs free energy is the energy that is needed or released by a reversible chemical process with constant pressure and temperature. Also known as the minimal thermal dynamic work required to drive the reaction (at constant pressure and temperature) or the other way around the maximum thermal dynamic work that the reaction can provide. The Gibbs free energy can be calculated by Equation B.2.

$$\Delta G = \Delta H - T\Delta S \tag{B.2}$$

With ΔH: the change in enthalpy, ΔS: the change in entropy, and T: the absolute temperature. This change in Gibbs free energy is the energy difference between the products and the reactants of the reaction in Equation B.1c. This change in Gibbs free energy can also be noted as $\Delta\bar{g}$, which is the change in Gibbs free energy per mole. The change in Gibbs free energy per mole can be calculated using Equation B.3.

$$\Delta\bar{g}_f = (\bar{g})_{products} - (\bar{g})_{reactants} \tag{B.3}$$

The change of Gibbs free energy for the reaction inside the fuel cell will be Equation B.4

$$\Delta\bar{g} = (\bar{g}_f)_{H_2O} - (\bar{g}_f)_{H_2} - \tfrac{1}{2}(\bar{g}_f)_{O_2} \tag{B.4}$$

For every mole H_2O produced, two moles of electrons travel through the electric system, each electron carrying a unit negative charge (e^-). The Faraday (F) constant represents the charge of a mole of electrons. There will thus be a charge of -2F. The electrical work done can be calculated by charge x voltage. The electrical work of a reversible system is the Gibbs free energy released by the reaction. This results in Equation B.5 (Larminie and Dicks, 2003).

$$\Delta \bar{g} = -2FV_r \tag{B.5a}$$

$$V_r = \frac{-\Delta \bar{g}}{2F} \tag{B.5b}$$

Under standard temperature and pressure, this results in a reversible voltage V_r of about 1.2 V for a single hydrogen cell without losses (Larminie and Dicks, 2003). For a fuel cell without losses, this reversible voltage, V_r, is equivalent to the open circuit voltage (OCV). The OCV is the voltage of the cell when no current is drawn. However, in real-life conditions, the voltage will be lower due to losses in the cell, which will be discussed next.

B-1-6 Efficiency and losses

For an ideally working fuel cell under isothermal conditions, the Gibbs free energy change of the reaction is completely converted into electrical energy, its maximum efficiency is given by Equation B.6. However there are multiple sources of fuel cell losses in practice, often called overpotentials. These overpotentials will lower the operating voltage of the fuel cell and are current dependent. A polarisation shows the relation between the cell voltage and the current. A typical polarisation curve can be seen in Figure B-4.

$$\eta_{max} = \frac{W_{max}}{\Delta H} = \frac{\Delta G}{\Delta H} \tag{B.6}$$

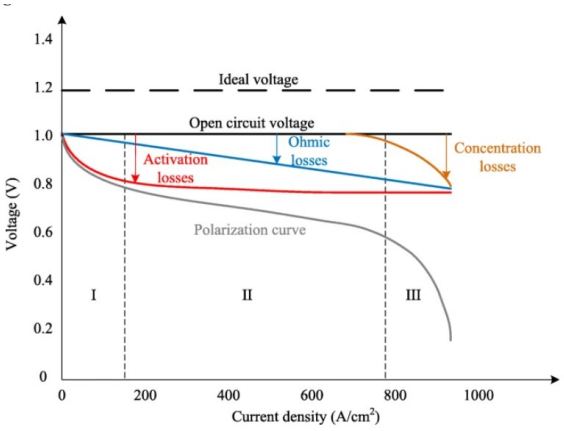

Figure B-4: Typical polarisation curve of a PEMFC. In grey the polarisation curve, in red the activation losses, in blue the ohmic losses and in yellow the concentration losses (Li et al., 2019).

Activation losses represent the slowness of the reaction taking place on the electrodes. A proportion of the generated voltage is lost in driving the electrons to or from the electrodes. These losses are the dominant losses of a fuel cell at low power (Larminie and Dicks, 2003).

Fuel crossover and internal currents: Generally, the electrolyte only conducts H^+ ions. In practice, a small amount of fuel and electrons can diffuse through the electrolyte. Voltage distributions due to imperfect cell composition can result in internal currents on the electrodes. Generally, the fuel loss due to fuel crossover and the internal current is small. However, it has a bigger effect on the OCV, being at least 0.3 V lower compared to the reversible voltage (Larminie and Dicks, 2003).

Ohmic losses: A voltage loss due to electric resistance of electrodes and other interconnections. Also, the resistance of the ions through the electrolyte membrane causes an ohmic loss. This loss is dominant in the middle part of the polarisation curve (Larminie and Dicks, 2003).

Concentration or mass-transport losses: These losses arise from the change in concentration of reactants at the surface of the electrodes. Insufficient concentration of reactants results in a larger voltage loss. This is the dominant loss at high power where mass transport capabilities are insufficient to supply reactants or collect the products for the reaction to take place efficiently (Larminie and Dicks, 2003).

BoP losses: The previously described losses only consider the losses inside the cell. The stack efficiency can be obtained by adding these losses. This is the efficiency of turning hydrogen into electric power. As earlier described, the fuel cell stack is not the only component of a PEMFC, the water pumps, compressors, controllers, etc., also draw power. Therefore, the total system efficiency is lower than the stack efficiency.

B-2 Degradation

The lifetime of the fuel cell is an important factor in the total cost of fuel cell operation. Over the lifetime, the previously described losses in the cell increase and efficiency drops, called degradation, resulting in higher fuel consumption. When the voltage loss becomes too large, the fuel cell has reached its end-of-life (EoL) condition, generally a performance loss of 10% is taken as the EoL condition (Ren et al., 2020). It is possible to use the fuel cell after the EoL condition. However, the power rating of the fuel cell can no longer be met. To mitigate the degradation mechanisms, a good understanding of the contributions to the overall ageing is important to see the relevance of mitigating each ageing mechanism. There are multiple sources of this degradation, and each cell component has different degradation mechanisms. Three loading conditions are often described to increase degradation substantially: load changing, start-stop cycling and idling. Each load condition has its own degradation mechanisms. Apart from the degradation due to the dynamic effects, ambient conditions also affects the degradation (Wu et al., 2008). These accelerating conditions are described next.

B-2-1 Ambient conditions

Impurities

Impurities in both the hydrogen and impurities in the air supply have a negative effect on fuel cell durability. Impurities such as ammonia can cause a lower proton conductivity of the MEA, which will increase the ohmic losses. Foreign substances can also decrease the mass transport capabilities of the GDL. Ending the introduction of the impurities, or recovery procedures may end the performance loss but it can also be permanent (Borup et al., 2007). The most common fuel impurities are Co, ammonia, hydrogen sulfide, hydrogen cyanide, hydrocarbons, formaldehyde, and formic acid (Borup et al., 2007). Fuel cell manufacturers often state the hydrogen purity requirement in the manufacturing sheet. The hydrogen that is considered in this research is made by electrolysis and not by natural gas reforming. Therefore, the purity of hydrogen is less of an issue. The most common air impurities are sulfur dioxide, nitrogen oxides, and particulate matter (Borup et al., 2007). These previous mentioned air impurities are also emitted by ICEs in ships, which could result in problems for hybrid ships that both use ICE and fuel cells.

Temperature and humidity

Both the temperature and the relative humidity (RH) of the fuel and air affect the durability of the fuel cell. The temperature and humidity of the cells are dependent on the operational conditions and are therefore not considered in this section. Humidifiers often increase the air and hydrogen of large-scale fuel cells and are therefore not dependent on the ambient conditions. However, sub-zero conditions can lead to fuel cell freezing which can lead to enhanced degradation. The nafion membrane inside the MEA contains water. It is reported that there are two states of water, chemically bounded to the nafion membrane and free water. This free water is prone to freezing at sub-zero temperatures while the bounded water does not freeze until -120°C. A fuel cell is often capable of self-starting at sub-zero temperatures. However, start-up during sub-zero conditions can lead to more severe degradation. Freezing is reported to cause adverse effects on the membrane. Also, it is reported that the mass transport properties of the GDL can change from freeze/ thaw cycles (Borup et al., 2007).

B-2-2 Operating conditions

The degradation contributions of load changing, start-stop cycling, idling, and high power were 56.5%, 33.0%, 4.7%, and 5.8%, respectively, for a fuel cell bus according to Pei et al. (2008). With start-stop cycling and load changing being dominant. Therefore these conditions are described more in-depth in the following sections.

Load cycling

In mobile applications, load changes happen regularly; due to acceleration and deceleration of the vehicle or vessel, the required power changes. Load changing is the harshest load condition of fuel cells, according to Ren et al. (2020). These load changes result in degradation due to multiple mechanisms, with the main causes: mechanical stress, potential cycling, and fuel starvation.

The fuel cell is relatively cold and wet at low currents and hot and dry at higher currents. Due to the load changes, the temperature and water content of the membrane change over time.The ionomer membrane swells with water uptake, this can cause stresses during cycling between high and low current because of the expansion and contraction of the ionomer due to the difference in humidity. These stresses contribute to mechanical failure of the membrane (Ren et al., 2020).

Load changes result in a fluctuating cell potential, generally between 0.6 V and 1 V (Borup et al., 2007). The anode will stay fairly close to the reversible hydrogen potential; therefore the potential of the cathode changes. When the potential rises quickly platinum can dissolve until a protective oxide layer is formed. This dissolution of the catalyst will lower the ECSA and increase the activation losses (Borup et al., 2007).

Mobile applications require relatively high power. Therefore, the fuel cell stacks consist of up to hundreds of cells in series with large area cells. Because the cells are connected in series, they must carry the same current as the neighbouring cells. When there is not enough fuel to support the current in a particular cell this can lead to fuel starvation, which can lead to the oxidation of the carbon support and the associated loss of ECSA due to the detachment of platinum particles (Borup et al., 2007). This lack of reactants can be caused by a sudden increase in the power demand. The mass transport capabilities of the cell might not be sufficient to directly follow the new demand (Ren et al., 2020). When a cell does not have enough fuel to support the current from the neighbouring cells the cell potential will rise until oxidation occurs at the carbon support leading to permanent damage (Borup et al., 2007). Similar to the previously described fuel starvation, there is a process called local fuel starvation. Cells with a large active area will have different fuel, air and coolant conditions on the inlet and outlet of the cell. Besides, small blockages in the flow channel due to water condensation can lead to areas with less fuel. Also, manufacturing errors in the flow channels lead to different fuel conditions across the cell. For regions where enough fuel is present, there is no problem. However, for locations on the cell where not enough fuel is present, the potential difference induced by the active, well-fueled part of the cell must still be established while maintaining the current. This can lead to a local reversed current, a current in the opposite direction to the current of the rest of the cell. The hydrogen reaction that occurs in the rest of the cell cannot sustain this reaction, the reaction that can facilitate this reverse current is the carbon corrosion reaction. Again, this carbon support corrosion leads to platinum dissolution and loss of mass transport capabilities (Borup et al., 2007).

Steady-state

This section investigates fuel cell degradation due to steady state operation. The idling and high power conditions will be separately investigated.

Idling, running the fuel cell with a close to zero power output will result in a high potential at the cathode because the current-related voltage losses are small. This high cathode potential will result in accelerated catalyst decay and the associated loss of ECSA (Ren et al., 2020). Due to the absence of gas consumption at low current there is a higher partial pressure of the reactant in the electrode. This will increase oxygen permeation to the anode, forming a hydrogen-oxygen interface which can lead to the formation of radicals (Ren et al., 2020). Chemical degradation is one of the major causes of fuel cell failure and said to be higher during idling (Ren et al., 2020). Hydroxyl or peroxy radicals are thought to attack polymer groups of the membrane. Also, hydrogen peroxide (H_2O_2) is thought to be formed during the oxygen reduction reaction and due to oxygen crossover, which can degrade the polymer membrane. The exact pathway of chemical degradation is still being researched. However, it is clear that it plays an essential role in membrane degradation (Bruijn et al., 2008).

High power, running the fuel cell close to the maximum rated capacity, can lead to multiple mechanisms that affect the fuel cell's durability. A large amount of water is formed at the cathode side of the cell at high power. This water must be transported out by the GDL. When the water transport capabilities of the GDL are insufficient, the fuel cell can be flooded. Due to the excess water, the required oxygen can no longer be supplied, leading to oxygen starvation and the resulting corrosion of the GDL and loss of ECSA (Ren et al., 2020). Besides, hot spot formation is thought to be present during the high power condition (Ren et al., 2020). A hot spot is a micro crack, or pinhole, in the membrane where oxygen can permeate through to the hydrogen, which causes an exothermic reaction. This exothermic reaction can worsen the pinhole creating a positive feedback mechanism (X. Zhang et al., 2017).

Start-stop

One of the main degradation mechanisms of fuel cells is start-stop cycling (Pei et al., 2008). The main contribution is the presence of a hydrogen-air interface (T. Zhang et al., 2018), resulting in a high cathode potential and oxidation of the carbon catalyst carrier. Due to this corrosion, the platinum catalyst can fall off the carbon support, decreasing the ECSA. When the fuel cell is turned off, air from the exhaust diffuses to the anode due to the concentration difference. When the fuel cell is turned on again, hydrogen will be supplied at the anode, leading to a reactive hydrogen-oxygen interface and a high cathode potential. Ettinghausen et al. (2011) pointed out that for long-term performance, carbon corrosion is more harmful than the dissolution of platinum. Carbon corrosion leads to a loss of the structural integrity of the porous electrode, which leads to lower mass transport properties because the porosity decreases. This loss of mass transport capability increases the concentration and mass transport losses (Ettingshausen et al., 2011).

Overview

In Figure B-5 a simplified overview of the degradation mechanisms of the operating and ambient conditions is given.

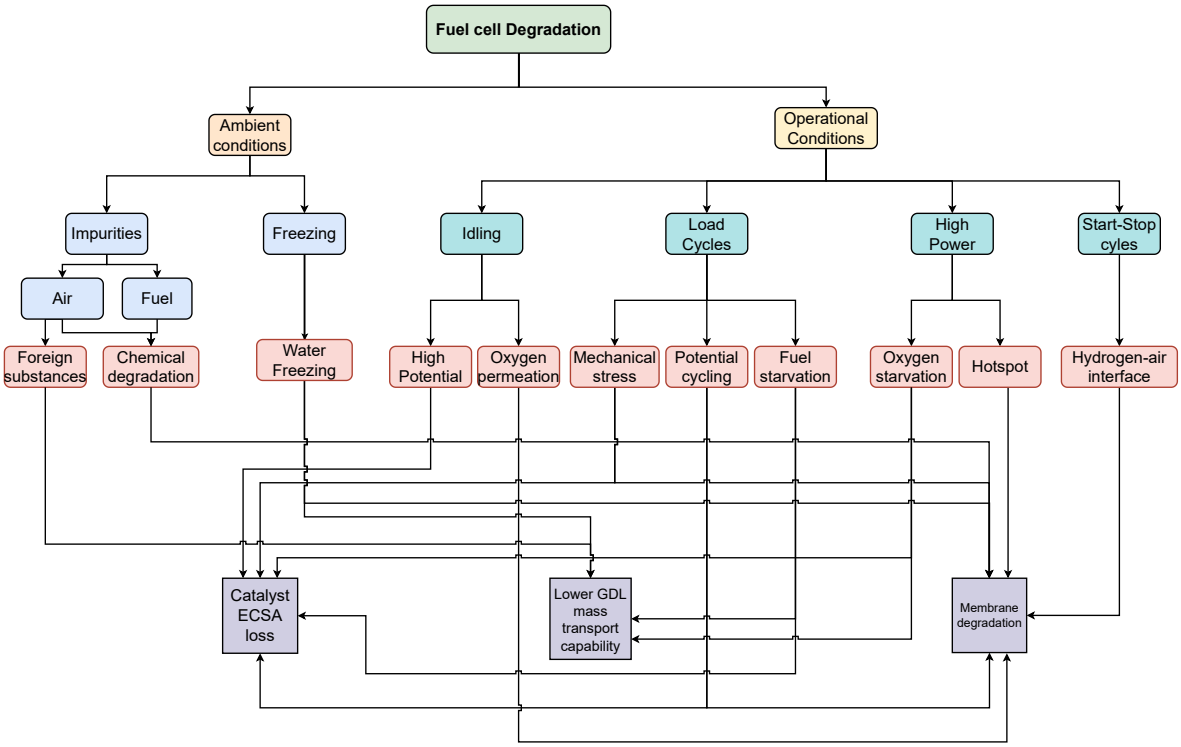

Figure B-5: Overview of the degradation mechanisms of operational and ambient conditions.

B-3 Degradation Mitigation

Fuel cell degradation mitigation can be performed on multiple levels. First, degradation can be mitigated by better cell design: more durable membranes, more stable catalyst, better flow field design, etc. Also, degradation mitigation can be done by controlling the BoP of the fuel cell, for example, changing the stoichiometric ratios of fuel and air prior to a load change to prevent fuel starvation. Fuel cell design and BoP control is not in the scope of work. Therefore, the focus will be on fuel cell degradation mitigation by reducing transient loading through temporary energy storage systems. In the following subsections, a strategy to mitigate degradation is investigated. First, the operational profile of the CTV is investigated to see how the operational profile of the CTV enhances the degradation.

B-3-1 Operational Profile

During operation, the CTV sails to many turbines each day to transfer the technicians to the turbines, resulting in a large amount short trips each day. The power demand often changes often during transfer: high power during the transit, reducing the power to approach the turbine and afterwards increase the power again during transfer, etc. Often more than fifteen of these transfer operations are performed each day. These power fluctuations result in high degradation due to load changes. Also, the CTV is on standby multiple times each day. Switching off the fuel cell each time the CTV is on standby would drastically shorten the lifetime as start-stop cycling is one of the major sources of degradation. However, leaving the fuel cell on for several hours with no power demand leads to high degradation due to idling. In either case, the degradation due to these standby times results in enhanced degradation.

B-3-2 Load changing mitigation and cost

To mitigate load changes, fuel cells are often combined with batteries, decreasing the number of load changes by supplying power during peak loads. This peak-shaving also results in a smaller fuel cell. The battery is charged during moments where the required energy is small, e.g. when the CTV is on standby. Mitigating idling and start-stop fuel cell degradation. In this section, an estimate is made to see whether it is beneficial to use a battery to account for load changes, by comparing the cost of a load change of the battery and fuel cell. The energy losses of the battery are not considered in the evaluation. It is expected that the battery losses are compensated by the increased efficiency of running the fuel cell at a lower power output. The efficiency of a fuel cell at low power can be as high as 60% compared to values below 45% at high power. The costs of two methods to account for a load change are compared. First, the fuel cell increases power or second, the battery supplies the additional load. As an example, the load change due to a transfer operation is considered. During such operations, the CTV approaches the turbine at low speed until the bow of the CTV touches the turbine. Then, engine power is increased to keep the CTV steady for crew transfer. We assume that a power of 500 kW is needed for the transfer operation and 50 kW of power is used during the approach, a load increase/decrease of 450 kW. The values used in the following sub-sections are shown in Table B-1.

	Value
Fuel cell price	1500 €/kW
Battery price	500 €/kWh
Maximum LFP battery cycle life	3000
Degradation due to a fuel cell load cycle	1 μV
Installed fuel cell capacity	600 kW
Load duration	5 min

Table B-1: Values used in battery and fuel cell load cycle cost evaluation

Fuel Cell

Fuel cell load cycle cost, C_{cycle_B} is based on 1 μV per cycle from idle to full power. It is assumed that the degradation due to a load cycle is proportional to the cycle's amplitude. Half a cycle, from idle to 50%, results in half the degradation. Therefore, the degradation due to the load change is multiplied by the amplitude of the load change divided by the installed power, 450 kW/P_{FC}. Based on the above criteria the cost related to one load cycle is calculated using Equation B.7. With, $C_{cycle_{FC}}$, the cost due to the load cycle of the fuel cell, $P_{FC_{installed}}$ the installed fuel cell capacity, and d_{cycle} the voltage decay of one full load cycle in μV, d_{EoL} the fuel cell EoL criteria of 10% loss at a voltage of 0.7 V, resulting in 70.000 μV. Based on this calculation, the cost of one cycle due to the transfer operation becomes €9.60.

$$C_{cycle_{FC}} = C_{FC} * P_{FC_{installed}} * \frac{d_{cycle}}{d_{EoL}} * \frac{350}{P_{FC}} \tag{B.7}$$

Battery

The battery degradation cost due to the energy throughput, C_{cycle_B} is calculated based on the maximum charge cycles of the battery. With EFC_B the equivalent number of discharge cycles, and Q_B the battery capacity. E_{cycle} is the energy supplied by the battery during one transfer operation, which is calculated by multiplying the required power by the duration. This results in battery degradation cost per cycle of €6.30.

$$C_{cycle_B} = C_B * \frac{E_{cycle}}{EFC_B * Q_B} \tag{B.8}$$

Sub-conclusion

From the previous calculations, it can be seen that the costs due to degradation are higher for the case where the fuel cell accounts for the load cycle as for the situation where the battery supplies the transient load. Besides the benefits of lower component degradation cost, using the batteries to mitigate the degradation due to start-stop cycling will further reduce the cost of operation. Therefore, the fuel cell will be combined with batteries in the concept of the fuel cell CTV. The fuel cell is used as a steady power source to supply the average energy demand and the battery is used to supply the energy during load transients.

B-4 Degradation modelling

Multiple possibilities exist to determine the lifetime of a fuel cell. For example, one can model the physical reactions that take place, for example, an ECSA dissolution model (Rinaldo et al., 2010). However, to get an accurate result, all (important) degradation mechanisms must be well understood, and it must be possible to quantify the reactions that are taking place.

This is however still a challenge as often models do not incorporate all the ageing effects. Also, due to a lack of experimental data, these models are hard to validate. For the purpose of lifetime estimation, which is the objective of this model in this research, the physical effects that are taking place are less important. More important is the degradation rate to determine the lifetime. For the above reasons, an empirical model will be made in this research. An example of an empirical model is the model of Pei et al. (2008). In this model, the cell voltage loss is described as a function of the individual ageing parameters: number of start-stop cycles, time at high power, time at idling and number of load changes. The parameters for these ageing mechanisms are obtained from literature. However, it is still challenging to obtain reliable information, as research often does not consider all the degradation effects. Therefore, information from multiple studies is combined, with different fuel cells and test environments. From Table-C-1 it can be seen that degradation rates deviate a lot between different studies. Because of the long duration of such research and high fuel cell prices, experiments are costly and are therefore performed on single cells or small kW range stacks. Therefore, the results of these studies are not necessarily true for large-scale fuel cells. Borup et al. (2007) pointed out that stacks in the order of several hundred square centimeter will experience different conditions between the inlet and outlet of the cell, which could lead to fuel distributions which cannot be tested in sub-scale experiments. Therefore, the degradation due to load changing might be worse on large marine fuel cells than on the small tested fuel cells.

B-5 Fuel cell size

From Fig. 4-6 it can be seen that the efficiency of the fuel cell decreases with increasing power. When sizing the fuel cell, one must make a choice between fuel cell efficiency and CAPEX of the fuel cell. Operating the fuel cell at a lower power would require more installed capacity. However, the hydrogen cost would be lower due to increased efficiency. To obtain the lowest LCoE, three important factors play a role if one would neglect additional maintenance costs due to increased system size: 1) the hydrogen price, 2) fuel cell system cost 3) the lifetime of the fuel cell. With these three parameters, the LCoE can be calculated using Equation. B.9.

$$LCoE = \frac{C_{H_2} + C_{FC}}{E_{Produced}} \tag{B.9}$$

The cost of hydrogen per kWh is calculated by dividing the cost in €/kg by the produced energy from one kg, which is the LHV of hydrogen multiplied by the fuel cell efficiency as a function of the power output η_{FC}. The efficiency is the fuel cell efficiency corresponding to the power of the fuel cell at which it is operated, as can be seen in Figure 4-6.

$$C_{H_2}[€/kWh] = \frac{C_{H_2}[€/kg]}{LHV_{H2} * \eta_{FC}(P_{FC})} \tag{B.10}$$

The fuel cell system cost per kWh produced energy can be calculated by dividing the cost of the fuel cell system by the amount of energy produced. The produced energy can be

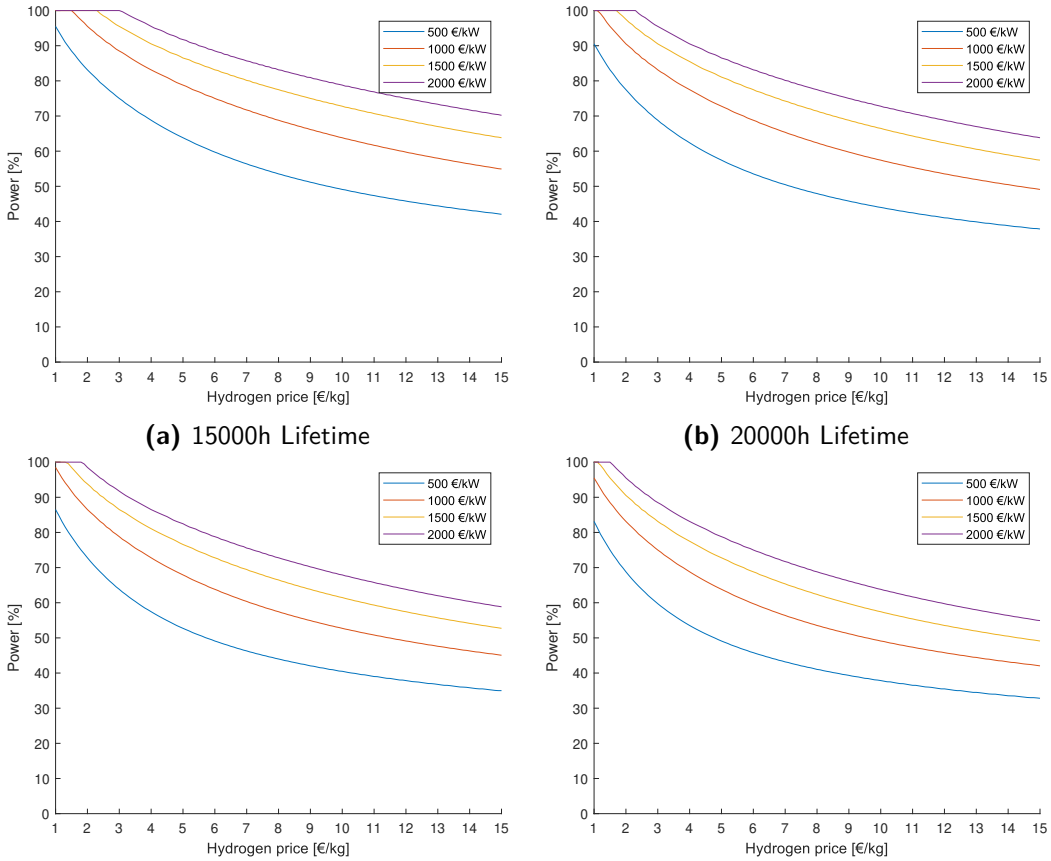

(a) 15000h Lifetime **(b)** 20000h Lifetime

(c) 25000h Lifetime **(d)** 30000h Lifetime

Figure B-6: Optimal fuel cell operating power for the lowest LCoE, produced by a fuel cell operating at a constant power, as a function of the hydrogen price for different lifetimes of the fuel cell and different fuel cell prices.

calculated by the lifetime of the fuel cell in hours multiplied by the power of the fuel cell (P_{FC}). The cost of the fuel cell is defined per kW of installed capacity, the maximum value of P_{FC} is therefore 1 kW.

$$C_{FC}[€/kWh] = \frac{C_{FC}[€/kW]}{L_{FC} * P_{FC}} \tag{B.11}$$

Combining Equation B.9, B.10, and B.11 gives the total LCoE. Minimising Equation B.12 results in the operating power P_{FC} of the fuel cell system with the lowest LCoE.

$$LCoE = \frac{C_{H_2}}{LHV_{H2} * \eta_{FC}} + \frac{C_{FC}}{L_{FC} * P_{FC}} \tag{B.12}$$

From Figure B-6 it can be seen that the optimal operating point for the lowest LCoE changes with the lifetime of the fuel cell. Often when a fuel cell system is designed, the smallest fuel cell system is chosen to reduce the CAPEX e.g (TNO, 2019b). However, Figure B-6 shows

that this is not necessarily the best method to have the lowest cost over the entire lifetime. The above optimal fuel cell power is only valid for a fuel cell that is operated at steady-state and when there are no differences in steady-state degradation rates for different power outputs.

C

Degradation rates

In this section, the the overall contributions of the ageing mechanisms are investigated from literature in an attempt to quantify the ageing mechanisms that take place. These degradation rates are used to calculate the lifetime of the fuel cell.

Start-stop cycles

Pei et al.(2008) performed experiments on a 100-cell PEM fuel cell stack with 280 cm^2 effective area. The size of the fuel cell is not stated but the high power condition of 100 A results in a cell voltage of 0.64 V, with 100 cells, results in a stack power of 6.4 kW at high the high power condition. A cell voltage decay of 0.00196 %/cycle was found at an operating voltage close to 0.7 V, resulting in 14 µV/cycle voltage decay. Qiu et al. (2015) investigated the impact of relative humidity cycles with intermittent start-stop cycles on a single cell. After 300 RH cycles and 40 start-stop cycles, the ECSA decreased by 48%, a very rapid decay. This higher degradation could be explained by the fact that tests are performed on a single cell instead of a complete stack. Hydrogen and oxygen crossover is one of the ageing mechanisms of start-stop cycles, it could be argued that this occurs more easily when the oxygen at the cathode only has to go through one cell to reach the hydrogen before a harmful reaction takes place. Zariksson (2011) found degradation rates of 69.7 µV/cycle and 92.5 µV/cycle for two different start and stop methods during single-cell experiments. Ettingshausen (2011) did a simulated start-stop cycle experiment where air intrusion at the cathode was mimicked for 500 cycles during single-cell experiments. An ECSA decay from 64.3 m^2 g^{-1} Pt at BoL to 19.3. A loss of roughly 80%, According to Wang et al. (2019) an ECSA loss of approximately 85% results in the EoL criteria of 10% performance loss. The value of 14 µV/cycle from Pei et al. (2008) is deemed the most representative for a large marine fuel cell of all degradation rates found.

Load cycling

Garcia-Sanchez et al. (2020) studied the degradation rate of three different load cycles and two steady-state degradation rates. The first cycle is a cycle between OCV and 0.2 Acm^{-2}, the second cycle between 0.2 Acm^{-2} and 1 Acm^{-2} and the third a complete cycle between OCV and 1 Acm^{-2}. The results of the experiments are displayed in Figure C-4. Interestingly, the highest degradation is obtained with a steady current density of 1 Acm^{-2} closely followed by a steady current density of 0.1 Acm^{-2}, which is not expected from the degradation mechanisms. According to the authors, this higher degradation is caused by membrane thinning when OCV was not included in the cycle. Bose et al. (2013) tested the 10 individual 50m^2 cells of a 100W fuel cell on cycling degradation. The results show variance between the degradation rates of the individual cells, with cells on the edges of the stack showing the highest degradation. After 480 hours of cycling, the average ECSA decrease was 42%, the stack voltage decreased by 2.8%, and the individual cell voltage was decreased up to 8%. During the 480h experiment, 4700 cycles were performed, resulting in an average decay rate of around 4μV. This however, also includes the degradation due to steady operation. Wang et al. (2018) studied the degradation behaviour on a stack made up out of 10 cells with an area of 330 cm^2. The stack was cycled between 25 $mAcm^{-2}$ and 600 $mAcm^{-2}$, after the stack voltage reached the steady-state, the stack current was held for 30s. The reported degradation rate was 1.0 V per cycle. Harzer et al. (2018) studied the degradation voltage loss due to cycling on 5cm^2 MEAs. The different tested load cycles are displayed in Figure C-2. The ECSA decay of these different load cycles are shown in Figure. C-3. It can be seen that the degradation at the triangular cycles: TW,TW-H, and TW-LUPL result in lower degradation compared to to the square wave. After 30000 TW cycles, the cell voltage decreased by roughly 0.04 V at 1 A/cm^2, or 1.3 μV/cycle. This is in the same order of magnitude of the results obtained in the research of Wang et al. (2018). From the previously discussed studies, it can be seen that degradation rates obtained from the experiments are very different, a value of 1 μV/cycle from Wang et al. (2018) is used in this research.

steady-state

In this section, we will discuss the degradation from a steady power demand. Rinaldo et al. (2010) made a physical model to describe the ECSA decay related to platinum dissolution and Pt nanoparticle size distribution. This model was then used by Y. Wang et al. (2019) to model the ECSA loss over time as a function of potential. The normalised ECSA decay for 5000 hours can be seen in Figure C-1. As expected, it can be seen that for higher potentials, the ECSA decay rate is much higher. Although this gives a good understanding of how the dissolution of platinum depends on the voltage, it does not give a complete picture as the degradation due to steady-state operation because only Pt dissolution is taken into account and not other effects such as membrane degradation. In the research of Pei et al. (2008) both the the degradation due to high power and idling are investigated. The performance decay

due to high power and idling are 0.00147 %/h and 0.00126 %/h, respectively. Which are in the same order of magnitude. If one would only look at degradation due to dissolution as described in the research of Y. Wang et al. a much lower performance degradation is expected for the high power condition. However, the degradation rate is higher for the high power condition. Indicating that other degradation rates besides platinum dissolution cannot be neglected. De Bruijn et al. (2008) reviewed long-term steady-state degradation rates. The results of the review can be seen in Table C-1. The first three degradation rates from Table C-1 are performed on a stack with a membrane thickness of 125 μm and show significantly less degradation compared to the other experiments with membranes between 25 μm and 50 μm. This indicates that also factors such as membrane degradation influences the durability. Besides, the RH and cyclic versus steady-state looks to greatly impact the durability from the results seen in Table-C-1. In accelerated membrane durability test performed by Macauley et al. (2016) the cell voltage was an important ageing factor for chemical membrane degradation. In conclusion, the cell voltage seems to be the largest influence on both the ECSA loss and chemical membrane degradation, the two main contributors to steady-state fuel cell degradation. The first three values of Table C-1 are used in the rest of this work.

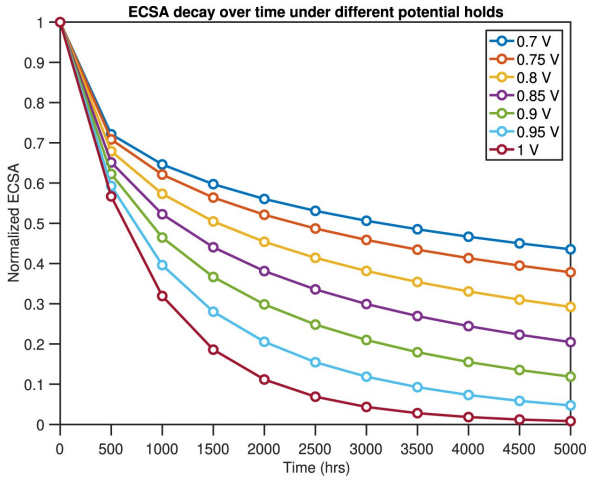

Figure C-1: Decay of normalised ECSA under different potentials over 5000 hours (Y. Wang et al., 2019).

Voltage decay μ h^{-1}	**Cell T** [°C]	**RH ano.** [%]	**RH cat.** [%]	**Voltage** [V]	**Current density** [J/ mA cm^{-2}]	**OCV in cyclee**	**Cyclic/SS**	**Membrane thickness** [μ m]
1	75	100	100	0.62	1,076	No	SS	125
1.4	75	100	100	0.82	538	No	SS	125
1.3	75	100	100	0.78	861	No	SS	125
1.5	75	57	74	0.7	259	No	SS	??
2.5	70	100	100	Cyclic	150-300	No	Cyclic	??
6	75	100	100	0.7	Not given	No	SS	36
6.4	70	100	100	0.62	800	No	SS	35
20	80	100	100	OCV	0	Yes	SS	25
25	80	100	100	0.77	200	No	SS	25
28	80	26	26	0.7	300	No	SS	??
29	80	26	26	0.7	300	No	SS	??
33	80	255	100	0.62	550	No	SS	50
2.5-50	75	80	80	0.66	300	No	SS	50
45	55	20	20	0.6-0.35	0-700	Yes	Cyclic	35
75	120	50	50	0.75	200	No	SS	??
75-114	80	26	26	0.7	0.01-300	Yes	Cyclic	??
95	55	20	20	0.59	500	No	SS	35
180	80	100	100	0.66	1,060	Yes	SS	50
210	80	26	26	0.7	0.01-300	No	Cyclic	??
Failure	80	100	100	Cyclic	Cyclic	Yes	Cyclic	50

Table C-1: A review of voltage decay rates in long-term PEMFC experiments, in increasing order of decay rate. Performed by de Bruijn et al. (2008)

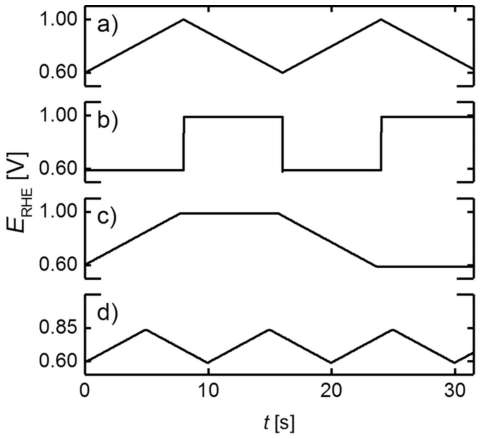

Figure C-2: Voltage profiles used in the voltage cycling experiment of Harzer et al.(2018). Respectively. a) Triangular wave (TW) between 0.6 and 1.0. b) square wave (SW), with a hold time of 8 s a 0.6 V and 1.0 V. c) Triangular wave with 8s potential hold at the 0.6V and 1V (TW–H); d) Triangular wave between 0.6 V and a lowered upper potential limit (TW–LUPL) of 0.85V.

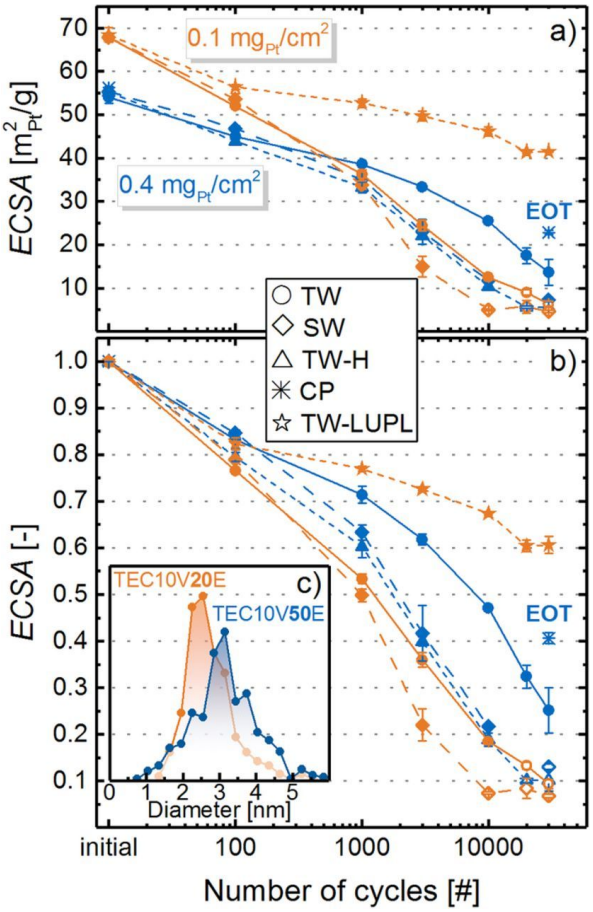

Figure C-3: Experimental ECSA measurements from the research of Harzer et al.(2018). Platinum loadings of 0.4 mg Pt/cm^2 are indicated with the blue symbols, and loadings of 0.1 mg Pt/cm^2 with orange symbols. The single point labelled CP, the blue star symbol placed at 30000 cycles depicts the ECSA after an 8-hour hold at 1.2 V_{cell},(Harzer et al., 2018).

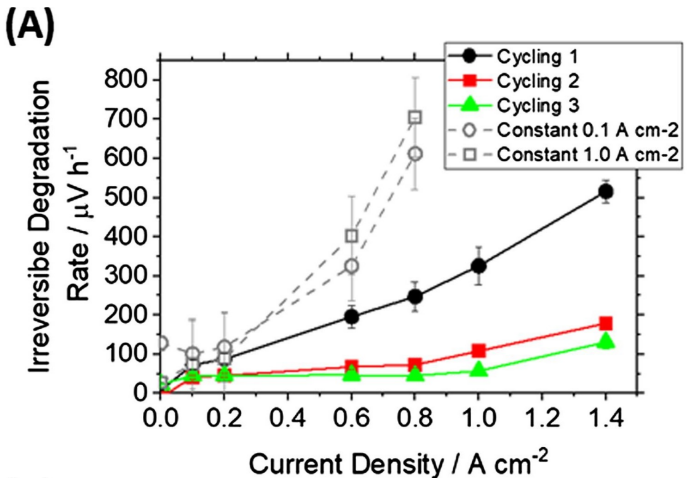

Figure C-4: Experimental results of the degradation study of Garcia-Sanchez et al.(2020).

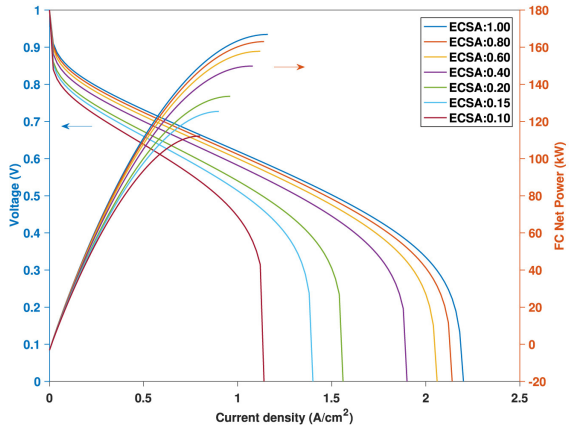

(a) Effect of diminishing ECSA on the polarization curve and fuel cell net power over time.

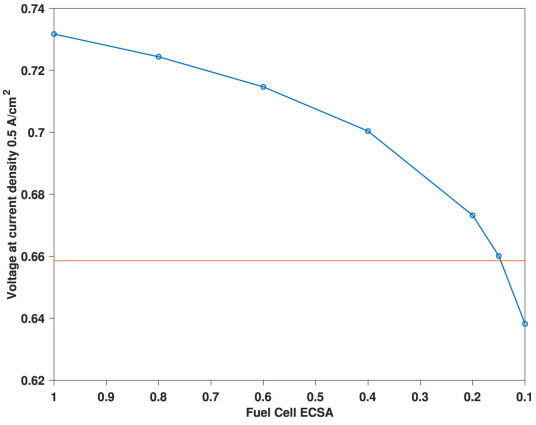

(b) Effect of diminishing ECSA on the voltage drop at 0.5 A/cm^2.

Figure C-5: Relationship between cell voltage and normalised ECSA values from the work of Wang et al. (2018).

D

Verification

To verify the results of the calculations performed by the model, a simple load profile is used. In this way the results that come out of this model can be predicted beforehand and compared to the model's outcome. The load profile used is a constant power of 1000 kW for one hour followed by a one-hour standby period and afterwards a one-hour transit back at 1000 kW.

Verification calculations

For the constant power load profile the total consumed energy can be calculated as follows.

$$E_{emotor} = 2 * \frac{1000}{\eta_{emotor}} = 2173.9kWh \tag{D.1}$$

The total used electricity for for Concept 2, 2A and 2B is as follows.

$$E_{elect} = \frac{E_{emotor}}{\eta_B} = 2415.5kWh \tag{D.2}$$

The battery capacity for Concept 2 is calculated based on the used capacity (95%-10% SoC) of the battery and the electric energy usage by the electric motor as follows:

$$Q_{B_{C2}} = \frac{E_{emotor}}{0.95 - 0.1} = 2557.5kWh \tag{D.3}$$

For Concept 3 the used fuel can be calculated with the ICE efficiency and the LHV of the fuel. As an example hydrogen is used.

$$m_{H_2} = 2 * \frac{1000}{\eta_{ICE} * LHV_{H_2}/3.6} = 162kg \tag{D.4}$$

The system dimensions and fuel and electricity consumption of the other concepts are hard to calculate beforehand therefore the outcome will be verified afterwards.

Simple load profile results

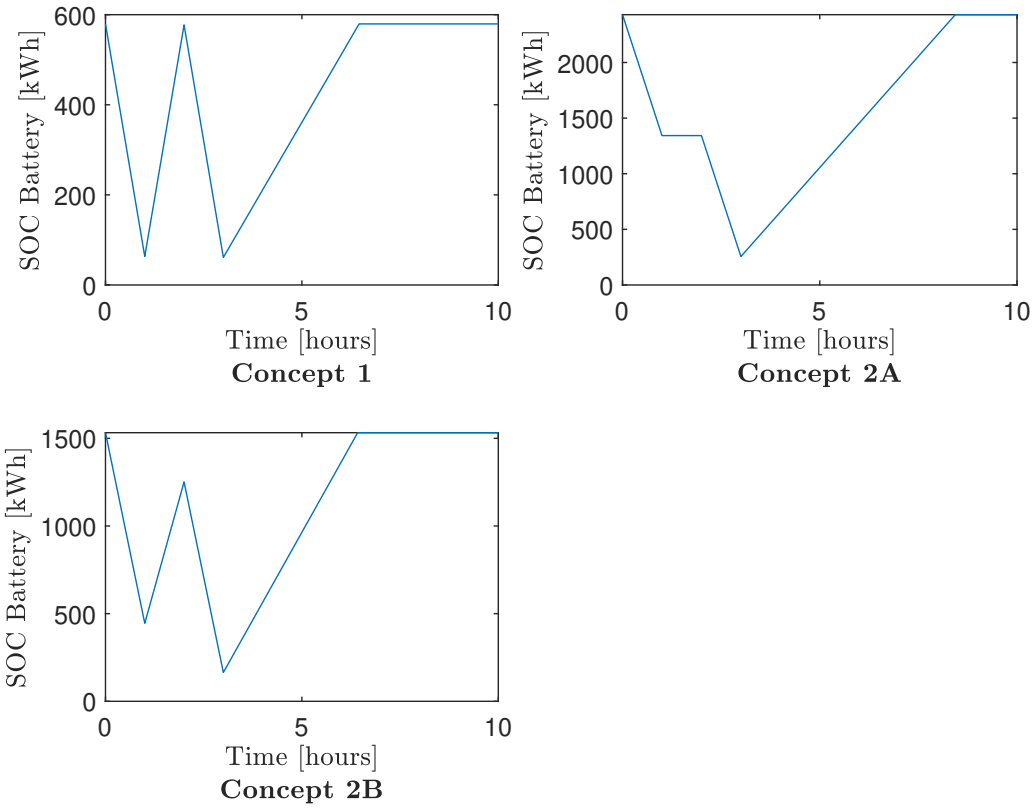

Figure D-1: SoC of Concept 1, Concept 2A, and Concept 2B for the load profile used for verification.

	Fuel				System			
	Elect. [kWh]	HVO [kg]	H2 [kg]	MeOH [kg]	Battery [kWh]	Fuel cell [kW]	ICE [kW]	GEN [kW]
Concept 1	576	0	113	0	610	628	0	0
Concept 2A	2416	0	0	0	2558	0	0	200
Concept 2B	2416	0	0	0	1613	0	0	200
Concept 3A	0	515	0	0	0	0	1176	0
Concept 3B	0	0	162	0	0	0	1176	0
Concept 3C	0	0	0	978	0	0	1176	0

Table D-1: Fuel consumption and component sizes for the verification load profile

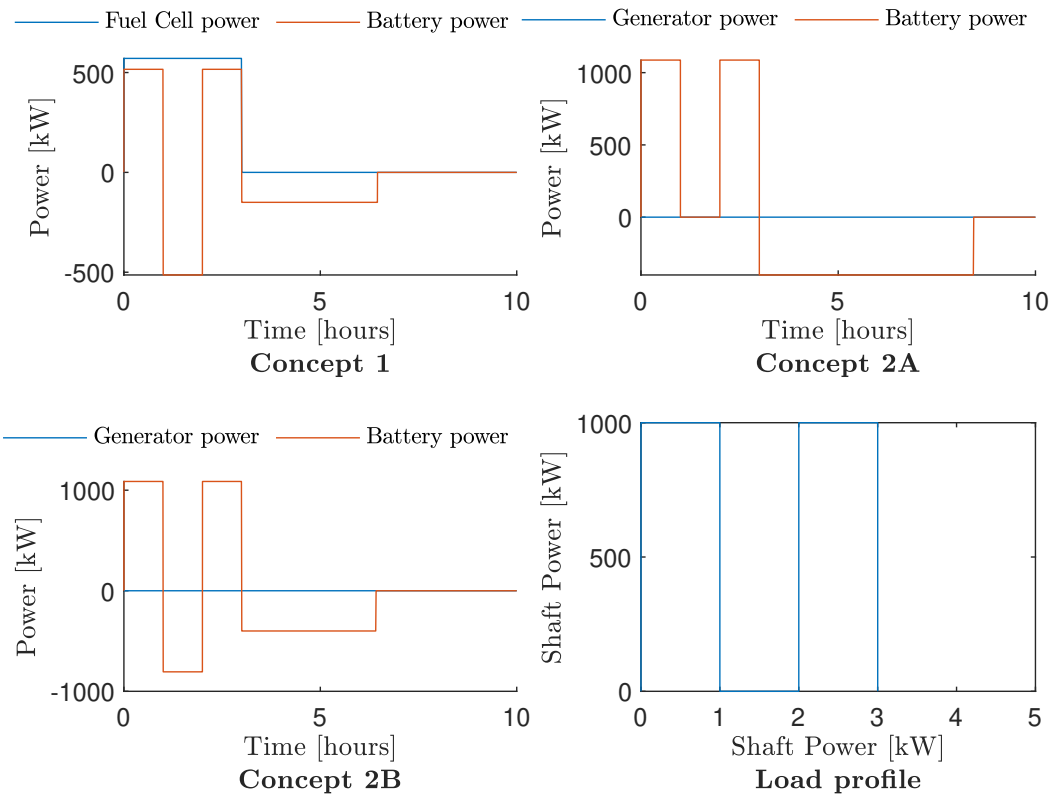

Figure D-2: Fuel cell, battery, and generator power of Concept 1, Concept 2A, and Concept 2B for the load profile used for verification.

Calculations

From Table D-1. It can be seen that the battery has a capacity of 628kW. The supplied energy of the battery can be calculated as follows

Concept 1

$$E_{bat} = Q_B * (0.95 - 0.1) = 518.5 \tag{D.5}$$

The fuel cell is sized using the 1.1 safety factor for installed power. The average fuel cell power is then:

$$P_{avg} = \frac{P_{FC_{installed}}}{1.1} = 570.9 \tag{D.6}$$

The supplied energy by the fuel cell is then:

$$E_{FC} = 3 * P_{avg} = 1712.7kWh \tag{D.7}$$

The total supplied power from the battery and fuel can then be calculated.

$$E_{tot_{C1}} = E_{FC} + E_{bat} = 518.5 + 1712.7 = 2231.2 \tag{D.8}$$

The electric losses of the battery storage during the 1 hour standby can be calculated as follows.

$$E_{B_{loss}} = 1 * P_{avg} * (1 - \eta_B) = 57.1 \tag{D.9}$$

The total energy can then be calculated as follows.

$$E_{used} = E_{tot_{C1}} - E_{B_{loss}} = 2231.2 - 57.1 = 2174.1 \tag{D.10}$$

E_{used} is approximately equivalent to E_{emotor}. Which verifies the calculation of the model. The slight error can be explained by the fact that the rounded value for the fuel cell size is used to calculate P_{avg}.

The fuel cell is around 50% efficient at 90% power output at beginning of life as can be seen in Figure 4-6. With the factor 0.95 for the fuel cell efficiency at half life, and 0.98 the converter efficiency. The hydrogen consumption can then be calculated as follows.

$$m_{H_2} = \frac{E_{FC}}{\frac{LHV_{H_2}}{3.6*0.5*0.95*0.98}} = 110.4kg \tag{D.11}$$

Which is about the same as the hydrogen consumption from Table D-1.

Concept 2B

From Table D-1 it can be seen that the battery from Concept 2B is 1613 kW. The total energy from the offshore charger can then be calculated as follows.

$$E_{charger_{OC}} = Q_B * C_{rate_OC} * t = 1613 * 0.5 * 1 = 806.5kWh \tag{D.12}$$

The usable capacity of the battery is calculated as follows.

$$E_{B_{use}} = Q_B * (SoC_{max} - SoCmin) = 1613 * (0.95 - 0.1) = 1371.05kWh \tag{D.13}$$

The total energy from the battery of Concept 2B is then calculated as follows.

$$E_B = E_{B_{use}} + E_{charger_{OC}} = 1371.05 + 806.5 = 2177.55kWh \tag{D.14}$$

Which is roughly the same as the used electricity by the electric motor, E_{emotor}. The difference can be explained by that in the model the battery is not discharged to a SoC of exactly 10%. Which, is indeed the case if the minimum SoC is investigated in the calculations, the minimum SoC is 164.5 instead of 161.3 kWh. This leaves a residual error of 0.4 kWh. What is considered sufficiently accurate for the this research purpose.

Sub-conclusion

From the previous sections it can be seen that the outcome of the model with the simplified load profile is indeed the same as what can be expected from the manual calculations of the component size and fuel calculations.

E

Emissions

In order to identify the environmental benefits of the alternative fuel options the the life cycle emissions are investigated in this section. In the following section GHGs are investigated. Because, different substances have different contributions to global warming, the emissions are expressed in CO_2 equivalent so that the individual contributors can be added. This is done using the global warming potential (GWP) on a 100-year timescale. In Table E-1 the GWP multiplication factors of different GHGs can be seen.

GHGs	**Time horizon of 100 years**
Carbon dioxide (CO_2)	1
Methane (CH_4)	25
Nitrous oxide (N_2O)	298

Table E-1: GWP multiplication values on a time horizon of 100 years to calculate the CO_2 equivalent GHG emissions

Fuel emissions

To determine the life-cycle emissions different phases are considered. First, the WTT emissions are the GHGs emitted during the production of the fuel. This normally includes the extraction of raw materials, fuel production, fuel compression for storage, and transporting the fuel. However, it is a challenge to obtain the correct values for the emissions during the transportation phase as life-cycle assessment studies from literature investigate different locations, therefore transportation emissions are not included. Next are the TTW emissions, the emissions from combustion of the fuel. The combined WTT and TTW emissions are the WTW emissions. For both WTT and TTW in CO_2 equivalent are based on a kWh of fuel. The reported values found online and in articles are often described in different units, e.g. in g CO_2-eq/kg fuel, to transfer this to g CO_2-eq/kWh of fuel, the fuel properties of Table 2-1 are used. For the TTW emissions of fuels which capture and utilise CO_2 during the production phase of the fuel, the CO_2 emissions are not included as due to the capture of CO_2 during production the CO_2 emissions are net-zero.

Benchmark - MGO

To be able to compare calculate a reduction from the alternative fuel options MGO is taken as a benchmark, as this is the fuel used to date. Hwang et al. (2019) compared the WTT and TTW of MGO and LNG fueled vessels. Two different scenarios are investigated, the import of MGO from Saudi Arabia and import from the U.S. to Korea with respective WTT values of 126.7 and 151.2 g CO_2-eq/kWh. The TTW is reported to be 274 g CO_2-eq/kWh. From TNO (2020) the WTT of MGO is reported to be 51 g CO_2-eq/kWh and the TTW to be 270 g CO_2-eq/kWh. The WTT on the emission factor website (CO2 emissiefactoren, 2022), a WTT of 70 g CO_2-eq/kWh is found and a TTW of 267.5 is found. The TTW emissions are similar for all considered sources. However, the WTT values vary substantially due to the included transportation emissions for the imported MGO from from Saudi Arabia and the U.S.. As MGO is only used as a benchmark, and transportation emissions are not included in this work, the lowest reported WTT values are used, TTW 51 g CO_2-eq/kWh, and WTT 270 g CO_2-eq/kWh from TNO (2020).

Electricity

According to Banou et al. (2016) the GHG emission of electricity based on offshore wind energy is 11 g CO_2-eq/kWh and 7 g CO_2-eq/kWh for the onshore counterpart. This difference can partly be explained by the vessels used to operate the wind farm, hence the topic of this work. In an review by Dolan and Garwin (2012) the median of wind energy from 49 references was 12 g CO_2-eq/kWh, the same order of magnitude as the values reported by Banou et al. (2016). 12 g CO_2-eq/kWh is used in this work.

Hydrogen

Bhandari et al. (2014) did a review on LCAs of hydrogen production with electrolysis. The reported value for the WTT of hydrogen production with electrolysis using wind power is 970 g CO_2eq/kg H_2. Using the LHV of hydrogen this results in 29.1 g CO_2-eq/kWh. The reported value for green hydrogen using wind energy on the emission factor website (CO2 emissiefactoren, 2022) reports a simular value of 32.8 g CO_2-eq/kWh. To store the hydrogen it needs to be either compressed or liquefied, processes that also consume energy and therefore contribute to the GHG emissions of hydrogen. The U.S. Department of Energy (2009) reported a minimum energy consumption 2.2 kWh/kg for compression to 350 Bar with fast fill, 3.2 kWh/kg to 700 Bar with fast fill, and 7 kWH/kg for liquefaction of hydrogen. Using the LHV of hydrogen this respectively results in 0.066, 0.096, and 0.21 kWh of electricity per kWh of hydrogen. Using the WTT of electricity results in an additional GHG emission of 0.7 g CO_2-eq/kWh for compression to 350 Bar, 1.1 g CO_2-eq/kWh to 700 Bar and 2.3 g CO_2-eq/kWh for liquefied hydrogen. From the previous values it can be seen that compression and liquefaction have a relative small effect on the total GHG emissions of hydrogen compared to

the production value of 29.1g CO_2-eq/kWh if renewable electricity is used. However, in this calculation only the required energy is taken into account and not the equipment needed for compression or liquefaction. Besides, the boil off of liquid hydrogen is not considered. The GHG emissions of hydrogen production including compression or liquefaction is rounded up to 32 g CO_2-eq/kWh, due to the small difference in emissions from compression or liquefaction no distinction is made between them. As hydrogen does not contains carbon there are no TTW emissions.

Methanol

Uusitalo et al. (2017) investigated the emissions of methanol production with CO_2 captured from ethanol and ammonia plants and electricity from solar, wind, and nuclear power plants. WTT emissions of 13.6 g CO_2eq/MJ is reported using wind energy, which is equivalent to 49 g CO_2-eq/kWh . To verify this number the hydrogen cost used for methanol production is compared to the hydrogen cost for pure hydrogen production. With the values obtained from the SMART PORT (2020) report, the hydrogen cost are roughly 19 euros per GJ for hydrogen and 33 euro for green methanol. It is assumed that the hydrogen consumption is directly proportional to the hydrogen cost. If we scale the emissions from hydrogen production with this hydrogen consumption a value of 54 g CO_2-eq/kWh is found, which is in the same order of magnitude as the 49 g CO_2-eq/kWh from Uusitalo et al. (2017). A WTT of 49 g CO_2-eq/kWh is used for methanol in the the rest of this work.

HVO

Soam and Hillman (2019) investigated the WTT GHG emissions of HVO and bio-diesel from different kind of feed-stocks, purpose grown feed-stocks and residual feed-stocks. HVO from residual feed-stock has a significantly lower emission impact as purpose grown feed-stocks, 50 g CO_2-eq/kWh versus values ranging between 90 g CO_2-eq/kWh and 250 g CO_2-eq/kWh for purpose-grown feed-stock HVO. As described in the Alternative fuel Section purpose grown HVO is not considered due to deforestation. The WTT and TTW emissions from the emission factor website (CO2 emissiefactoren, 2022), are 28.5g and 3.9g CO_2-eq/kWh respectively. The average of the previous studies of HVO based on waste streams of vegetable oils is used, a WTT of 39 g CO_2-eq/kWh. For the TTW the value of 3.9 g CO_2-eq/kWh is taken (CO2 emissiefactoren, 2022). Within these TTW the CO_2 emissions are neglected because of relatively short cyclic behaviour of the carbon in the vegetable oil. During the grow of the crops the CO_2 is extracted from the atmosphere which is released again during combustion and therefore does not contribute to the global warming effect.

Overview

An overview of the WTT, TTW, and WTW emissions that will be used for the GHG calculations can be seen in Table 4-7.

	WTT	TTW	WTW
MGO	51	270	321
HVO	39	4.5	43.5
Wind energy	12	0	12
Hydrogen	32	0	32
Methanol	49	3.9	52.9

Table E-2: Overview of WTT, TTW, and WTW of different fuels in g Co2-eq per kWh of fuel.

Component production GHG emissions

The GHG emissions of the production of the various components of the power generating system and the fuel storage systems are considered in this section. Both the emissions of material production/extraction as the electricity during the production process are considered.

Simons and Azimov (2021) did a comparative LCA study on different power generating systems for heavy-duty transport applications. According to this study the GHG emission of the battery of a heavy-duty PEMFC-battery truck is 8511 kg CO_2-eq for a battery with a capacity of 75 kWh. This equals 114 kg CO_2-eq/kWh. For the production of a 190 kW fuel cell system a value of 8456 kg CO_2-eq was found, this equals 45 kg CO_2-eq/kW. Finally, for the production of a diesel engine with a similar size as the previous PEMFC a value of 8043 kg Co_2-eq/kW was found. This results in 42 kg CO_2-eq/kW. An overview of the results can be seen in Table 4-8. For the electric motor a permanent magnet synchronous machine (PMSM) is used for both the electric machine used for power generating as for the electric machine connected to the ICE in the genset. Nordelof et al. (2019) did an LCA on the production of various PMSMs. For a 100kW PMSM produced in Sweden a value of 520 kg Co_2-eq was found or 5.2 kg Co_2-eq/ kW. For the genset the combined GHG emissions of the ICE and PMSM is used, 47 kg CO_2-eq/kW.

Another large component is the fuel storage system. For compressed hydrogen strong carbon fiber storage tanks are needed. According to a study of Elgowainy et al. (2012) the production of a 350 bar compressed 5.6 kg hydrogen storage system resulted in 2210 kg CO_2-eq, 368 kg CO_2-eq per kg of hydrogen storage. In the Elgowainy et al. (2012) liquid hydrogen storage is not evaluated, the value of cryogenic compressed hydrogen storage is evaluated. For the production of a cryogenic compressed hydrogen storage tank a value of 260 kg CO_2-eq per kg of hydrogen storage was found. It is assumed that the carbon fiber wrap around the

Component	Unit	GHG	Source
ICE	kW	42	(Simons and Azimov, 2021)
Fuel cell	kW	45	(Simons and Azimov, 2021)
Lithium-ion battery	kWh	114	(Simons and Azimov, 2021)
PMSM	kW	5	(Nordelof et al., 2019)
Genset	kW	47	(Simons and Azimov, 2021, Nordelof et al., 2019)
Compressed hydrogen storage	kg	368	(Elgowainy et al., 2012)
Cryogenic hydrogen storage	kg	200*	(Elgowainy et al., 2012)

Table E-3: GHG emissions of different power generating system components in kg CO_2-eq per indicated unit. *Estimated based on the values for cryogenic compressed hydrogen storage

aluminium liner is the only difference between cryogenic compressed hydrogen storage and normal cryogenic storage. Subtraction results in a value around 200kg CO_2-eq per kg of hydrogen storage. The resulting values used in this research are displayed in Table E-3.

F

Additional results

Transit	Storage method		Transit	Storage method		Transit	Storage method		Transit	Storage method	
[km]	Concept 1	Concept 3B	[km]	Concept 1	Concept 3B	[km]	Concept 1	Concept 3B	[km]	Concept 1	Concept 3B
5	Compressed	Compressed	29	Cryogenic	Cryogenic	53	Cryogenic	Cryogenic	77	Cryogenic	Does not fit
6	Compressed	Compressed	30	Cryogenic	Cryogenic	54	Cryogenic	Cryogenic	78	Cryogenic	Does not fit
7	Compressed	Compressed	31	Cryogenic	Cryogenic	55	Cryogenic	Cryogenic	79	Cryogenic	Does not fit
8	Compressed	Compressed	32	Cryogenic	Cryogenic	56	Cryogenic	Cryogenic	80	Cryogenic	Does not fit
9	Compressed	Compressed	33	Cryogenic	Cryogenic	57	Cryogenic	Cryogenic	81	Cryogenic	Does not fit
10	Compressed	Compressed	34	Cryogenic	Cryogenic	58	Cryogenic	Cryogenic	82	Cryogenic	Does not fit
11	Compressed	Compressed	35	Cryogenic	Cryogenic	59	Cryogenic	Cryogenic	83	Cryogenic	Does not fit
12	Compressed	Compressed	36	Cryogenic	Cryogenic	60	Cryogenic	Cryogenic	84	Cryogenic	Does not fit
13	Compressed	Compressed	37	Cryogenic	Cryogenic	61	Cryogenic	Cryogenic	85	Cryogenic	Does not fit
14	Compressed	Compressed	38	Cryogenic	Cryogenic	62	Cryogenic	Cryogenic	86	Cryogenic	Does not fit
15	Compressed	Cryogenic	39	Cryogenic	Cryogenic	63	Cryogenic	Cryogenic	87	Cryogenic	Does not fit
16	Compressed	Cryogenic	40	Cryogenic	Cryogenic	64	Cryogenic	Cryogenic	88	Cryogenic	Does not fit
17	Compressed	Cryogenic	41	Cryogenic	Cryogenic	65	Cryogenic	Cryogenic	89	Cryogenic	Does not fit
18	Compressed	Cryogenic	42	Cryogenic	Cryogenic	66	Cryogenic	Cryogenic	90	Cryogenic	Does not fit
19	Compressed	Cryogenic	43	Cryogenic	Cryogenic	67	Cryogenic	Cryogenic	91	Cryogenic	Does not fit
20	Compressed	Cryogenic	44	Cryogenic	Cryogenic	68	Cryogenic	Does not fit	92	Does not fit	Does not fit
21	Compressed	Cryogenic	45	Cryogenic	Cryogenic	69	Cryogenic	Does not fit	93	Does not fit	Does not fit
22	Compressed	Cryogenic	46	Cryogenic	Cryogenic	70	Cryogenic	Does not fit	94	Does not fit	Does not fit
23	Compressed	Cryogenic	47	Cryogenic	Cryogenic	71	Cryogenic	Does not fit	95	Does not fit	Does not fit
24	Cryogenic	Cryogenic	48	Cryogenic	Cryogenic	72	Cryogenic	Does not fit	96	Does not fit	Does not fit
25	Cryogenic	Cryogenic	49	Cryogenic	Cryogenic	73	Cryogenic	Does not fit	97	Does not fit	Does not fit
26	Cryogenic	Cryogenic	50	Cryogenic	Cryogenic	74	Cryogenic	Does not fit	98	Does not fit	Does not fit
27	Cryogenic	Cryogenic	51	Cryogenic	Cryogenic	75	Cryogenic	Does not fit	99	Does not fit	Does not fit
28	Cryogenic	Cryogenic	52	Cryogenic	Cryogenic	76	Cryogenic	Does not fit	100	Does not fit	Does not fit

Table F-1: Hydrogen storage method of Concept 1 and Concept 3B

	Original profile	Second profile	Third profile	Foruth profile
Transit speed to/from windpark [kts]	19	19	19	19
Transit speed in windpark [kts]	12	12	12	12
Manouvring speed [Kts]	3	3	3	3
Average transit distance between trubines [m]	2000	1500	2500	2000
Average daily standby time [h]	3:30	2:30	4.45	3:30
Average transfer duration [min]	6	4	5	6
Average manoeuvring duration [min]	3	3	3	3
Days of operation per year	330	330	330	330
Power during transfer / push-on [kW]	500	600	400	600
Service teams	3	2	1	1
Nr. of turbines visited by service teams 1	1	1	1	1
Troubleshoot teams	2	2	3	1
Nr. of turbines visited by troubleshoot teams	3	3	3	3
Number of daily transfer operations	18	9	20	8

Table F-2: Values for additional 50 km transit operational profile

	5km				25km				50 km				75 km			
	Elect. [kWh]	HVO [kg]	H2 [kg]	MeOH [kg]	Elect. [kWh]	HVO [kg]	H2 [kg]	MeOH [kg]	Elect. [kWh]	HVO [kg]	H2 [kg]	MeOH [kg]	Elect. [kWh]	HVO [kg]	H2 [kg]	MeOH [kg]
Concept 1	915	0	67	0	793	0	168	0	806	0	247	0	494	0	366	0
Concept 2A	2104	0	0	0	2497	0	0	460	2303	0	0	1354	2109	0	0	2249
Concept 2B	2105	0	0	0	3487	0	0	0	5215	0	0	0	5780	0	0	541
Concept 3A	0	448	0	0	0	743	0	0	0	1111	0	0	0	1480	0	0
Concept 3B	0	0	141	0	0	0	234	0	0	0	350	0	0	0	466	0
Concept 3C	0	0	0	852	0	0	0	1412	0	0	0	2111	0	0	0	2811

Table F-3: Fuel consumption

G

Gripper system

Another possibility to reduce the emissions of a CTV is by reducing the fuel consumption. During the operation of a CTV a large part of the energy is consumed during the transfer operation. Because, a relatively high power is used to remain a no slip contact with the turbine for up to 15 minutes each transfer. With a large amount of transfers each day this results in a significant amount of the total energy. There are system that can grab the boat-landings, in this way the CTV does not have to remain trust during the transfer operation. An example system can be seen in Figure G-1. Besides reduced fuel consumption, this also increases the safety of the transfer as the risk of a slipping contact between the CTV and the turbine is reduced. If the average transfer duration is 5 min, 15 times a day, and 500kW of power is assumed for the transfer operation this system would reduce the energy consumption by 625kWh each day. With 330 days of operations each year this would result in an energy reduction of 2 GWh during a 10 year period, equivalent to 470t MGO with an engine efficiency of 37%, resulting in a large cost reduction. This would result in an GHG reduction of 1.9 million kg CO_2 equivalent within 10 years (CO2 emissiefactoren, 2022).

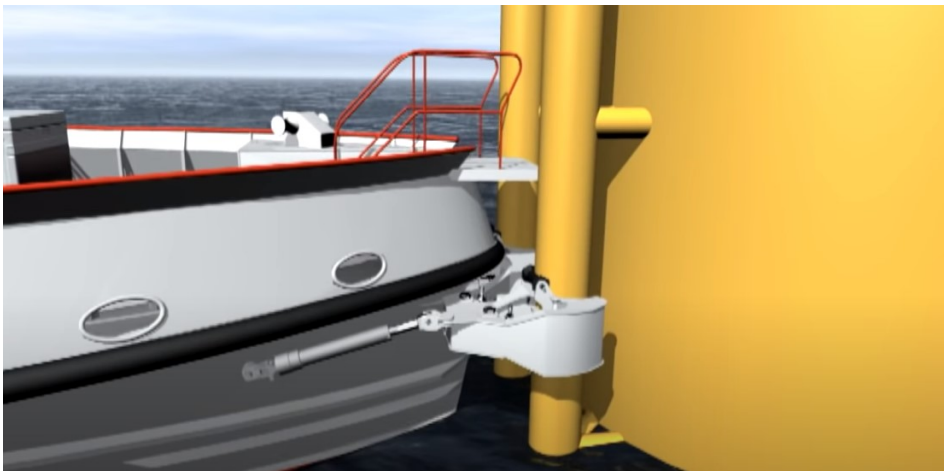

Figure G-1: Crew transfer gripper system. (Mobimar, 2021)

Bibliography

Argon national labratory. (2018). *Energy systems d3 2016 toyota mirai*. Retrieved April 12, 2022, from https://www.anl.gov/es/energy-systems-d3-2016-toyota-mirai

Baleta, J., Vujanović, M., Pachler, K., & Duić, N. (2015). Numerical modeling of urea water based selective catalytic reduction for mitigation of nox from transport sector. *Journal of Cleaner Production*, *88*, 280–288.

Ballard Power Systems. (2022). *Marine modules*. Retrieved April 5, 2022, from https://www.ballard.com/fuel-cell-solutions/fuel-cell-power-products/marine-modules

BEHYDRO. (2022). *Motoren*. Retrieved May 12, 2022, from https://www.behydro.be/

Bhandari, R., Trudewind, C., & Zapp, P. (2014). Life cycle assessment of hydrogen production via electrolysis a review. *Journal of cleaner production*, *85*, 151–163.

BICX. (2022). *Bunker index*. Retrieved May 11, 2022, from https://www.bunkerindex.com/prices/portfreels_xmdo.php?port_id=637

BloombergNEF. (2021). *Battery pack prices fall to an average of $132/kwh, but rising commodity prices start to bite*. Retrieved June 17, 2022, from https://about.bnef.com/blog/battery-pack-prices-fall-to-an-average-of-132-kwh-but-rising-commodity-prices-start-to-bite/

Bonou, A., Laurent, A., & Olsen, S. (2016). Life cycle assessment of onshore and offshore wind energy-from theory to application. *Applied Energy*, *180*, 327–337.

Borup, R., Meyers, J., Pivovar, B., Seung, K. Y., Mukundan, R., Garland, N., Myers, D., Wilson, M., Garzon, F., Wood, D., et al. (2007). Scientific aspects of polymer electrolyte fuel cell durability and degradation. *Chemical reviews*, *107*(10), 3904–3951.

Bose, A., Babburi, P., R.Kumar, Myers, D., Mawdsley, J., & Milhuff, J. (2013). Performance of individual cells in polymer electrolyte membrane fuel cell stack under-load cycling conditions. *Journal of Power Sources*, *243*, 964–972.

Bruijn, F. D., G.J.M, V. D., & Janssen. (2008). Durability and degradation issues of pem fuel cell components. *Fuel cells*, *8*(1), 3–22.

Choi, C., Yu, S., Han, I., Kho, B., Kang, D., Lee, H., Seo, M., Kong, J., Kim, G., Ahn, J., et al. (2016). Development and demonstration of pem fuel-cell-battery hybrid system for propulsion of tourist boat. *International Journal of Hydrogen Energy*, *41*(5), 3591–3599.

CO2 emissiefactoren. (2022). *Brandstoffen voertuigen*. Retrieved May 11, 2022, from https://www.co2emissiefactoren.nl/lijst-emissiefactoren/#brandstoffen_voertuigen

Corvus Energy. (2022). *Energy storage solutions*. Retrieved April 5, 2022, from https://corvusenergy.com/products/energy-storage-solutions/

cryoworld. (2021). *Liquid hydrogen storage: Status and future perspectives*. Retrieved April 13, 2022, from https://www.utwente.nl/en/tnw/ems/research/ats/chmt/m13-hendrie-derking-cryoworld-chmt-2019.pdf

Cwind. (2022). *Hybrid ses*. Retrieved June 21, 2022, from https://cwind.global/wp-content/uploads/2019/07/CWind-SE-CTV-Datasheet-CW072-Final-website.pdf

Dankwa, J. A. Y., Abdulfatah, A., Afrane, S., Jin, C., & Liu, H. (2021). Reviewing two decades of cleaner alternative marine fuels: Towards imo's decarbonization of the maritime transport sector. *Journal of Cleaner Production*, *320*, 128871.

Dolan, S., & Heath, G. (2012). Life cycle greenhouse gas emissions of utility-scale wind power: Systematic review and harmonization. *Journal of Industrial Ecology*, *16*, S136–S154.

Elgowainy, A., Reddi, K., & Wang, M. (2012). *Life-cycle analysis of hydrogen on board storage options* (tech. rep.). Argonne National Laboratory. https://www.hydrogen.energy.gov/pdfs/review13/an034_elgowainy_2013_o.pdf

EngineeringToolbox. (2022). *Fuels - higher and lower calorific values*. Retrieved April 6, 2022, from https://www.engineeringtoolbox.com/fuels-higher-calorific-values-d_169.html

Ettingshausen, F., KleemannJ, J., Marcu, A., Toth, G., & Roth, H. F. C. (2011). Dissolution and migration of platinum in pemfcs investigated for start/stop cycling and high potential degradation. *Fuel Cells*, *11*(2), 238–245.

FullTank. (2022). *Brandstofprijzen*. Retrieved May 11, 2022, from https://fulltank.nl/nl/brandstofprijzen/

Garcia-Sanchez, D., T. Morawietz, T., p.da Rocha, Hiesgen, R., P.Gazdzicki, & K.A.Friedrich. (2020). Local impact of load cycling on degradation in polymer electrolyte fuel cells. *Applied Energy*, *259*, 114210.

Gianni, M., a. Pietra, & Taccani, R. (2021). Outlook of future implementation of pemfc and sofc onboard cruise ships. *E3S Web of Conferences*, *238*.

Government of the Netherlands. (2020). *Offshore wind energy*. Retrieved April 7, 2022, from https://www.government.nl/topics/renewable-energy/offshore-wind-energy

Guo, M., Fu, Z., Ma, D., Ji, N., Song, C., & Liu, Q. (2015). A short review of treatment methods of marine diesel engine exhaust gases. *Procedia Engineering*, *121*, 938–943.

Harzer, G., Schwämmlein, J., Ghosh, A. D. S., & Gasteiger, H. (2018). Cathode loading impact on voltage cycling induced pemfc degradation: A voltage loss analysis. *Journal of The Electrochemical Society*, *165*(6), F3118.

Hwang, S., Jeong, B., Jung, K., Kim, M., & Zhou, P. (2019). Life cycle assessment of lng fueled vessel in domestic services. *Journal of Marine Science and Engineering*, *7*(10), 359.

IACCSEA. (2013). *Marine scr-cost benefit analysis*. Retrieved April 12, 2022, from https://www.iaccsea.com/wp-content/uploads/2018/12/IACCSEA-Marine-SCR-Cost-benefit-analysis-2013.pdf

IMO. (2018). *Initial imo ghg strategy*. Retrieved May 14, 2022, from https://www.imo.org/en/MediaCentre/HotTopics/Pages/Reducing-greenhouse-gas-emissions-from-ships.aspx

Inal, O., Charpentier, J., & Deniz, C. (2022). Hybrid power and propulsion systems for ships: Current status and future challenges. *Renewable and Sustainable Energy Reviews*, *156*, 111965.

Kim, K., Roh, G., Kim, W., & Chun, K. (2020). A preliminary study on an alternative ship propulsion system fueled by ammonia: Environmental and economic assessments. *Journal of marine science and engineering*, *8*(3), 183.

Kobayashi, H., Hayakawa, A., Somarathne, A., Kunkuma, K., & Okafor, E. (2019). Science and technology of ammonia combustion. *Proceedings of the Combustion Institute*, *37*(1), 109–133.

Larminie, J., & Dicks, A. (2003). *Fuel cell systems explained* (2th ed.). John Wiley & Sons Ltd.

Łebkowski, A. (2020). Analysis of the use of electric drive systems for crew transfer vessels servicing offshore wind farms. *Energies*, *13*(6), 1466.

Li, Z., Zheng, Z., Xu, L., & Lu, X. (2019). A review of the applications of fuel cells in microgrids: Opportunities and challenges. *BMC Energy*, *1*(1), 1–23.

Macauley, N., Watson, M., Lauritzen, M., Knights, S., Wang, G., & Kjeang, E. (2016). Empirical membrane lifetime model for heavy duty fuel cell systems. *Journal of Power Sources*, *336*, 240–250.

MAN Energy Solutions. (2022). *Methanol for the maritime energy transition*. Retrieved May 9, 2022, from https://www.man-es.com/marine/strategic-expertise/future-fuels/methanol

McKinlay, C., Turnock, S., & Hudson, D. (2021). Route to zero emission shipping: Hydrogen, ammonia or methanol? *International Journal of Hydrogen Energy*, *46*(55), 28282–28297.

MEARSK. (2022). *Maersk supply service launches new venture company, stillstrom, to deliver offshore vessel charging*. Retrieved April 5, 2022, from https://www.maersksupplyservice.com/2022/01/25/maersk-supply-service-launches-venture-company-stillstrom/

Mobimar. (2021). *Boat landing gripper system*. Retrieved April 13, 2022, from https://www.mobimar.com/commercial-vessels/trimaran-concept/wind-farm-crew-transfer-vessel/mobimar-23-wind-when-safety-priority

Moiras, S., Papapostolou, C., Ktenidis, P., & Kaldellis, J. (2017). Nox emission reduction in marine diesel engines.

Nedstack. (2022). *Marine power installations*. Retrieved April 5, 2022, from https://nedstack.com/en/pemgen-solutions/maritime-power-installations

Nicholas, M. (2019). *Estimating electric vehicle charging infrastructure costs across major us metropolitan areas*. Retrieved April 6, 2022, from https://theicct.%20org/sites/default/files/publications/ICCT%5C_EV%5C_Charging%5C_Cost%5C_20190813.%20pdf

Njord OFFSHORE. (2022). *26m ips multipurpose crew transfer vessels*. Retrieved June 21, 2022, from https://njordoffshore.com/wp-content/uploads/2019/08/Njord-26m-Quad-IPS-12pax.pdf

Nordelof, A., Grunditz, E., Lundmark, S., Tillman, A., Alatalo, M., & Thiringer, T. (2019). Life cycle assessment of permanent magnet electric traction motors. *Transportation Research Part D: Transport and Environment*, *67*, 263–274.

Offshore. (2022). *World's first offshore charging station completes sea trials*. Retrieved April 5, 2022, from https://www.offshore-mag.com/renewable-energy/article/14232807/worlds-first-offshore-charging-station-completes-sea-trials

Pei, P., Chang, Q., & Tang, T. (2008). A quick evaluating method for automotive fuel cell lifetime. *International Journal of Hydrogen Energy*, *33*(14), 3829–3836.

Preger, Y., Barkholtz, H., Fresquez, A., Campbell, D., Juba, B., Romàn-Kustas, J., Ferreira, S., & Chalamala, B. (2020). Degradation of commercial lithium-ion cells as a function of chemistry and cycling conditions. *Journal of The Electrochemical Society*, *167*(12), 120532.

Qiu, Y., Zhong, H., Wang, M., & Zhang, H. (2015). Effect of relative humidity cycles accompanied by intermittent start/stop switches on performance degradation of membrane electrode assembly components in proton exchange membrane fuel cells. *Journal of Power Sources*, *283*, 171–180.

Ren, P., Pei, P., Li, Y., Wu, Z., Chen, D., & Huang, S. (2020). Degradation mechanisms of proton exchange membrane fuel cell under typical automotive operating conditions. *Progress in Energy and Combustion Science*, *80*, 100859.

Rinaldo, S. G., Stumper, J., & Eikerling, M. (2010). Physical theory of platinum nanoparticle dissolution in polymer electrolyte fuel cells. *The Journal of Physical Chemistry C*, *114*(13), 5773–5785.

SGS Inspire. (2021). *Europe: Pure hvo available in nine european countries*. Retrieved May 19, 2022, from https://inspire.sgs.com/news/102941/europe--pure-hvo-available-in-nine-european-countries

Simons, S., & Azimov, U. (2021). Comparative life cycle assessment of propulsion systems for heavy-duty transport applications. *Energies*, *14*(11), 3079.

SMART PORT. (2020). *Power-2-fuel cost analysis* (tech. rep.). https://smartport.nl/wp-content/uploads/2020/09/Cost-Analysis-Power-2-Fuel_def_2020.pdf

Soam, S., & Hillman, K. (2019). Factors influencing the environmental sustainability and growth of hydrotreated vegetable oil (hvo) in sweden. *Bioresource Technology Reports*, *7*, 100244.

StatLine. (2022). *Aardgas en elektriciteit, gemiddelde prijzen van eindverbruikers*. Retrieved May 11, 2022, from https://www.bunkerindex.com/prices/portfreels_xmdo.php?port_id=637

TNO. (2019a). *Feasibility study for a zero emission, battery-electric powertrain for the gouwenaar ii*. Retrieved April 6, 2022, from https://repository.tno.nl/islandora/object/uuid%5C%3A1163fe91-bb12-4aee-98cb-e5ad0321a57a

TNO. (2019b). *Feasibility study for a zero emission, hydrogen fuel cell powertrain for the gouwenaar ii*. Retrieved April 2, 2022, from https://repository.tno.nl/islandora/object/uuid%5C%3A09736677-e299-47bf-86b4-930d3c125fae

TNO. (2020). *Green maritime methanol: Wp3 factsheet and comparison with diesel and lng*. Retrieved April 20, 2022, from https://repository.tno.nl//islandora/object/uuid:31be5cf6-3b22-4405-a911-982ec5f902fd

TNO. (2022). *E-fuels: Towards a more sustainable future for truck transport, shipping and aviation*. Retrieved April 21, 2022, from https://smartport.nl/wp-content/uploads/2020/09/20-11482-whitepaper-Voltachem-10.pdf

Trillos, J., Wilken, D., Brand, U., & Vogt, T. (2021). Life cycle assessment of a hydrogen and fuel cell ropax ferry prototype. *Progress in life cycle assessment 2019* (pp. 5–23). Springer.

TWI. (2022). *What are technology readiness levels (trl)?* Retrieved May 12, 2022, from https://www.twi-global.com/technical-knowledge/faqs/technology-readiness-levels

U.S Department of Energy. (2009). *Hydrogen and fuel cells program*. Retrieved April 1, 2022, from https://www.hydrogen.energy.gov/pdfs/9013_energy_requirements_for_hydrogen_gas_compression.pdf

U.S Department of Energy. (2020). *Doe hydrogen heavy duty truck targets*. Retrieved June 21, 2022, from https://www.energy.gov/sites/prod/files/2020/02/f71/fcto-compressed-gas-storage-workshop-2020-adams.pdf

Uusitalo, V., Väisänen, S., Inkeri, E., & r. Soukka. (2017). Potential for greenhouse gas emission reductions using surplus electricity in hydrogen, methane and methanol production via electrolysis. *Energy conversion and management*, *134*, 125–134.

van Biert, L., Godjevac, M., k. Visser, & Aravind, P. (2016). A review of fuel cell systems for maritime applications. *Journal of Power Sources*, *327*, 345–364.

Verhelst, S., Turner, J. W., Sileghem, L., & Vancoillie, J. (2019). Methanol as a fuel for internal combustion engines. *Progress in Energy and Combustion Science*, *70*, 43–88.

VOLVO PENTA. (2022). *Volvo penta d13*. Retrieved April 5, 2022, from https://www.volvopenta.com/marine/products/inboard-shaft/inboard-shaft-engine-range/d13/

Wang, G., Huang, F., Yu, Y., Wen, S., & z. Tu. (2018). Degradation behavior of a proton exchange membrane fuel cell stack under dynamic cycles between idling and rated condition. *international journal of hydrogen energy*, *43*(9), 4471–4481.

Wang, J., Liu, P., Hicks-Garner, J., Sherman, E., Soukiazian, S., Verbrugge, M., Tataria, H., Musser, J., & Finamore, P. (2011). Cycle-life model for graphite-lifepo4 cells. *Journal of power sources*, *196*(8), 3942–3948.

Wang, X., Shipurkar, U., Haseltalab, A., Polinder, H., & Negenborn, F. C. R. (2021). Sizing and control of a hybrid ship propulsion system using multi-objective double-layer optimization. *IEEE Access*, *9*, 72587–72601.

Wang, Y., Advani, S. M. S., & Prasad, A. (2019). Power management system for a fuel cell/battery hybrid vehicle incorporating fuel cell and battery degradation. *International Journal of Hydrogen Energy*, *44*(16), 8479–8492.

Wu, J., Yuan, X. Z., Martin, J. J., Wang, H., Zhang, J., Shen, J., Wu, S., & Merida, W. (2008). A review of pem fuel cell durability: Degradation mechanisms and mitigation strategies. *Journal of Power Sources*, *184*(1), 104–119.

WWF. (2022). *8 things to know about palm oil*. Retrieved May 12, 2022, from https://www.wwf.org.uk/updates/8-things-know-about-palm-oil

Xing, H., Stuart, C., Spence, S., & Chen, H. (2021). Alternative fuel options for low carbon maritime transportation: Pathways to 2050. *Journal of Cleaner Production*, *297*, 126651.

Yang, J., Chang, Y., Zhang, L., Hao, Y., Yan, Q., & Wang, C. (2018). The life-cycle energy and environmental emissions of a typical offshore wind farm in china. *Journal of Cleaner Production*, *180*, 316–324.

YANMAR. (2020). *Cleaner exhaust gas for ocean and sky more convenience for vessels*. Retrieved June 18, 2022, from https://www.yanmar.com/media/news/2020/08/14010405/scr_system_en.pdf

Zakrisson, E. (2011). The effect of start/stop strategy on pem fuel cell degradation characteristics.

Zhang, J. (2008). *Pem fuel cell electrocatalysts and catalyst layers: Fundamentals and applications*. Springer Science & Business Media.

Zhang, T., Wang, P., Chen, H., & Pei, P. (2018). A review of automotive proton exchange membrane fuel cell degradation under start-stop operating condition. *Applied energy*, *223*, 249–262.

Zhang, X., Yang, D., Luo, M., & z. Dong. (2017). Load profile based empirical model for the lifetime prediction of an automotive pem fuel cell. *International Journal of Hydrogen Energy*, *42*(16), 11868–11878.